TRITA-MEK Technical Report 2000:11 ISSN 0348-467X ISRN KTH/MEK/TR--00/11--SE

Modeling of magnetohydrodynamic turbulence

by

Ola Widlund

November, 2000 Technical Reports from Royal Institute of Technology Department of Mechanics SE-100 44 Stockholm, Sweden Typsatt i AMS-IATEX.

Akademisk avhandling som med tillstånd av Kungliga Tekniska Högskolan i Stockholm framlägges till offentlig granskning för avläggande av teknologie doktorsexamen fredagen den 15 december, 2000, kl. 10.15 i Kollegiesalen, Administrationsbyggnaden, Kungliga Tekniska Högskolan, Valhallavägen 79, Stockholm.

© Ola Widlund, 2000 Norstedts Tryckeri AB, Stockholm, 2000

Modeling of magnetohydrodynamic turbulence

Ola Widlund

Faxén Laboratory Department of Mechanics, Royal Institute of Technology SE-100 44 Stockholm, Sweden

November, 2000

Abstract

Conventional one-point turbulence closures have been extended with an additional transported scalar for modeling of magnetohydrodynamic (MHD) turbulence. The new scalar, α , captures the length scale anisotropy and tendency towards two-dimensionality, which is a characteristic feature of MHD turbulence, and allows accurate modeling of the Joule dissipation of turbulence. The concept has been used for both a full Reynolds stress closure, and a three-equation $K-\varepsilon-\alpha$ model. An exact transport equation for α was derived from the governing equations. All terms in the equation require modeling, however. The proposed model transport equation for α includes terms for magnetic dissipation, nonlinear energy transfer, and effects of mean shear and strain. Modeling of the magnetic and strain-related terms was based on rapid distortion analysis of the linearized equations, while modeling of nonlinear effects is phenomenological in nature. For homogeneous turbulence, the model was compared with linear theory, direct numerical simulations and experiments. For turbulence subjected to a strong magnetic field, the model reproduces the energy and length scale evolution predicted by linear theory. When nonlinear effects are of importance, it predicts energy decay and length scale evolution in agreement with experiments. The eddy viscosity and Reynolds stress versions of the model coincide with the respective conventional models in the absence of a magnetic field. The objective of this project has been to develop efficient MHD turbulence models for engineering applications, especially for modeling of continuous steel casting. The novel MHD turbulence models appear to be numerically robust, and they have been implemented in a commercial flow solver, together with electromagnetic equations for the Lorentz forces in the mean momentum equations.

Descriptors: Turbulence model, magnetohydrodynamics, MHD, magnetohydrodynamic turbulence, computational fluid dynamics, continuous casting, dimensionality, Reynolds stresses, eddy viscosity

Contents

Preface		vii
Chapter	1. Introduction	1
Chapter 2.1. 2.2. 2.3. 2.4. 2.5.	2. Basic concepts Governing equations Reynolds decomposition Reynolds stresses and turbulent kinetic energy Conventional turbulence closures The quasistatic approximation of magnetic flux density	7 7 7 10 11 14
Chapter 3.1. 3.2. 3.3. 3.4. 3.5.	3. MHD turbulence modeling Spectral analysis of homogeneous MHD turbulence Modeling of the Joule dissipation An exact equation for α Inhomogeneous effects Implementation in a commercial flow solver	19 20 23 27 28 31
Chapter 4.1. 4.2.	4. Concluding summary The MHD turbulence closure Summary of papers	33 33 35
Chapter 5.1. 5.2. 5.3.	5. Future challenges Understanding nonlinear inertial effects Including effects of walls and inhomogeneities Modeling of anisotropic turbulent transport	38 38 39 41
Acknowledgments		43
Bibliography		44
Paper 1		49
Paper 2		75
Paper 3		103
Paper 4		115
Paper 5		133
Paper 6		179
Paper 7		187

Preface

This thesis considers the modeling of magnetohydrodynamic (MHD) turbulence, by including additional structural information in conventional Reynolds stress and eddy-viscosity closures. The thesis is based on and contains the following papers.

- **Paper 1.** O. WIDLUND, S. ZAHRAI & F. H. BARK (1998) Development of a Reynolds stress closure for modeling of homogeneous MHD turbulence. *Phys. Fluids* **10**, 1987–1996.
- Paper 2. O. Widlund, S. Zahrai & F. H. Bark (2000) Structure information in rapid distortion analysis and one-point modeling of axisymmetric magnetohydrodynamic turbulence. *Phys. Fluids* 12, 2609–2620.
- Paper 3. O. Widlund & G. Tallbäck (2000) Modeling of anisotropic turbulent transport in simulations of liquid metal flows in magnetic fields. 3rd Int. Symposium on Electromagnetic Processing of Materials, EPM2000, Nagoya, Japan, April 3-6, 2000. ISIJ.
- **Paper 4.** O. Widlund (2000) MHD turbulence modeling: Effects of mean strain on dimensionality anisotropy. To be submitted.
- **Paper 5.** O. Widlund (2000) Implementation of MHD model equations in CFX 4.3. Technical Report TRITA-MEK 2000:10, Dept. of Mechanics, KTH, Stockholm.
- **Paper 6.** O. Widlund (2000) Modeling anisotropic MHD turbulence in simulations of liquid metal flows. *4th International PAMIR Conference*, Presqu'île de Giens, France, 18-22 September, 2000. PAMIR.
- **Paper 7.** O. Widlund (2000) Nonlinear effects in modeling of homogeneous MHD turbulence Comparison with experiment To be submitted.

Compared to already published versions, the papers have here been typeset in a consistent format, and minor typos have been corrected.

CHAPTER 1

Introduction

Faraday and his contemporaries were already in the early 19th century aware of the interaction between a magnetic field, and an object moving through it [13]. They knew, that if an electrically conducting solid object or a fluid moves through a magnetic field, an electric current is generated. The current induces a magnetic field of its own, which distorts the original field. The current also interacts with the magnetic field to create forces, which tend to counteract the original motion.

The interest for the interaction between conducting fluids and magnetic fields increased in the end of the 19th century, when astrophysicists realized that electrically conducting ionized gases (plasmas) are abundant in the universe, together with strong magnetic fields. The concentration of gases is naturally very low, but the effects can be dramatic because the time scales and length scales are extremely large. In 1919, Larmor presented a brief communication with the title "How could a rotating body such as the Sun become a magnet?" [19]. One of the explanations suggested by Larmor was that the rotating motion of the sun induces electrical currents, which themselves produce the magnetic field necessary for their creation. The result is a self-exciting hydrodynamic dynamo (see, e.g., Moffatt [27]). Much later geophysicists embraced the dynamo theory for explaining how the rotation of the earth causes its liquid core to generate the earth magnetic field. The term "magnetohydrodynamics" was introduced by the Swedish astrophysicist Hannes Alfvén in 1942 [3], when he, in a classical paper in *Nature*, reported the first mathematical deduction of magnetohydrodynamic wave motion, later known as Alfvén waves. At about this time, the formal theory of magnetohydrodynamics (MHD) was finding its present form (see, e.g., Shercliff [35]).

The first electromagnetic pumps and generators were conceived around 1920, and especially since the second world war, MHD has found wide-spread practical and industrial application. Electromagnetic pumping of liquid metal coolants was, for example, standard practice in the early nuclear reactor designs, and MHD is a cornerstone in modern research on controlled thermonuclear fusion. In a fusion reactor, the hot plasma is confined using magnetic fields, and liquid metal "blankets" are used both for cooling and moderation. Magnetic fields are used in materials processing for heating, levitation (to avoid contamination), stirring, and flow control. In the manufacture of semi-conductor substrates, magnetic fields are applied in the crystal growth process to control the detrimental effect of natural convection. In the metallurgical industry, magnetic fields are commonly used for stirring and braking of liquid metal flows.

A process of particular relevance for this thesis is the continuous casting of steel. In this process, the liquid steel is continuously supplied to a water cooled copper mold through a submerged inlet pipe. The strong momentum of the injected liquid steel causes recirculation in the mold and this may lead to inclusion of particles and impurities, that would otherwise migrate to the slag layer at the surface. The fluid motion in the mold can be damped and controlled by applying a static magnetic field across the mold. The field is provided by a so-called *electromagnetic brake* (EMBR), a device often used to improve quality and productivity in continuous casting operations. The primary effect of the magnetic field is here to brake the mean flow; the motion of the fluid through the magnetic field induces Lorentz forces, which tend to counteract the motion perpendicular to the magnetic field. Another effect is magnetic dissipation of turbulence, or Joule dissipation, which reduces the turbulent transport of heat and momentum. Figure 1.1 illustrates the effect of a localized magnetic field on the mean flow in the mold. The momentum of the inlet jet is reduced and redirected. The penetration depth of the jet is thus considerably reduced, as is the entrapment of oxide particles and gas bubbles. The meniscus, i.e., the near-wall interface between liquid steel and the slag layer, will be calmer and the

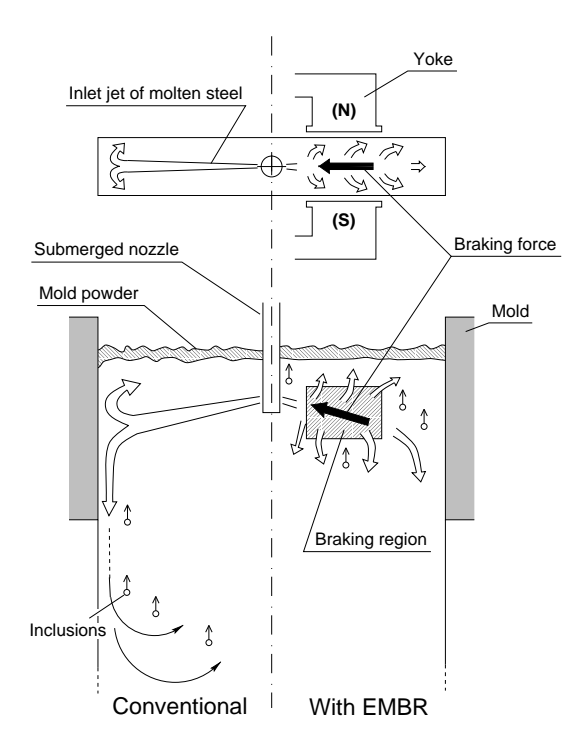


FIGURE 1.1 Outline of flow field and transport of inclusions in continuous slab casting. The left side of the figure is for conventional casting, without magnetic braking. On the right side, an electromagnetic brake (EMBR) has been applied to brake the momentum of the inlet jet.

surface temperature higher. The increased stability of the process often leads to a substantial reduction of cracks in the surface of the product.

Manufacturers of magnetic brakes use numerical flow simulations to optimize their designs and verify that they meet performance specifications (see, e.g., Lehman et al. [22]), and steel producers use simulations to optimize their processes [39, 43]. The most economic way of simulating turbulent flows is to solve equations for the mean flow velocities, mean temperatures, etc. The effects of the turbulent fluctuations on the mean flow are accounted for by including model equations for statistical turbulence quantities. Common quantities used in turbulence models are the kinetic energy of the turbulence (turbulence intensity), and quantities related to length scales or time scales of the largest turbulent eddies, which account for most of the turbulent transport. The extension of commercial numerical flow solvers to include the effects a magnetic field on the mean flow is relatively straightforward, but the effect of the magnetic field on turbulence is more difficult to incorporate. The magnetic forces act preferentially on motion perpendicular to the magnetic field. One consequence of this is that turbulent structures are elongated in the direction of the magnetic field. These structural changes are very important for a correct description of Joule dissipation of turbulence, but the effects are not captured by conventional turbulence models.

If we look at the effects of a magnetic field in more detail, it is useful to define a few dimensionless numbers. The interaction between the fluid flow and the magnetic field is characterized by the magnetic Reynolds number. For an incompressible Newtonian fluid with constant density ρ , magnetic permeability μ and electric conductivity σ , the magnetic Reynolds number is defined as

$$Rm \equiv \mu \sigma U L = \frac{UL}{\lambda}, \tag{1.1}$$

where U and L are characteristic velocity and length scales of the flow, and $\lambda = 1/(\mu\sigma)$ is the magnetic field diffusivity. Lehnert [23] was the first to formulate the dimensionless number (1.1) and recognize the analogy with the hydrodynamic Reynolds number $\mathrm{Re} = UL/\nu$ (where ν is the kinematic viscosity). The magnetic Reynolds number can be interpreted as a ratio of the time scales for diffusion of magnetic field perturbations, and flow convection. In most industrial and laboratory-scale liquid metal flows, magnetic diffusion dominates, and the magnetic Reynolds number is very low, $\mathrm{Rm} \ll 1$. This means that the distortion of the magnetic field due to the flow is negligible, and our theoretical treatment of the electromagnetic equations can be simplified considerably.

Regarding magnetic effects on the flow, the strength of magnetic effects relative to inertial mechanisms is measured by the *magnetic interaction parameter*, defined as

$$N \equiv \frac{\sigma B^2}{\rho} \frac{L}{U},\tag{1.2}$$

where B is the flux density of the magnetic field. N is the ratio of inertial forces and magnetic Lorentz forces, characterized by time scales L/U and $\rho/(\sigma B^2)$, respectively.

Lehnert [24] studied the decay of turbulence in an imposed magnetic field He considered the final period of decay, where both magnetic and viscous forces are present (Re $\ll 1$), but nonlinear effects are negligible. Lehnert formulated the linearized induction and momentum equations, and derived a law of decay for the spectral energy tensor (see Sec. 3.1.3). He noted that the asymptotic state of decay is two-dimensional with respect to the magnetic field, so that surviving turbulent structures are very long the direction of the magnetic field. Moffatt later continued along the same lines [26]; He used Lehnert's linearized equations, focusing on the case of high Reynolds number, $\text{Re} \gg 1$, and strong magnetic fields, $N \gg 1$, where also viscous effects can be neglected. For the case of low magnetic Reynolds number, Moffatt found that turbulent kinetic energy decays as $K \sim (t/\tau_m)^{-1/2}$, where $\tau_m = \rho/(\sigma B^2)$ is the magnetic time scale. It is interesting to note that this often cited result follows already from integration of Lehnert's decay law for the spectral energy. Moffatt further showed that, although the final state of decay is two-dimensional (no variation in the direction of the field), linear theory predicts that the remaining turbulent kinetic energy is partitioned equally between fluctuations parallel with, and perpendicular to the magnetic field.

Sommeria and Moreau [37], and Davidson [11] used dimensional arguments to estimate the development of length scale anisotropy during the linear phase of decay. If l_{\perp} and l_{\parallel} , respectively, are length scales in the perpendicular and parallel directions relative to the magnetic field, they found that $l_{\parallel} \sim (t/\tau_m)^{1/2}$, if l_{\perp} is assumed to change only slowly. Davidson argued that the field-parallel component of angular momentum is conserved during decay in a magnetic field, and this lead to the energy decay rate found earlier by Lehnert and Moffatt.

A scale estimate of the magnetic term in the linearized equations shows that the magnetic Joule dissipation, μ , of turbulent kinetic energy, K, is

$$\mu \sim rac{1}{ au_m} \left(rac{l_\perp}{l_\parallel}
ight)^2 K$$

(see, e.g., Davidson [11]). Even if Joule dissipation dominates initially, it will diminish with growing anisotropy of the length scales, and we will eventually reach a point where nonlinear inertial effects are no longer negligible. If the initial interaction parameter is N_0 , Alemany et al. [2], and Sreenivasan and Alboussière [38] have estimated that the duration of the linear phase of decay is $t_{\text{lin}} \sim \tau_m N_0^{4/3}$. The role of nonlinear inertial mechanisms in MHD turbulence is still not well understood, but they are expected to increase the Joule dissipation rate, by transferring energy to regions of spectral space where Joule dissipation is strong (see, e.g., Moreau [28]).

Most of the MHD experiments reported on in the literature are studies of pipe and channel flows, both laminar and turbulent. Magnetic fields are generally found to reduce the level of turbulence, and delay transition from laminar to turbulent flow. The monograph by Branover on MHD duct flows [5], and the review by Lielausis [25] provide good overviews of experimental results. The thesis of Burr [6] is an example of more recent work.

The experimental setup used by Alemany et al. [2], and later Caperan and Alemany [8], is unique as it is probably the only one where wall effects are negligible. They studied the decay of homogeneous grid generated turbulence in a magnetic field. The initial interaction parameter was of order unity, so nonlinear effects should be important. They found the energy decay rate $K \sim t^{-1.7}$, which is significantly faster than the theoretical results for the linear case mentioned earlier.

The most accurate approach to numerical modeling is direct numerical simulations (DNS), where one resolves all turbulent fluctuations in time and space. Already in 1976, Schumann used DNS to study the decay of homogeneous turbulence in a magnetic field [34]. In a more recent study, Zikanov and Thess [44] applied an artificial forcing to study the development of two-dimensional turbulence. Noguchi et al. [30, 17] have performed DNS of a plane channel flow in a weak magnetic field ($N \ll 1$). Homogeneous MHD turbulence has also been studied using spectral models, like the eddy-damped quasi-normal Markovian (EDQNM) approximation, and the direct-interaction approximation (DIA). See Nakauchi et al. [29] and Shimomura [36] for applications of EDQNM and a two-scale version of DIA, respectively.

The turbulence models generally used for computation of complex flows in industrial applications rely on statistical quantities for modeling of turbulent transport. One of the most popular models, the K- ε model, include transport equations for the turbulent kinetic energy, K, and the viscous dissipation rate, ε . Turbulent transport in the mean equations is then modeled by defining a turbulent viscosity as a function of the variables K and ε . In more advanced models, transport equations are introduced for the Reynolds stresses appearing in the mean momentum equations. The Reynolds stresses are statistical second moments of velocity fluctuations in all directions. Conventional turbulence closures carry no information about length scale anisotropies, however, and this makes it difficult to incorporate MHD effects in a physically realistic way. Ji and Gardner [16] proposed a modification of a low-Re K- ε model for modeling of MHD pipe flows. They used an exponential damping function to model a decrease of the Joule dissipation with increasing magnetic field strength (as measured by a bulk interaction parameter). More recently, Kenjereš and Hanjalić [18] suggested significant improvements of this model.

The objective of the work presented in this thesis has been to develop an effective and numerically robust engineering turbulence closure for industrial MHD applications. The closure developed here differ from earlier work by introducing an additional transported scalar variable for the length scale anisotropy information we need for modeling of the Joule dissipation. The definition of the new dimensionality anisotropy variable α is such that the Joule dissipation of homogeneous turbulence can be expressed exactly as

$$\mu = \frac{2\sigma B^2}{\rho} \alpha K.$$

A transport equation for the variable α can be derived from the governing equations, but all terms require modeling. The resulting model equation for α includes effects of mean strain, nonlinear energy transfer, and magnetic dissipation.

The magnetic terms in the ε and Reynolds stress equations can also be modeled in terms of α . The scalar α and its transport equation can thus be used for an MHD extension of conventional turbulence closures, for example in a three-equation "K- ε - α " model, or an eight-equation "Reynolds stress- α " model.

CHAPTER 2

Basic concepts

2.1. Governing equations

With spatial coordinates \mathbf{x} and time t, the Navier–Stokes and continuity equations for the instantaneous velocity field $u_i(\mathbf{x},t)$ of an incompressible fluid are

$$\frac{\partial u_i}{\partial t} + u_j \frac{\partial u_i}{\partial x_j} = -\frac{1}{\rho} \frac{\partial p}{\partial x_i} + \nu \frac{\partial^2 u_i}{\partial x_j \partial x_j} + f_i, \tag{2.1}$$

$$\frac{\partial u_i}{\partial x_i} = 0, (2.2)$$

where $p(\mathbf{x}, t)$ is the pressure field, ρ is constant fluid density, ν is the kinematic viscosity, and f_i is the magnetic Lorentz force, as governed by the Maxwell equations. Using lower-case letters to denote instantaneous values, we have

$$f_i = \frac{1}{\rho} \epsilon_{ikn} j_k b_n. \tag{2.3}$$

The electric current density j_i is given by Ohm's law,

$$j_i = \sigma(e_i + \epsilon_{ikn} u_k b_n), \tag{2.4}$$

where e_i is the electric field and b_i the magnetic flux density. The scalar electrostatic potential ϕ is defined by

$$e_i = -\frac{\partial \phi}{\partial x_i}. (2.5)$$

In the absence of free charges, the electric current density is divergence free. If the conductivity σ is constant, the divergence of Ohm's law (2.4), together with (2.5), therefor yields

$$\frac{\partial^2 \phi}{\partial x_i \partial x_i} = \epsilon_{ijk} \frac{\partial}{\partial x_i} (u_j b_k). \tag{2.6}$$

2.2. Reynolds decomposition

The instantaneous variables above can be split into mean and fluctuating parts, using the so-called Reynolds decomposition. We define the mean of a quantity v as the ensemble average over an infinite number of realizations,

$$\langle v \rangle = \lim_{N \to \infty} \frac{1}{N} \sum_{n=1}^{N} v_n. \tag{2.7}$$

For the quantities in the Navier–Stokes equations, the Reynolds decomposition is defined by

$$u_{i}(\mathbf{x},t) \equiv \langle u_{i}(\mathbf{x},t) \rangle + u'_{i}(\mathbf{x},t) = U_{i}(\mathbf{x},t) + u'_{i}(\mathbf{x},t),$$

$$p(\mathbf{x},t) \equiv \langle p(\mathbf{x},t) \rangle + p'(\mathbf{x},t) = P(\mathbf{x},t) + p'(\mathbf{x},t),$$

$$f_{i}(\mathbf{x},t) \equiv \langle f_{i}(\mathbf{x},t) \rangle + f'_{i}(\mathbf{x},t) = F_{i}(\mathbf{x},t) + f'_{i}(\mathbf{x},t),$$
(2.8)

where we have used capital letters to denote the mean quantities, and primes to denote the fluctuating parts. Reynolds decompositions for the electromagnetic quantities are defined in the same way, except for the magnetic flux density: the mean magnetic flux density is the sum of the induced mean flux density \mathbf{B}_I (due to the mean flow), and the applied external magnetic field \mathbf{B}_0 ,

$$b_i(\mathbf{x}, t) \equiv \langle b_i(\mathbf{x}, t) \rangle + b_i'(\mathbf{x}, t) = B_i(\mathbf{x}, t) + b_i'(\mathbf{x}, t), \tag{2.9}$$

where

$$B_i(\mathbf{x},t) = B_{Ii}(\mathbf{x},t) + B_{0i}(\mathbf{x}). \tag{2.10}$$

The external magnetic field \mathbf{B}_0 is here assumed steady, but not necessarily homogeneous. For electric current, electric potential, and electric field, we have

$$j_{i}(\mathbf{x},t) \equiv J_{i}(\mathbf{x},t) + j'_{i}(\mathbf{x},t),$$

$$\phi(\mathbf{x},t) \equiv \Phi(\mathbf{x},t) + \phi'(\mathbf{x},t),$$

$$e_{i}(\mathbf{x},t) \equiv E_{i}(\mathbf{x},t) + e'_{i}(\mathbf{x},t).$$
(2.11)

2.2.1. Mean equations. The ensemble averaged Navier–Stokes and continuity equations, often called the Reynolds equations, are

$$\frac{\partial U_i}{\partial t} + U_j \frac{\partial U_i}{\partial x_j} = -\frac{1}{\rho} \frac{\partial P}{\partial x_i} + \frac{\partial}{\partial x_j} \left(\nu \frac{\partial U_i}{\partial x_j} - \langle u_i' u_j' \rangle \right) + F_i, \qquad (2.12)$$

$$\frac{\partial U_i}{\partial x_i} = 0. \qquad (2.13)$$

We see that the statistical second moments of the velocity fluctuations appear on the right-hand side of the mean momentum equations; the quantities $-\rho \langle u_i' u_j' \rangle$ are the *Reynolds stresses*.

The interaction between the velocity field and the magnetic field is characterized by the magnetic Reynolds number. For an incompressible Newtonian fluid with magnetic permeability μ and electrical conductivity σ , the magnetic Reynolds number is defined as,

$$Rm \equiv \mu \sigma U L, \tag{2.14}$$

where U is a characteristic velocity scale, and L is the integral length scale. The magnetic Reynolds number can be interpreted as the ratio between the diffusion time scale of the magnetic field, and the time scale of the velocity field. In most industrial and laboratory-scale flows, the magnetic Reynolds number is very low, $Rm \ll 1$. This means that the distortion of the magnetic field due to the flow is negligible. The treatment of the electromagnetic equations can then be simplified considerably by applying the inductionless, or quasistatic approximation, in which we can neglect the flow-induced magnetic flux densities \mathbf{B}_I and \mathbf{b} beside the external field \mathbf{B}_0 . We use the quasistatic approximation

here without further motivation, and refer to Sec. 2.5 for a discussion about the underlying scale arguments in the context of Reynolds averaging.

We introduce the Reynolds decomposed quantities into Eqs. (2.3) through (2.6). Ensemble averaging yields the following equations for the mean electromagnetic quantities,

$$\nabla^2 \Phi = \nabla \cdot (\mathbf{U} \times \mathbf{B} + \langle \mathbf{u}' \times \mathbf{b}' \rangle) \approx \nabla \cdot (\mathbf{U} \times \mathbf{B}_0), \tag{2.15}$$

$$\mathbf{E} = -\nabla\Phi,\tag{2.16}$$

$$\mathbf{J} = \sigma(\mathbf{E} + \mathbf{U} \times \mathbf{B} + \langle \mathbf{u}' \times \mathbf{b}' \rangle) \approx \sigma(\mathbf{E} + \mathbf{U} \times \mathbf{B}_0), \tag{2.17}$$

$$\mathbf{F} = \frac{1}{\rho} (\mathbf{J} \times \mathbf{B} + \langle \mathbf{j}' \times \mathbf{b}' \rangle) \approx \frac{1}{\rho} \mathbf{J} \times \mathbf{B}_0, \tag{2.18}$$

where the relative errors of the approximation are of order Rm, or smaller.

Most commercial codes for turbulent flow simulations solve the Reynolds averaged equations, (2.12) and (2.13), with additional turbulence model equations for predicting the Reynolds stresses $\langle u_i'u_j'\rangle$. One way to include the Lorentz force in the mean momentum equation is to solve also Eq. (2.15) for the mean electric potential equation, with appropriate boundary conditions; the Lorentz force can then be computed from Eqs. (2.16) through (2.18), with due attention given to the conservation of electric current.

2.2.2. Fluctuation equations. If we subtract the mean Reynolds equations from the instantaneous Navier–Stokes and continuity equations, we are left with the equations for the fluctuating velocity and pressure fields,

$$\frac{\partial u_i'}{\partial t} + U_j \frac{\partial u_i'}{\partial x_j} = -u_j' \frac{\partial U_i}{\partial x_j} - \frac{1}{\rho} \frac{\partial p'}{\partial x_i} + \nu \frac{\partial^2 u_i'}{\partial x_j \partial x_j} + \frac{\partial}{\partial x_j} (\langle u_i' u_j' \rangle - u_i' u_j') + f_i',$$
(2.19)

$$\frac{\partial u_i'}{\partial x_i} = 0. {(2.20)}$$

We use the same procedure to obtain equations for the fluctuating electromagnetic quantities, and again apply the quasistatic approximation,

$$\nabla^2 \phi' = \nabla \cdot (\mathbf{U} \times \mathbf{b}' + \mathbf{u}' \times \mathbf{B} + \mathbf{u}' \times \mathbf{b}' - \langle \mathbf{u}' \times \mathbf{b}' \rangle)$$

$$\approx \nabla \cdot (\mathbf{u}' \times \mathbf{B}_0).$$
(2.21)

$$\mathbf{e}' = -\nabla \phi', \tag{2.22}$$

$$\mathbf{j}' = \sigma(\mathbf{e}' + \mathbf{U} \times \mathbf{b}' + \mathbf{u}' \times \mathbf{B} + \mathbf{u}' \times \mathbf{b}' - \langle \mathbf{u}' \times \mathbf{b}' \rangle)$$

$$\approx \sigma(\mathbf{e}' + \mathbf{u}' \times \mathbf{B}_0),$$
(2.23)

$$\mathbf{f}' = \frac{1}{\rho} (\mathbf{J} \times \mathbf{b}' + \mathbf{j}' \times \mathbf{B} + \mathbf{j}' \times \mathbf{b}' - \langle \mathbf{j}' \times \mathbf{b}' \rangle)$$

$$\approx \frac{1}{\rho} \mathbf{j}' \times \mathbf{B}_{0}.$$
(2.24)

2.3. Reynolds stresses and turbulent kinetic energy

The velocity fluctuations enter the mean equations (2.12) as the *a priori* unknown Reynolds stresses $-\rho \langle u'_i u'_i \rangle$.

A transport equation for the Reynolds stress tensor $R_{ij} \equiv \langle u'_i u'_j \rangle$ can be derived by multiplying the Navier–Stokes equations (2.1) by u_k , ensemble averaging, and subtracting the mean part (the latter is Eq. (2.12) multiplied by U_k). This yields (see, e.g., Hallbäck *et al.* [15], Sec. 3.4)

$$\frac{\partial R_{ij}}{\partial t} + U_j \frac{\partial R_{ij}}{\partial x_j} = P_{ij} + \Pi_{ij} - \varepsilon_{ij} - \frac{\partial}{\partial x_m} \left(J_{ijm} - \nu \frac{\partial R_{ij}}{\partial x_m} \right) + \langle u_i' f_i' \rangle + \langle u_j' f_i' \rangle,$$
(2.25)

where

$$P_{ij} \equiv -R_{im} \frac{\partial U_j}{\partial x_m} - R_{jm} \frac{\partial U_i}{\partial x_m}, \qquad (2.26)$$

$$\Pi_{ij} \equiv \frac{2}{\rho} \langle p' s'_{ij} \rangle, \text{ with } s'_{ij} \equiv \frac{1}{2} \left(\frac{\partial u'_i}{\partial x_j} + \frac{\partial u'_j}{\partial x_i} \right),$$
(2.27)

$$\varepsilon_{ij} \equiv 2\nu \left\langle \frac{\partial u_i'}{\partial x_m} \frac{\partial u_j'}{\partial x_m} \right\rangle, \tag{2.28}$$

$$J_{ijm} \equiv \langle u'_i u'_j u'_m \rangle + \frac{1}{\rho} \left(\langle u'_j p' \rangle \delta_{im} + \langle u'_i p' \rangle \delta_{jm} \right). \tag{2.29}$$

In (2.27), s'_{ij} is the fluctuating strain rate tensor. ε_{ij} is the viscous dissipation tensor. Only the production term P_{ij} and part of the transport term in (2.25) are explicit in the Reynolds stress tensor R_{ij} . All other terms require modeling.

The pressure terms in the Reynolds stress transport (RST) equation have been split into two parts. The pressure-strain rate correlation Π_{ij} is traceless and represents intercomponent energy transfer; it thus has no counterpart in the transport equation for the turbulent kinetic energy $K \equiv R_{ii}/2$. The pressure term in J_{ijm} represents pressure-gradient work (Tennekes & Lumley [41]); it has here been lumped with the triple correlation responsible for turbulent transport, so that J_{ijm} represents spatial redistribution.

There is a problem with closure of the RST equations for two reasons, as noted by Reynolds & Kassinos [32]. First there is the *non-linearity* of the Navier–Stokes equations; a formally derived equation for a higher-order moment will contain terms of the next higher order. Second, the terms involving the fluctuating pressure represent *non-local interactions*.

The traditional theoretical treatment of the pressure–strain rate correlation (2.27) is based on the formal solution of a Poisson equation for the fluctuating pressure field. The divergence of (2.19), together with (2.20), yields

$$-\frac{1}{\rho}\nabla^2 p' = 2\frac{\partial U_i}{\partial x_i}\frac{\partial u_j'}{\partial x_i} + \frac{\partial^2}{\partial x_i\partial x_j}\left(u_i'u_j' - \langle u_i'u_j'\rangle\right) - \frac{\partial f_i'}{\partial x_i}.$$
 (2.30)

The integration of the Poisson equation is usually subject to a number of local homogeneity assumptions (see, e.g., Chou [9]). One of these is that the mean velocity gradients are assumed homogeneous, so that they can be extracted from the integrals. For the MHD problem at hand, we split the pressure–strain term

into three traceless parts, representing the contributions from the respective terms in the pressure Poisson equation (2.30),

$$\Pi_{ij} = \Pi_{ij}^{(r)} + \Pi_{ij}^{(s)} + \Pi_{ij}^{(m)}. \tag{2.31}$$

The rapid part $\Pi_{ij}^{(r)}$ here represents interaction of turbulence with the mean velocity field. The slow term $\Pi_{ij}^{(s)}$ represents non-linear turbulence–turbulence interactions, generally acting to restore a turbulence field to isotropy. The magnetic part $\Pi_{ij}^{(m)}$ represents interaction between turbulence and Lorentz forces. In this thesis, we treat the magnetic part of the traceless pressure–strain

In this thesis, we treat the magnetic part of the traceless pressure–strain term together with the explicit body-force terms in (2.25). All effects of the magnetic field are thus incorporated into a *Joule dissipation tensor*, defined as

$$\mu_{ij} \equiv -\langle u_i' f_j' \rangle - \langle u_j' f_i' \rangle - \Pi_{ij}^{(m)}. \tag{2.32}$$

(The dissipative nature of μ_{ij} will be demonstrated in Sec. 3.1.)

An equation for turbulent kinetic energy $K \equiv R_{ii}/2$ is obtained by taking the trace of (2.25),

$$\frac{\partial K}{\partial t} + U_j \frac{\partial K}{\partial x_j} = P_K - \varepsilon - \frac{\partial}{\partial x_m} \left(J_m - \nu \frac{\partial K}{\partial x_m} \right) - \mu, \tag{2.33}$$

where

$$P_K \equiv -\langle u_i' u_m' \rangle \frac{\partial U_i}{\partial x_m}, \tag{2.34}$$

$$\varepsilon \equiv \nu \left\langle \frac{\partial u_i'}{\partial x_m} \frac{\partial u_i'}{\partial x_m} \right\rangle, \tag{2.35}$$

$$J_m \equiv \frac{1}{2} \langle u_i' u_i' u_m' \rangle + \frac{1}{\rho} \langle u_m' p' \rangle, \qquad (2.36)$$

$$\mu \equiv \frac{1}{2}\mu_{ii} = -\langle u_i' f_i' \rangle. \tag{2.37}$$

Here P_K and ε are the turbulence production and viscous dissipation, respectively, while J_m represents turbulent transport, and μ is the scalar Joule dissipation of turbulent kinetic energy.

In the following section we briefly discuss conventional turbulence closures, which do not consider effects of the Lorentz force. Modeling of the Joule dissipation terms μ_{ij} and μ is discussed in Chapter 3.

2.4. Conventional turbulence closures

The mean momentum equation (2.12) must be closed by providing a model for the Reynolds stresses $-\rho \langle u_i' u_j' \rangle$, or by defining closed model transport equations for them. In practical applications we often want to predict also the transport of a scalar, for example temperature (or enthalpy), or the concentration of a chemical species. Consider a scalar q, for which a Reynolds decomposition defines mean and fluctuating parts Q and q', respectively. The mean transport equation can be written

$$\frac{\partial Q}{\partial t} + U_j \frac{\partial Q}{\partial x_j} = \frac{\partial}{\partial x_j} \left(\frac{\Gamma_Q}{\rho} \frac{\partial Q}{\partial x_j} + \langle u_i' q' \rangle \right) + S_Q, \tag{2.38}$$

where ρS_Q is a volume source of the scalar. Turbulent fluctuations contribute to the transport of the mean quantity through the turbulent Reynolds flux $-\rho \langle u'_i q' \rangle$, which must also be quantified by some kind of turbulence model.

If we consider the case without external body forces, conventional turbulence models can be put into two broad classes; eddy viscosity models, and Reynolds stress transport (RST) models. The most common eddy viscosity model is the K- ε model.

2.4.1. Reynolds stress transport models. A full Reynolds stress closure features transport equations for each of the six independent components of the Reynolds stress tensor $R_{ij} \equiv \langle u'_i u'_j \rangle$, complemented by a transport equation for scalar viscous dissipation, ε . The turbulent transport in the mean momentum equation (2.12) is thus accounted for without further modeling.

The Reynolds flux term in the scalar equation is usually modeled as

$$-\langle u_i'q'\rangle = \frac{C_s}{\sigma_Q} \frac{K}{\varepsilon} R_{ij} \frac{\partial Q}{\partial x_j}, \qquad (2.39)$$

where C_s is a model constant, and σ_Q is the turbulent Prandtl number for the scalar (Daly & Harlow, [10]). The use of the Reynolds stresses in this model makes the turbulent diffusion anisotropic, and governed by the velocity fluctuations in different directions.

In the Reynolds stress equation (2.25), only the production term P_{ij} is exact, and all other terms require modeling. With the most common model (Launder, Reece & Rodi [20]), we have

$$\begin{split} P_{ij} &\equiv -R_{ik} \frac{\partial U_j}{\partial x_k} - R_{jk} \frac{\partial U_i}{\partial x_k}, \\ \Pi_{ij}^{(s)} &= -C_1 \frac{\varepsilon}{K} \left(R_{ij} - \frac{2}{3} K \delta_{ij} \right), \\ \Pi_{ij}^{(r)} &= -\gamma \left(P_{ij} - \frac{2}{3} P_{kk} \delta_{ij} \right), \\ \varepsilon_{ij} &= \frac{2}{3} \varepsilon \delta_{ij}, \\ J_{ijm} &= -\frac{C_s}{\sigma_{RS}} \frac{K}{\varepsilon} R_{ml} \frac{\partial R_{ij}}{\partial x_l}. \end{split}$$

Here $K \equiv R_{ii}/2$, while the scalar viscous dissipation ε is given by a model transport equation (neglecting molecular transport),

$$\frac{\partial \varepsilon}{\partial t} + U_j \frac{\partial \varepsilon}{\partial x_j} = C_{\varepsilon 1} \frac{\varepsilon}{K} P_{ii} / 2 - C_{\varepsilon 2} \frac{\varepsilon^2}{K} + \frac{\partial}{\partial x_j} \left(\frac{C_s}{\sigma_{\varepsilon}} \frac{K}{\varepsilon} R_{jk} \frac{\partial \varepsilon}{\partial x_k} \right).$$

This particular Reynolds stress model has nondimensional model constants $C_{\varepsilon 1}$, $C_{\varepsilon 2}$, C_1 , γ , C_s , σ_{RS} , and σ_{ε} .

Wall boundary conditions for the discretized equations are generally applied using wall functions. The mean velocity and the value of ε are then prescribed some small distance from the wall, within the logarithmic region of the boundary layer. The Reynolds stress equations are solved assuming the wall-normal

gradient is zero, and the source terms are evaluated in a way consistent with the logarithmic law of the wall.

2.4.2. Eddy viscosity models. In eddy viscosity models, the Reynolds stresses are modeled using the so-called Boussinesq hypothesis, relating Reynolds stress anisotropy to the mean strain tensor:

$$-\langle u_i'u_j'\rangle = -\frac{2}{3}K\delta_{ij} + \nu_T S_{ij}, \qquad (2.40)$$

where ν_T is the turbulent viscosity, $K \equiv \langle u_i' u_i' \rangle / 2$ is the turbulent kinetic energy, and

$$S_{ij} \equiv rac{1}{2} \left(rac{\partial U_i}{\partial x_j} + rac{\partial U_j}{\partial x_i}
ight)$$

is the mean strain tensor.

The widely used two-equation $K-\varepsilon$ model contains transport equations for the turbulent kinetic energy K, and the viscous dissipation rate ε . The turbulent viscosity in (2.40) is given by a constitutive relationship,

$$\nu_T = C_\mu \frac{K^2}{\varepsilon},\tag{2.41}$$

where C_{μ} is a nondimensional model constant. If (2.40) is inserted into the mean momentum equation, we get

$$\frac{\partial U_i}{\partial t} + U_j \frac{\partial U_i}{\partial x_j} = -\frac{1}{\rho} \frac{\partial P}{\partial x_i} + \frac{\partial}{\partial x_j} \left[(\nu + \nu_T) \frac{\partial U_i}{\partial x_j} \right]. \tag{2.42}$$

In analogy with (2.40) we have the eddy diffusivity hypothesis, which expresses the Reynolds flux as

$$-\langle u_i'q'\rangle = \frac{\nu_T}{\sigma_Q} \frac{\partial Q}{\partial x_i},\tag{2.43}$$

where σ_Q is a turbulent Prandtl number.

The most common formulation of the $K-\varepsilon$ model is that of Launder and Spalding [21]. The exact production term (2.34) is modeled using the Boussinesq hypothesis (2.40), so that

$$P_K = 2\nu_T S_{ij} S_{ji}. (2.44)$$

If we neglect molecular diffusion, the model transport equations for K and ε are

$$\frac{\partial K}{\partial t} + U_j \frac{\partial K}{\partial x_j} = P_K - \varepsilon + \frac{\partial}{\partial x_j} \left[\frac{\nu_T}{\sigma_K} \frac{\partial K}{\partial x_j} \right], \tag{2.45}$$

$$\frac{\partial \varepsilon}{\partial t} + U_j \frac{\partial \varepsilon}{\partial x_j} = C_{\varepsilon 1} \frac{\varepsilon}{K} P_K - C_{\varepsilon 2} \frac{\varepsilon^2}{K} + \frac{\partial}{\partial x_j} \left[\frac{\nu_T}{\sigma_{\varepsilon}} \frac{\partial \varepsilon}{\partial x_j} \right]. \tag{2.46}$$

Here $C_{\varepsilon 1}$, $C_{\varepsilon 2}$, σ_K and σ_{ε} are nondimensional model constants.

In the standard high-Reynolds number version of the $K-\varepsilon$ model, the treatment of wall boundary conditions is the same as described above for the Reynolds stress model.

2.5. The quasistatic approximation of magnetic flux density

In the following we derive scale estimates for the induced mean and fluctuating magnetic flux densities. Based on these scale estimates, we formulate the quasistatic, or inductionless, approximation of the Reynolds-decomposed electromagnetic equations.

2.5.1. The induction equation. We assume a Reynolds decomposition of the magnetic flux density into mean and fluctuating parts, as defined in (2.9) and (2.10),

$$b_i \equiv B_i + b_i'$$

where the mean magnetic flux density is understood to be the sum of a steady¹ external magnetic field \mathbf{B}_0 and the mean induced field \mathbf{B}_I due to the fluid motion,

$$B_i = B_{0i} + B_{Ii}.$$

An equation for the instantaneous magnetic field can be found by combining Ohm's law, $\mathbf{j} = \sigma(\mathbf{e} + \mathbf{u} \times \mathbf{b})$, with Ampere's law, $\nabla \times \mathbf{b} = \mu_0 \mathbf{j}$. In the latter, the current density \mathbf{j} is related only to the induced field (no externally imposed currents), and $\nabla \times \mathbf{B}_0 = 0$ in the flow domain. We then obtain

$$\nabla \times (\mathbf{B}_I + \mathbf{b}') = \mu_0 \sigma(\mathbf{e} + \mathbf{u} \times \mathbf{b}).$$

Taking the curl of this, using Faraday's law $\nabla \times \mathbf{e} = -\partial \mathbf{b}/\partial t$ and some algebra, we get the *induction equation*,

$$\frac{\partial b_i}{\partial t} + u_j \frac{\partial b_i}{\partial x_j} = b_j \frac{\partial u_i}{\partial x_j} + \frac{1}{\mu_0 \sigma} \frac{\partial^2 (B_{Ii} + b_i')}{\partial x_j \partial x_j}.$$
 (2.47)

2.5.2. Scale estimates of induced magnetic flux density. A Reynolds decomposition of (2.47) yields the mean induction equation,

$$\frac{\partial B_i}{\partial t} + U_j \frac{\partial B_i}{\partial x_j} = B_j \frac{\partial U_i}{\partial x_j} + \left\langle b_j' \frac{\partial u_i'}{\partial x_j} \right\rangle - \left\langle u_j' \frac{\partial b_i'}{\partial x_j} \right\rangle + \frac{1}{\mu_0 \sigma} \frac{\partial^2 B_{Ii}}{\partial x_j \partial x_j}, \tag{2.48}$$

from which we should be able to find a scale estimate B_I for the mean induced magnetic flux density. In order to obtain a scale estimate b for fluctuating magnetic flux density, we derive a transport equation for $\langle b'_i b'_i \rangle$ by taking the scalar product of the instantaneous flux density b_i and the induction equation (2.47). Ensemble averaging, and subtraction of an equation for $B_i B_i$ (not shown here), yields

$$\begin{split} \frac{\partial \left\langle b_{i}^{\prime}b_{i}^{\prime}\right\rangle }{\partial t} + U_{j}\frac{\partial \left\langle b_{i}^{\prime}b_{i}^{\prime}\right\rangle }{\partial x_{j}} &= -2\left\langle b_{i}^{\prime}u_{j}^{\prime}\right\rangle \frac{\partial B_{i}}{\partial x_{j}} - \frac{\partial}{\partial x_{j}}\left\langle b_{i}^{\prime}b_{i}^{\prime}u_{j}^{\prime}\right\rangle \\ &+ 2B_{j}\left\langle b_{i}^{\prime}\frac{\partial u_{i}^{\prime}}{\partial x_{j}}\right\rangle + 2\left\langle b_{i}^{\prime}b_{j}^{\prime}\right\rangle \frac{\partial U_{i}}{\partial x_{j}} + 2\left\langle b_{i}^{\prime}b_{j}^{\prime}\frac{\partial u_{i}^{\prime}}{\partial x_{j}}\right\rangle \\ &- \frac{2}{\mu_{0}\sigma}\left\langle \frac{\partial b_{i}^{\prime}}{\partial x_{j}}\frac{\partial b_{i}^{\prime}}{\partial x_{j}}\right\rangle + \frac{1}{\mu_{0}\sigma}\frac{\partial^{2}\left\langle b_{i}^{\prime}b_{i}^{\prime}\right\rangle }{\partial x_{j}\partial x_{j}}. \end{split} \tag{2.49}$$

¹In the analysis, the external field could in principle be slowly time dependent, provided its time scale is large compared with the time scales of the turbulence (the external field may otherwise excite turbulence).

If the magnitude of the external field is B_0 , we can assume that $B_0 > B_I$, and $B_I \ge b$ (these assumptions can be verified a posteriori). We further allow the mean velocity field and the turbulent velocity fluctuations to be characterized by separate velocity scales U and u, respectively (in a homogeneous shear flow without magnetic effects, there is only one relevant velocity scale so that $U \sim u$). The characteristic length scale of all mean field gradients is L.

For a correct scale estimate of the turbulent correlations, we must consider the strength of correlation between pairs of fluctuating quantities, and determine sensible length-scale estimates for the fluctuation gradients $\partial b'_i/\partial x_j$ and $\partial u'_i/\partial x_j$.

If we consider the correlation $\langle (\partial u'_i/\partial x_j)^2 \rangle$ (which governs the viscous dissipation of turbulent kinetic energy) the largest contribution comes from the smallest scales in the spectrum. It is usually estimated as

$$\left\langle \left(\frac{\partial u_i'}{\partial x_j} \right)^2 \right\rangle \sim \frac{u^2}{\lambda^2},$$

where λ is the so-called Taylor microscale, which relates to the integral scale L through

$$\lambda \sim \text{Re}^{-1/2} L,\tag{2.50}$$

where $\text{Re} = uL/\nu$ is the hydrodynamic Reynolds number (see, e.g., Tennekes & Lumley [41], Sec. 3.2). For high-Reynolds number flows, λ is thus much smaller than the integral scale L of the largest eddies. Looking at the corresponding magnetic term $\langle (\partial b_i'/\partial x_j)^2 \rangle$, however, we should note that the magnetic diffusivity is several orders of magnitude larger than the kinematic viscosity, and the magnetic Reynolds number Rm is presumably smaller than unity. This means that all but the largest-scale magnetic fluctuations will be effectively smeared out by the magnetic diffusivity; there is in fact no significant separation of scales between the energy-containing and the dissipating magnetic fluctuations. The appropriate scale estimate for the correlation $\langle (\partial b_i'/\partial x_j)^2 \rangle$ is therefor b^2/L^2 . We conclude that $\partial u_i'/\partial x_j \sim u/\lambda$, while $\partial b_i'/\partial x_j \sim b/L$.

In estimating the correlation between two fluctuating quantities, Tennekes & Lumley [41] noted that two quantities cannot interact strongly unless they are "tuned to the same frequency band". They found that the correlation coefficient scales with the ratio (≤ 1) of the time-scales involved. A correlation between u_i' and $\partial u_i'/\partial x_j$ is thus proportional to both the ratio of their time scales (L/u and λ/u , respectively) and their individual scale estimates, so that

$$\left\langle u_i' \frac{\partial u_i'}{\partial x_j} \right\rangle \sim \frac{\lambda}{u} \frac{u}{L} \frac{u^2}{\lambda} = u^3 / L$$

Note that from (2.50) this is smaller by a factor of $\mathrm{R}e^{1/2}$ than the estimate u^3/λ we would get if the two quantities were perfectly correlated. The time and length scales of the magnetic fluctuations presumably follow those of the large turbulent eddies responsible for their creation, with length scale L and time scale L/u (which applies to both b_i' and $\partial b_i'/\partial x_j$).

Assuming that the transient term in (2.49) can be neglected (steady-state conditions), the remaining terms of the $\langle b'_i b'_i \rangle$ equation can now be estimated as

$$U_j \frac{\partial \langle b_i' b_i' \rangle}{\partial x_j} \sim \frac{b^2 U}{L} \tag{2.51}$$

$$2\left\langle b_i'u_j'\right\rangle \frac{\partial B_i}{\partial x_j} \sim \frac{bB_0u}{L} \tag{2.52}$$

$$\frac{\partial}{\partial x_j} \langle b_i' b_i' u_j' \rangle \sim \frac{b^2 u}{L} \tag{2.53}$$

$$2B_j \left\langle b_i' \frac{\partial u_i'}{\partial x_j} \right\rangle \sim B_0 \frac{\lambda}{L} \frac{bu}{\lambda} = \frac{bB_0 u}{L}$$
 (2.54)

$$2\left\langle b_i'b_j'\right\rangle \frac{\partial U_i}{\partial x_j} \sim \frac{b^2 U}{L} \tag{2.55}$$

$$2\left\langle b_i'b_j'\frac{\partial u_i'}{\partial x_j}\right\rangle \sim \frac{\lambda}{L}\frac{b^2u}{\lambda} = \frac{b^2u}{L}$$
 (2.56)

$$\frac{2}{\mu_0 \sigma} \left\langle \frac{\partial b_i'}{\partial x_j} \frac{\partial b_i'}{\partial x_j} \right\rangle \sim \frac{1}{\mu_0 \sigma} \frac{b^2}{L^2} = \frac{1}{\text{Rm}} \frac{b^2 U}{L}$$
 (2.57)

$$\frac{1}{\mu_0 \sigma} \frac{\partial^2 \langle b_i' b_i' \rangle}{\partial x_i \partial x_j} \sim \frac{1}{\mu_0 \sigma} \frac{b^2}{L^2} = \frac{1}{\text{Rm}} \frac{b^2 U}{L}.$$
 (2.58)

For small Rm, Eq. 2.14, and $u \leq U$, the terms (2.51), (2.53), (2.55), and (2.56) will be smaller than (2.57) and (2.58). At least one of the terms (2.52) and (2.54), containing B_0 , should presumably be of the same order as (2.57) and (2.58), so that

$$\frac{1}{\mathrm{Rm}} \frac{b^2 U}{L} \sim \frac{b B_0 u}{L}.$$

The scale estimate for the magnetic fluctuations is thus

$$b \sim \frac{u}{U} \text{Rm} B_0. \tag{2.59}$$

For the terms of the mean induction equation equation (2.48), we have (using (2.59) and neglecting the transient term)

$$U_j \frac{\partial B_i}{\partial x_j} \sim \frac{UB_0}{L},\tag{2.60}$$

$$B_j \frac{\partial U_i}{\partial x_j} \sim \frac{UB_0}{L},\tag{2.61}$$

$$\left\langle b_j' \frac{\partial u_i'}{\partial x_j} \right\rangle \sim \frac{ub}{L} \sim \operatorname{Rm} \frac{u}{U} \frac{uB_0}{L},$$
 (2.62)

$$\left\langle u_j' \frac{\partial b_i'}{\partial x_j} \right\rangle \sim \frac{ub}{L} \sim \operatorname{Rm} \frac{u}{U} \frac{uB_0}{L},$$
 (2.63)

$$\frac{1}{\mu_0 \sigma} \frac{\partial^2 B_{Ii}}{\partial x_i \partial x_j} \sim \frac{1}{\mu_0 \sigma} \frac{B_I}{L^2} = \frac{1}{\text{Rm}} \frac{U B_I}{L}.$$
 (2.64)

If Rm $\ll 1$ and $u \leq U$, the terms (2.62) and (2.63) are smaller than (2.60) and (2.61). At least one of the latter two should balance (2.64), so that

$$rac{UB_0}{L} \sim rac{1}{\mathrm{Rm}} rac{UB_I}{L}.$$

This gives the scale estimate

$$B_I \sim \text{Rm}B_0. \tag{2.65}$$

The scale relations (2.59) and (2.65) form the basis for the quasistatic or inductionless approximation, in which the induced mean and fluctuating magnetic fields can be neglected beside the larger external field \mathbf{B}_0 , provided Rm is low.

Comparing the scale estimates for b and B_I , we finally note that $b/B_I \sim u/U$; the mean velocity field is responsible for the induced mean magnetic flux density, and the turbulent velocity fluctuations induce magnetic fluctuations.

2.5.3. Quasistatic approximation of the electromagnetic equations. The scale estimates for \mathbf{B}_I and \mathbf{b}' can now be used to motivate the approximations in Sec. 2.2.1 and 2.2.2.

The mean electric potential equations is

$$\nabla^2 \Phi = \nabla \cdot (\mathbf{U} \times \mathbf{B} + \langle \mathbf{u}' \times \mathbf{b}' \rangle) \approx \nabla \cdot (\mathbf{U} \times \mathbf{B}_0). \tag{2.66}$$

The approximation is due to the scale estimates

$$\mathbf{U} \times \mathbf{B} \sim U B_0,$$

 $\langle \mathbf{u}' \times \mathbf{b}' \rangle \sim u B_0 \mathrm{Rm} u / U,$

which show that $\mathbf{U} \times \mathbf{B} \gg \langle \mathbf{u}' \times \mathbf{b}' \rangle$, if $u \leq U$ and $\mathrm{Rm} \ll 1$. The equation for the fluctuating potential is

$$\nabla^2 \phi' = \nabla \cdot (\mathbf{U} \times \mathbf{b}' + \mathbf{u}' \times \mathbf{B} + \mathbf{u}' \times \mathbf{b}' - \langle \mathbf{u}' \times \mathbf{b}' \rangle). \tag{2.67}$$

The last two terms are of order ub, and vanish beside the second term, $\mathbf{u}' \times \mathbf{B} \sim uB_0$. The first term is estimated using the scale relation (2.59) for b, so that

$$\mathbf{U} \times \mathbf{b}' \sim U \mathrm{Rm} B_0 u / U = \mathrm{Rm} u B_0$$
.

Note that this estimate is not altered by the gradient operator in (2.67), because the length scale of the largest eddies is governed by the length scale of the mean velocity gradients. The second term in (2.67) is larger than the others by a factor of Rm^{-1} so that

$$\nabla^2 \phi' \approx \nabla \cdot (\mathbf{u}' \times \mathbf{B}_0). \tag{2.68}$$

The decomposition of the electric field yields

$$\mathbf{E} = -\nabla \Phi, \quad \mathbf{e}' = -\nabla \phi'.$$

Assuming there are no external electric fields, Eqs. (2.67) and (2.68) suggest that $|\mathbf{E}| \sim UB_0$, and $|\mathbf{e}'| \sim uB_0$.

If we again use the approximations of the cross-product terms from (2.66) and (2.67), we get the current equations

$$\mathbf{J} = \sigma(\mathbf{E} + \mathbf{U} \times \mathbf{B} + \langle \mathbf{u}' \times \mathbf{b}' \rangle) \approx \sigma(\mathbf{E} + \mathbf{U} \times \mathbf{B}_0), \tag{2.69}$$

$$\mathbf{j}' = \sigma(\mathbf{e}' + \mathbf{U} \times \mathbf{b}' + \mathbf{u}' \times \mathbf{B} + \mathbf{u}' \times \mathbf{b}' - \langle \mathbf{u}' \times \mathbf{b}' \rangle)$$

$$\approx \sigma(\mathbf{e}' + \mathbf{u}' \times \mathbf{B}_0).$$
(2.70)

The mean Lorentz force becomes

$$\mathbf{F} = \frac{1}{\rho} (\mathbf{J} \times \mathbf{B} + \langle \mathbf{j}' \times \mathbf{b}' \rangle) \approx \frac{1}{\rho} (\mathbf{J} \times \mathbf{B}_0), \tag{2.71}$$

based on the scale relations $\mathbf{J} \sim \sigma U B_0$ and $\mathbf{j}' \sim \sigma u B_0$, deduced from Eqs. (2.69) and (2.70) (under the assumption that $|\mathbf{E}| \sim U B_0$, and $|\mathbf{e}'| \sim u B_0$). Subtracting (2.71) from the instantaneous equation gives

$$\mathbf{f}' = \frac{1}{\rho} (\mathbf{J} \times \mathbf{b}' + \mathbf{j}' \times \mathbf{B} + \mathbf{j}' \times \mathbf{b}' - \langle \mathbf{j}' \times \mathbf{b}' \rangle). \tag{2.72}$$

Applying the scale relations for J and j' shows that the terms in (2.72) have the same relative magnitudes as the terms of the potential equation (2.67). With the same arguments we get

$$\mathbf{f}'pproxrac{1}{
ho}\mathbf{j}' imes\mathbf{B}_0.$$

CHAPTER 3

MHD turbulence modeling

For turbulence subjected to a steady external magnetic field, **B**, the model equations for K, R_{ij} , and ε discussed in Sec. 2.4 must be complemented with sink terms to account for magnetic (Joule) dissipation. If we let μ and μ_{ε} be the Joule sink terms in the K and ε equations, respectively, dimensional analysis yields

$$\mu = d_1 \frac{\sigma B^2}{\rho} K,$$
$$\mu_{\varepsilon} = d_2 \frac{\sigma B^2}{\rho} \varepsilon,$$

where $\sigma B^2/\rho$ is the inverse of a magnetic time scale, and the coefficients d_1 and d_2 are dimensionless (see, e.g., Branover [5], Sec. 2-3).

Unfortunately, the coefficients d_1 and d_2 are not constants, but depend on the structure and length scale distribution of the turbulence. One effect of the magnetic field is that turbulent structures tend to grow in the direction of the magnetic field and, as a consequence, d_1 (and d_2) will decrease. Sommeria and Moreau [37] found that

$$d_1 \sim \left(rac{l_\perp}{l_\parallel}
ight)^2,$$

where l_{\perp} and l_{\parallel} are turbulent length scales perpendicular to, and parallel with the magnetic field, respectively.

In a few recent model proposals, the variation of d_1 and d_2 is estimated in terms of variables of a conventional turbulence closure. With the rationale that the length scale anisotropy in a steady flow should depend on the strength of the magnetic field, relative to inertial effects, Ji and Gardner [16] proposed a modification of a low-Re K- ε model where they let d_1 and d_2 be proportional to an exponential damping function,

$$\exp(-cN_m),$$

where N_m is the mean-flow (or bulk) interaction parameter,

$$N_m = \frac{\sigma B^2 L}{\rho U}.$$

For less obvious reasons, they included the same damping function in the constitutive relationship (2.41) for the turbulent viscosity, ν_T . More recently, Kenjereš and Hanjalić [18] suggested some significant improvements of this model; they dropped the damping function in the equation for ν_T , and replaced N_m with a

turbulent interaction parameter $N = \sigma B^2 K/(\rho \varepsilon)$, based on the local turbulence variables

The central idea developed in this thesis is to include in the closure an additional transported scalar variable for the length scale anisotropy information we need for modeling of the Joule dissipation. The definition of the new variable α is such that the Joule dissipation of homogeneous turbulence can be expressed exactly as

$$\mu = \frac{2\sigma B^2}{\rho} \alpha K.$$

3.1. Spectral analysis of homogeneous MHD turbulence

Spectral analysis offers several important advantages for the study of homogeneous turbulence. In the spectral domain, we deal with two-point velocity correlations; one-point quantities like the Reynolds stresses are formed through spherical integration over spectral space. The non-locality of the pressure fluctuations is tractable, as we can solve the Poisson equations for the pressure fluctuations explicitly, and eliminate pressure from the Navier–Stokes equations. Finally, the Poisson equation for the electrostatic potential is easy to deal with, and the Lorentz force as well as the magnetic Joule dissipation of turbulence can be written in closed form. (See also Batchelor [4], Lehnert [24], and Hallbäck [14]).

3.1.1. Fourier transform of fluctuations. We consider the case of homogeneous turbulence, allowing for homogeneous mean velocity gradients,

$$U_{i,m}(t) = \frac{\partial U_i}{\partial x_m}.$$

The fluctuating quantities may each be expanded in an infinite Fourier series if we consider a flow domain which is periodic in all spatial directions. The dimensions of the flow domain may depend on time in a way that conserves the volume of the domain. We define the Fourier expansions for the fluctuating velocity and pressure fields as

$$u'_{i}(\mathbf{x},t) = \sum \hat{u}_{i}e^{i\mathbf{k}\cdot\mathbf{x}},$$
$$p'(\mathbf{x},t) = \sum \hat{p}e^{i\mathbf{k}\cdot\mathbf{x}}.$$

Fourier transformation of the fluctuation equations (2.19) and (2.20) yields

$$\frac{d\hat{u}_i}{dt} = -U_{i,j}\hat{u}_j - i\frac{k_i}{\rho}\hat{p} - ik_j(\widehat{u'_i u'_j}) - \nu k^2 \hat{u}_i + \hat{f}_i,$$
(3.1)

$$ik_i\hat{u}_i = 0, (3.2)$$

complemented by an equation for the rate of change of the wave number, due to the mean strain,

$$\frac{dk_i}{dt} + U_{j,i}k_j = 0.$$

Fourier transformation of the electromagnetic fluctuation equations (2.21) through (2.24) yields

$$\hat{\mathbf{f}} = \frac{1}{\rho} \hat{\mathbf{j}} \times \mathbf{B}_0, \tag{3.3}$$

$$\hat{\mathbf{j}} = \sigma(\hat{\mathbf{e}} + \hat{\mathbf{u}} \times \mathbf{B_0}), \tag{3.4}$$

$$\hat{\mathbf{e}} = -i\mathbf{k}\hat{\phi},\tag{3.5}$$

$$-k^2\hat{\phi} = i\mathbf{k} \cdot (\hat{\mathbf{u}} \times \mathbf{B}_0). \tag{3.6}$$

We can find an explicit expression for the transformed fluctuating Lorentz force (see, e.g., Schumann [34]). From (3.5) and (3.6) we have

$$\hat{\mathbf{e}} = -\frac{\mathbf{k} \cdot (\hat{\mathbf{u}} \times \mathbf{B}_0)}{k^2} \mathbf{k} = -\frac{1}{k^2} \mathbf{k} \times (\mathbf{k} \times [\hat{\mathbf{u}} \times \mathbf{B}_0]) - \hat{\mathbf{u}} \times \mathbf{B}_0,$$

where we made use of the vector identity $\mathbf{a} \times (\mathbf{b} \times \mathbf{c}) = (\mathbf{a} \cdot \mathbf{c})\mathbf{b} - (\mathbf{a} \cdot \mathbf{b})\mathbf{c}$. Using (3.3) and (3.4), we get

$$\mathbf{\hat{f}} = -\frac{\sigma}{\rho k^2} \left[\mathbf{k} \times (\mathbf{k} \times (\mathbf{\hat{u}} \times \mathbf{B}_0)) \right] \times \mathbf{B}_0.$$

In the following we use **B** without subscript for the external magnetic field.

The pressure field \hat{p} can be eliminated from the transformed fluctuation equations (3.1) by twice taking the cross-product with \mathbf{k} . Using the continuity condition (3.2) and some algebra, we finally get a complete set of equations as

$$\frac{d\hat{u}_i}{dt} = -U_{i,j}\hat{u}_j + 2\frac{k_i k_m}{k^2} U_{m,j}\hat{u}_j - ik_j(\widehat{u'_i u'_j}) + i\frac{k_i k_m k_j}{k^2}(\widehat{u'_m u'_j}) - \nu k^2 \hat{u}_i - \frac{\sigma}{\rho} \frac{(\mathbf{B} \cdot \mathbf{k})^2}{k^2} \hat{u}_i,$$
(3.7)

$$\frac{dk_i}{dt} = -U_{j,i}k_j. (3.8)$$

3.1.2. The spectral energy and Reynolds stress tensors. The spectral energy tensor is defined as the ensemble averaged second moments of $\hat{\mathbf{u}}$,

$$\hat{\Phi}_{ij}(\mathbf{k},t) = \langle \hat{u}_i(-\mathbf{k},t)\hat{u}_j(\mathbf{k},t)\rangle = \langle \hat{u}_i^*\hat{u}_j\rangle,$$

which correspond to the two-point velocity correlations in physical space. Here \hat{u}_i^* is the complex conjugate of \hat{u}_i . The time derivative of $\hat{\Phi}_{ij}$ is

$$\frac{d}{dt}\langle \hat{u}_i^* \hat{u}_j \rangle = \left\langle \hat{u}_i^* \frac{d\hat{u}_j}{dt} \right\rangle + \left\langle \frac{d\hat{u}_i^*}{dt} \hat{u}_j \right\rangle.$$

The dynamical equations for $\tilde{\Phi}_{ij}$ can now be derived by inserting (3.7). We further rewrite the convolution integrals in the second line of Eq. (3.7) as

$$\widehat{u'_m u'_n}(\mathbf{k}) = \int \hat{u}_m(\mathbf{k} - \mathbf{k}') \hat{u}_n(\mathbf{k}') d^3 \mathbf{k}',$$

and introduce the triple correlation and its complex conjugate

$$\hat{T}_{ijk}(\mathbf{k}, \mathbf{k}') \equiv \langle \hat{u}_i(\mathbf{k} - \mathbf{k}') \hat{u}_j(\mathbf{k}') \hat{u}_k(-\mathbf{k}) \rangle ,$$

$$\hat{T}_{ijk}^*(\mathbf{k}, \mathbf{k}') \equiv \langle \hat{u}_i(\mathbf{k}' - \mathbf{k}) \hat{u}_j(-\mathbf{k}') \hat{u}_k(\mathbf{k}) \rangle .$$

This yields

$$\frac{d}{dt}\hat{\Phi}_{ij}(\mathbf{k},t) = -U_{i,m}\hat{\Phi}_{mj} - U_{j,m}\hat{\Phi}_{im}
+2\frac{k_i k_m}{k^2} U_{m,n}\hat{\Phi}_{nj} + 2\frac{k_j k_m}{k^2} U_{m,n}\hat{\Phi}_{in}
+ik_m \left\{ \Delta_{in} \int \hat{T}^*_{mnj}(\mathbf{k}, \mathbf{k}') d^3 \mathbf{k}' - \Delta_{jn} \int \hat{T}_{mni}(\mathbf{k}, \mathbf{k}') d^3 \mathbf{k}' \right\}
-2\nu k^2 \hat{\Phi}_{ij} - 2\frac{\sigma}{\rho} \frac{(\mathbf{B} \cdot \mathbf{k})^2}{k^2} \hat{\Phi}_{ij},$$
(3.9)

where $\Delta_{ij} \equiv \delta_{ij} - \frac{k_i k_j}{k^2}$.

The components of the Reynolds stress tensor represent the ensemble averaged velocity correlations in the one-point limit, $R_{ij} = \langle u'_i u'_j \rangle$. For homogeneous turbulence they can be expressed in terms of the spectral energy tensor,

$$R_{ij}(t) = \int \hat{\Phi}_{ij}(\mathbf{k}, t) d^3\mathbf{k}.$$

Integration of the dynamical equations of the spectral energy tensor produces the spectral representation of the Reynolds stress transport (RST) equations we introduced in Sec. 2.3,

$$\frac{dR_{ij}(t)}{dt} = P_{ij} + \Pi_{ij}^{(r)} + \Pi_{ij}^{(s)} - \varepsilon_{ij} - \mu_{ij}, \tag{3.10}$$

with

$$\begin{split} P_{ij} &= -U_{i,k}R_{kj} - U_{j,k}R_{ki}, \\ \Pi_{ij}^{(r)} &= 2U_{m,n} \int \left(\frac{k_i k_m}{k^2} \hat{\Phi}_{nj} + \frac{k_j k_m}{k^2} \hat{\Phi}_{ni}\right) d^3\mathbf{k}, \\ \Pi_{ij}^{(s)} &= \int i k_m \left\{ \Delta_{in} \int \hat{T}_{mnj}^*(\mathbf{k}, \mathbf{k}') d^3\mathbf{k}' \right. \\ &\left. - \Delta_{jn} \int \hat{T}_{mni}(\mathbf{k}, \mathbf{k}') d^3\mathbf{k}' \right\} d^3\mathbf{k}, \\ \varepsilon_{ij} &= 2\nu \int k^2 \hat{\Phi}_{ij} d^3\mathbf{k}, \\ \mu_{ij} &= 2\frac{\sigma}{\rho} \int \frac{(\mathbf{B} \cdot \mathbf{k})^2}{k^2} \hat{\Phi}_{ij} d^3\mathbf{k}, \end{split}$$

where P_{ij} is the turbulence production, $\Pi_{ij}^{(r)}$ and $\Pi_{ij}^{(s)}$ are rapid and slow pressure—strain terms, respectively, and ε_{ij} is the dissipation rate tensor. As mentioned in Sec. 2.3, the Joule dissipation μ_{ij} includes the explicit body force terms, as well as their contribution to the redistributive pressure—strain interaction; see Eq. (2.32).

Of the terms in Eq. (3.10), only the production term is explicit in the mean velocity gradients and the Reynolds stresses themselves. All other terms must be modeled in some way, as discussed in Sec. 2.4.1

3.1.3. The "angular" energy distribution. If we assume magnetic dissipation dominates in Eq. (3.9), all other terms may be neglected. The resulting linear equation is similar to that of Lehnert [24], but we here neglect also the viscous term ($\text{Re} \gg 1$).

Let the magnetic field **B** be in the k_3 -direction, and introduce spherical coordinates,

$$\mathbf{k} = k \{ \sin \theta \sin \varphi, \sin \theta \cos \varphi, \cos \theta \},$$

where φ is an azimuthal angle about **B**, and θ is the angle between **k** and **B**. Contraction of (3.9) then yields an evolution equation for spectral energy $\hat{E} \equiv \hat{\Phi}_{ii}/2$,

$$\frac{d\hat{E}(\mathbf{k},t)}{dt} = -\hat{\mu},\tag{3.11}$$

$$\hat{\mu} = \hat{E} \frac{\sigma B^2}{\rho} \cos^2 \theta. \tag{3.12}$$

Here $\hat{\mu}$ represents a spectral Joule dissipation. If we let $E_0(k)$ be an isotropic initial energy spectrum, the solution to (3.11) can be written as a function of the angle θ ,

$$\hat{E}(\theta, t) = E_0(k) \exp\left(-\frac{\sigma B^2}{\rho} t \cos^2 \theta\right). \tag{3.13}$$

Figure 3.1 shows a polar plot of \hat{E} and $\hat{\mu}$ as functions of θ , as given by (3.13) and (3.12) for a few points in time. Joule dissipation acts selectively on energy located about the axis parallel with the magnetic field, and the remaining energy tends to be concentrated near the perpendicular plane. Note also that the relative magnitude of the Joule dissipation decreases rapidly, as the energy near the k_{\parallel} -axis is depleted. (Schumann [34] used a similar illustration for the individual components of $\hat{\Phi}_{ij}$).

In the more general case, where also viscous and nonlinear inertial effects are important, the situation can be illustrated as in Fig. 3.2 (similar to that of Moreau [28]). Joule dissipation is largest in a cone about an axis parallel with the magnetic field (shaded region). Outside the dotted circle, the turbulent structures a small enough for viscous dissipation to be significant. Nonlinear inertial mechanisms cause what we can call angular energy transfer, transferring energy from the energy-containing region near the k_{\perp} -plane, to the region where Joule dissipation is strong. The nonlinear mechanisms thus enhance Joule dissipation.

3.2. Modeling of the Joule dissipation

For modeling purposes, the rapid pressure–strain term $\Pi_{ij}^{(r)}$ is often written as

$$\Pi_{ij}^{(r)} = 2U_{k,n}(M_{inkj} + M_{jnki}),$$

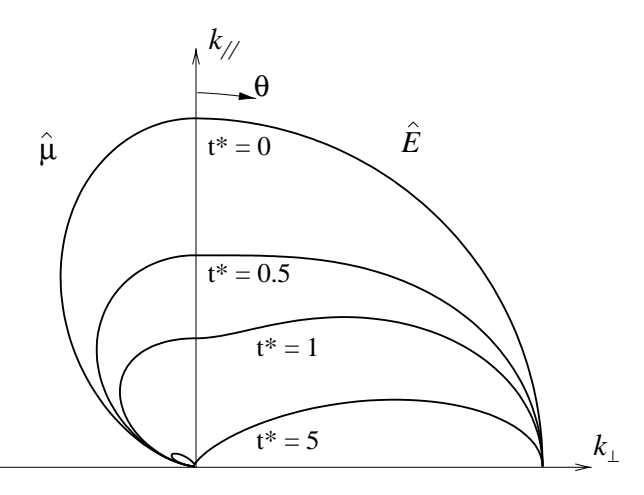


FIGURE 3.1 Polar plot of \hat{E} and $\hat{\mu}$ as functions of θ , for a couple of moments in time. The data is computed using Eqs. (3.13) and (3.12) (assuming $E_0 = 1$). Time t^* is here relative to the magnetic time scale, i.e. $t^* = t\sigma B^2/\rho$.

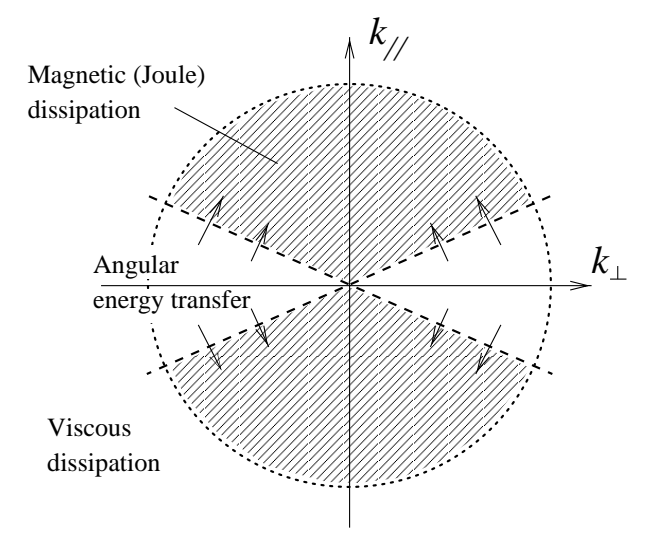


FIGURE 3.2 Illustration of the general case, where also nonlinear and viscous effects are important. Joule dissipation is largest in a cone about an axis parallel with the magnetic field (shaded region). Viscous dissipation is significant outside the dotted circle, where wavenumbers are large (small scales). Nonlinear inertial mechanisms cause angular energy transfer, which transfers energy from the energy-containing region near the k_{\perp} -plane, to the region where Joule dissipation is strong. (Moreau [28].)

where we have introduced the fourth-rank tensor

$$M_{ijpq} \equiv \int \frac{k_p k_q}{k^2} \hat{\Phi}_{ij}(\mathbf{k}, t) d^3 \mathbf{k}. \tag{3.14}$$

The Joule dissipation tensor may be exactly expressed in terms of the M-tensor [42],

$$\mu_{ij}(t) = 2\frac{\sigma B^2}{\rho} N_{pq} M_{ijpq}, \qquad (3.15)$$

where

$$N_{ij} = \frac{1}{R^2} B_i B_j = n_i n_j,$$

and n_i is the direction unit vector of the magnetic field.

In classical turbulence modeling, the M-tensor is generally modeled in terms of the Reynolds stress tensor alone, or rather in its nondimensional version, the anisotropy tensor

$$a_{ij} \equiv \frac{R_{ij}}{K} - \frac{2}{3}\delta_{ij}.$$

Although models of this kind seem to do well in many irrotational mean flows, they fail to predict, for example, the complex behavior of turbulence subjected to rapid rotation. One of the problems with a model in terms of **R** only is that it includes only information about the distribution of turbulent kinetic energy into Reynolds stress components, while the original **M**-tensor contains information also about the distribution of length scales in different directions. Reynolds [31] and Reynolds & Kassinos [32] therefore discussed the possibility to include other tensors in models for rapid rotation (see also Cambon [7]). For this purpose they introduced the *structure dimensionality tensor* **Y**, defined by

$$Y_{ij} \equiv \int \frac{k_i k_j}{k^2} \hat{\Phi}_{nn}(\mathbf{k}) d^3 \mathbf{k} = M_{nnij}. \tag{3.16}$$

From the definition follows that $Y_{ii} = 2K$.

The dimensionality tensor **Y** carries length scale information which seems to be vital for successful modeling of MHD turbulence. If we contract (3.15), the scalar Joule dissipation $\mu = \mu_{ii}/2$ can be expressed as

$$\mu(t) = \frac{\sigma B^2}{\rho} N_{ij} M_{nnji}$$

$$= \frac{\sigma B^2}{\rho} N_{ij} Y_{ji}$$

$$= \frac{\sigma B^2}{\rho} K \left(N_{ij} y_{ji} + \frac{2}{3} \right).$$
(3.17)

In the last equality we have introduced the normalized dimensionality anisotropy tensor, defined by

$$y_{ij} \equiv \frac{Y_{ij}}{K} - \frac{2}{3}\delta_{ij}.$$

In analogy with the Reynolds stress anisotropy tensor, this tensor is traceless and the values of its diagonal components are limited to the finite interval [-2/3, 4/3]

(see, e.g., Reynolds [31]). A value of y_{11} close to -2/3, for example, indicates that the energy-containing eddies are relatively long in the x_1 direction, while a value of 4/3 would indicate that they are relatively short in the x_1 direction.

Inspired by Eq. (3.17), it was proposed in **Paper 1** (Widlund *et al.* [42]), that a model for MHD turbulence should include a model transport equation for a normalized dimensionality anisotropy variable α , defined as

$$\alpha \equiv \frac{N_{ij}Y_{ji}}{2K}. (3.18)$$

The variable α is thus the normalized component of **Y** which is in the direction of the magnetic field. It follows from the discussion above that $0 \le \alpha \le 1$, and that $\alpha = 1/3$ for isotropic turbulence. In the limit of two dimensional (2D) turbulence, $\alpha = 0$.

With this new transported scalar, the Joule dissipation in homogeneous turbulence can expressed exactly as

$$\mu = \frac{2\sigma B^2}{\rho} K\alpha. \tag{3.19}$$

Widlund *et al.* proposed a coordinate invariant tensor function for modeling of the Joule dissipation tensor μ_{ij} in the Reynolds stress equations:

$$\mu_{ij}(t) = 2\frac{\sigma B^2}{\rho} K F_{ij}(a_{kl}, n_m, \alpha), \qquad (3.20)$$

where F_{ij} is a second-rank symmetric tensor function of the form

$$F_{ij} = \frac{G(\alpha, I_{na})}{K} R_{ij} + \frac{H(\alpha)}{2K} (n_i n_k R_{kj} + n_j n_k R_{ki})$$

$$= G(\alpha, I_{na}) \left[a_{ij} + \frac{2}{3} \delta_{ij} \right]$$

$$+ H(\alpha) \left[\frac{1}{2} (n_i n_k a_{kj} + n_j n_k a_{ki}) + \frac{2}{3} n_i n_j \right].$$
(3.21)

G and H are here functions of α and I_{na} , as indicated, and $I_{na} \equiv n_i n_k a_{ki}$ is the only relevant invariant of the terms in F_{ij} . A model equation for viscous dissipation ε should also include a magnetic destructions term. Based on the Joule dissipation term (3.19), and simple dimensional arguments, the magnetic destruction of ε can be modeled as

$$\mu_{\varepsilon} = C_{\varepsilon\alpha} \frac{2\sigma B^2}{\rho} \varepsilon\alpha. \tag{3.22}$$

In **Paper 1**, Widlund *et al.* proposed a simple phenomenological transport equation for the new closure variable α ,

$$\frac{d\alpha}{dt} = \pi_{\alpha} - \mu_{\alpha},\tag{3.23}$$

with

$$\pi_{\alpha} = C_{\alpha 2} \frac{\varepsilon}{K} \left(\frac{1}{3} - \alpha \right), \tag{3.24}$$

$$\mu_{\alpha} = C_{\alpha 1} \frac{2\sigma B^2}{\rho} \alpha^2. \tag{3.25}$$

Here μ_{α} represents magnetic destruction, driving the turbulence towards the two dimensional (2D) state ($\alpha = 0$). The term π_{α} is a linear return-to-isotropy term of Rotta type [33]. It represents nonlinear angular energy transfer (see Sec. 3.1.3), and promotes a return to the isotropic state ($\alpha = 1/3$).

3.3. An exact equation for α

The main features of the phenomenological transport equation proposed for α in **Paper 1** are confirmed in **Paper 2** and **Paper 4**, based on an equation derived for the complete tensor **Y**. We have

$$\frac{dY_{ij}}{dt} = P_{ij}^{Y} + \Pi_{ij}^{Y} + \pi_{ij}^{Y} - \varepsilon_{ij}^{Y} - \mu_{ij}^{Y}, \tag{3.26}$$

where

$$\begin{split} P_{ij}^Y &= -2U_{p,m} \int \frac{k_i k_j}{k^2} \hat{\Phi}_{mp} d^3 \mathbf{k} \\ \Pi_{ij}^Y &= -U_{n,j} Y_{ni} - U_{n,i} Y_{nj} + 2U_{m,n} \int \frac{k_i k_j k_m k_n}{k^4} \hat{\Phi}_{pp} d^3 \mathbf{k} \\ \pi_{ij}^Y &= \int i k_m \frac{k_i k_j}{k^2} \int \left(\hat{T}_{mpp}^*(\mathbf{k}, \mathbf{k}') - \hat{T}_{mpp}(\mathbf{k}, \mathbf{k}') \right) d^3 \mathbf{k}' \ d^3 \mathbf{k} \\ \varepsilon_{ij}^Y &= 2\nu \int k_i k_j \hat{\Phi}_{nn} d^3 \mathbf{k} \\ \mu_{ij}^Y &= 2 \frac{\sigma}{\rho} \int \frac{(\mathbf{B} \cdot \mathbf{k})^2}{k^2} \frac{k_i k_j}{k^2} \hat{\Phi}_{nn} d^3 \mathbf{k}. \end{split}$$

Like the Reynolds stress tensor \mathbf{R} , the dimensionality tensor has trace 2K, so that contraction of equation (3.26) yields an equation for turbulent kinetic energy. The different terms on the right-hand side of (3.26) have been grouped and labeled according to their physical origin, and the way they contribute to the turbulent kinetic energy. P_{ij}^Y represents turbulence production, as the contracted term equals the contraction P_{ii} of production in the Reynolds stress equations. The traceless term Π_{ij}^Y represents what we can call mean deformation energy transfer, and corresponds to the rapid pressure–strain term in the Reynolds stress equations. The non-linear term π_{ij}^Y is also traceless, corresponding to slow pressure–strain in the Reynolds stress equations. ε_{ij}^Y and μ_{ij}^Y represent viscous and Joule dissipation, respectively.

Let $N_{ij} \equiv n_i n_j$. We take the time derivative of the definition (3.18), and insert (3.26) to obtain an evolution equation for α :

$$\frac{d\alpha}{dt} = P_{\alpha} + \Pi_{\alpha} + \pi_{\alpha} - \varepsilon_{\alpha} - \mu_{\alpha}, \tag{3.27}$$

where

$$\begin{split} P_{\alpha} &= \frac{1}{2K} \left(N_{ik} P_{ki}^{Y} - 2\alpha P_{K} \right), \\ \Pi_{\alpha} &= \frac{1}{2K} N_{ik} \Pi_{ki}^{Y}, \\ \pi_{\alpha} &= \frac{1}{2K} N_{ik} \pi_{ki}^{Y}, \\ \varepsilon_{\alpha} &= \frac{1}{2K} \left(N_{ik} \varepsilon_{ki}^{Y} - 2\alpha \varepsilon \right), \\ \mu_{\alpha} &= \frac{1}{2K} \left(N_{ik} \mu_{ki}^{Y} - 2\alpha \mu \right). \end{split}$$

The properties of the last two terms were examined in **Paper 2**, using rapid distortion theory and the linearized version of Eq. (3.9) (neglecting mean strain and the nonlinear term). ε_{α} is expected to be small, and can be conveniently absorbed in the return-to-isotropy model (3.24) proposed in **Paper 1** for the nonlinear term π_{α} . With the simple model term (3.25) proposed for μ_{α} , the model was found to give the desired asymptotic behavior, for long times, if the coefficient $C_{\alpha 1}$ was adjusted to give good agreement with rapid distortion results for small values of α (see **Paper 2** and **Paper 7** for details).

The mean strain terms P_{α} and Π_{α} were analyzed in **Paper 4**. Unfortunately Π_{α} depends on all components of **Y**, not only on $N_{ik}Y_{ki}$. A model of Π_{α} in terms of α was found to be appropriate only if **Y** is reasonably symmetric about an axis parallel with the magnetic field. This should fortunately be the case wherever magnetic effects are important.

The nonlinear inertial mechanisms behind the term π_{α} are currently not well understood; some progress is made in **Paper 7**, and ideas for future work are discussed briefly in Sec. 5.1.

3.4. Inhomogeneous effects

Spectral analysis is a powerful tool for analyzing homogeneous turbulence. On the other hand, the assumption of homogeneity is fundamental for the analysis, and it is difficult to see how the results could be generalized to account for effects of walls and mean-flow inhomogeneities.

Apart from boundary conditions, inhomogeneity effects appear through the Poisson equations for fluctuating pressure and fluctuating electric potential. The elimination of these quantities in the spectral analysis accounts only for the spatially homogeneous solution to the Poisson equations. The fluctuating pressure appears mainly in the pressure–strain rate terms, where it acts to redistribute energy between the Reynolds stress components; it has no net effect on the turbulent kinetic energy. The fluctuating electric potential, however, appears in the scalar Joule dissipation of turbulent kinetic energy. Below we derive an expression for the scalar Joule dissipation of homogeneous turbulence in physical space. This allows us to see where assumptions of homogeneity enter the analysis. The analysis largely follows that of Chou, for the pressure–strain terms [9].

We here use plain lower-case letters (without primes) to denote fluctuating quantities. If the external magnetic field ${\bf B}$ is homogeneous, the Poisson equation

for fluctuating electric potential is

$$-\nabla^2 \phi = -B_k \epsilon_{ijk} \frac{\partial u_j}{\partial x_i}.$$
 (3.28)

Successive differentiations are commutative, so that the gradient of ϕ also satisfies a Poisson equation,

$$-\nabla^2 \frac{\partial \phi}{\partial x_i} = -B_k \epsilon_{njk} \frac{\partial^2 u_j}{\partial x_n x_i}.$$
 (3.29)

Eqs. (3.28) and (3.29) have integral solutions

$$\phi(\mathbf{x}) = -B_k \epsilon_{ijk} \int \frac{\partial u_j'}{\partial x_i'} G(\mathbf{x}, \mathbf{x}') dV', \qquad (3.30)$$

$$\frac{\partial \phi}{\partial x_i}(\mathbf{x}) = -B_k \epsilon_{njk} \int \frac{\partial^2 u_j'}{\partial x_i' \partial x_n'} G(\mathbf{x}, \mathbf{x}') dV', \tag{3.31}$$

where we have used primed quantities to denote variables of integration, and $G(\mathbf{x}, \mathbf{x}')$ is the Poisson Green function. We here assume the latter is defined to account for boundary conditions, and note that the spatially homogeneous solution, with boundary conditions prescribed in infinity, is governed by the "homogeneous" Green function

$$G^{\text{hom}}(\mathbf{x}, \mathbf{x}') = \frac{1}{4\pi |\mathbf{x}' - \mathbf{x}|}.$$
 (3.32)

From Eqs. (2.22) through (2.24), we have the scalar Joule dissipation as

$$\mu(\mathbf{x}) = -\langle f_i u_i \rangle$$

$$= \frac{\sigma}{\rho} \left[B_k \epsilon_{ijk} \left\langle u_i \frac{\partial \phi}{\partial x_j} \right\rangle + B^2 \langle u_i u_i \rangle - B_i B_k \langle u_k u_i \rangle \right], \tag{3.33}$$

where the quantity $\langle u_i u_j \rangle$ are the Reynolds stresses. The first term in (3.33) can be rewritten using (3.31). Since \mathbf{x} and \mathbf{x}' are independent, $\mathbf{u}(\mathbf{x})$ is unaffected by differentiation over \mathbf{x}' , and some algebra yields

$$\mu(\mathbf{x}) = \frac{\sigma}{\rho} \left[B_k \epsilon_{kij} B_q \epsilon_{qps} \int \frac{\partial^2 \langle u_i u_p' \rangle}{\partial x_j' \partial x_s'} G(\mathbf{x}, \mathbf{x}') dV' + B^2 \langle u_i u_i \rangle - B_i B_k \langle u_k u_i \rangle \right].$$
(3.34)

We here recognize $\langle u_i u_p' \rangle$ as the two-point velocity correlation.

Let \mathbf{r} be the difference vector of \mathbf{x} and \mathbf{x}' , such that

$$r_i = x_i' - x_i,$$

and the distance between the points is $r = |\mathbf{x}' - \mathbf{x}|$. Differentiation and integration inside the integral in (3.34) is with respect to \mathbf{x}' , keeping \mathbf{x} constant, so a change of coordinates from \mathbf{x}' and \mathbf{x} , to \mathbf{x} and \mathbf{r} , yields $dV' = dr_1 dr_2 dr_3$, and

$$\int \frac{\partial^2 \langle u_i u_p' \rangle}{\partial x_j' \partial x_s'} G(\mathbf{x}, \mathbf{x}') dV' = \int \frac{\partial^2 \langle u_i u_p' \rangle}{\partial r_j \partial r_s} G(\mathbf{x}, \mathbf{x}') dV'.$$

Following Chou [9], we introduce two conservation relations for the two-point velocity correlations. Due to the continuity condition, we have $\partial u'_n/\partial x'_n = 0$. For the ensemble averaged two-point correlation this yields

$$\frac{\partial \langle u_i u_n' \rangle}{\partial x_n'} = \frac{\partial \langle u_i u_n' \rangle}{\partial r_n} = 0, \tag{3.35}$$

assuming \mathbf{x} is kept constant during differentiation. Chou argued, that if we are not too close to flow boundaries, this conservation relation is approximately symmetric with respect to points \mathbf{x}' and \mathbf{x} , so that (still \mathbf{x} constant)

$$\frac{\partial \langle u_n u_i' \rangle}{\partial r_n} \approx 0. \tag{3.36}$$

Let us now assume coordinates oriented so that $\mathbf{B} = B\mathbf{e}_3$. Equation (3.34) yields

$$\mu(\mathbf{x}) = \frac{\sigma B^2}{\rho} \left[\int \left\{ \frac{\partial^2 \langle u_1 u_1' \rangle}{\partial r_2^2} + \frac{\partial^2 \langle u_2 u_2' \rangle}{\partial r_1^2} - \frac{\partial^2}{\partial r_1 \partial r_2} \left(\langle u_1 u_2' \rangle + \langle u_2 u_1' \rangle \right) \right\} G(\mathbf{x}, \mathbf{x}') dV' + \langle u_1 u_1 \rangle + \langle u_2 u_2 \rangle \right].$$
(3.37)

Due to the first conservation relation (3.35),

$$\begin{split} \frac{\partial \langle u_1 u_2' \rangle}{\partial r_2} &= -\frac{\partial \langle u_1 u_1' \rangle}{\partial r_1} - \frac{\partial \langle u_1 u_3' \rangle}{\partial r_3}, \\ \frac{\partial \langle u_1' u_2 \rangle}{\partial r_1} &= -\frac{\partial \langle u_2 u_2' \rangle}{\partial r_2} - \frac{\partial \langle u_2 u_3' \rangle}{\partial r_3}, \end{split}$$

so that the last term of the integrand in (3.37) is

$$\frac{\partial^{2}}{\partial r_{1}\partial r_{2}} \left(\langle u_{1}u_{2}' \rangle + \langle u_{2}u_{1}' \rangle \right) =
- \frac{\partial^{2}\langle u_{1}u_{1}' \rangle}{\partial r_{1}^{2}} - \frac{\partial^{2}\langle u_{2}u_{2}' \rangle}{\partial r_{2}^{2}} - \frac{\partial^{2}\langle u_{1}u_{3}' \rangle}{\partial r_{1}\partial r_{3}} - \frac{\partial^{2}\langle u_{2}u_{3}' \rangle}{\partial r_{2}\partial r_{3}}.$$
(3.38)

The second conservation relation (3.36) gives

$$\frac{\partial \langle u_1 u_3' \rangle}{\partial r_1} + \frac{\partial \langle u_2 u_3' \rangle}{\partial r_2} \approx -\frac{\partial \langle u_3 u_3' \rangle}{\partial r_3}.$$

Away from the walls, the last two terms in (3.38) can then be approximated by

$$-\frac{\partial^2 \langle u_1 u_3' \rangle}{\partial r_1 \partial r_3} - \frac{\partial^2 \langle u_2 u_3' \rangle}{\partial r_2 \partial r_3} \approx -\frac{\partial^2 \langle u_3 u_3' \rangle}{\partial r_3^2}.$$
 (3.39)

We may now collect and rearrange the terms of (3.37) as follows (note the use of index notation to represent summation),

$$\mu \approx \frac{\sigma B^{2}}{\rho} \left[-\int \frac{\partial^{2} \langle u_{n} u_{n}' \rangle}{\partial r_{3}^{2}} G(\mathbf{x}, \mathbf{x}') dV' + \int \left\{ \frac{\partial^{2} \langle u_{1} u_{1}' \rangle}{\partial r_{n} \partial r_{n}} + \frac{\partial^{2} \langle u_{2} u_{2}' \rangle}{\partial r_{n} \partial r_{n}} \right\} G(\mathbf{x}, \mathbf{x}') dV' + \langle u_{1} u_{1} \rangle + \langle u_{2} u_{2} \rangle \right].$$
(3.40)

For comparison with the spectral expression (3.14) for homogeneous turbulence, we note that the definition of the **M** tensor in physical space is (see, e.g., [15], Sec. 3.8.2)

$$M_{ijpq} \equiv -\int \frac{\partial^2 \langle u_i u_j' \rangle}{\partial r_p \partial r_q} G^{\text{hom}}(\mathbf{x}, \mathbf{x}') dV',$$

and that, for homogeneous turbulence, contraction of the second index pair yields the Reynolds stresses,

$$M_{ijnn} = \langle u_i u_i \rangle.$$

Sufficiently far away from flow boundaries, the general Green function $G(\mathbf{x}, \mathbf{x}')$ in Eq. (3.40) can be replaced by the homogeneous $G^{\text{hom}}(\mathbf{x}, \mathbf{x}')$. The second integral in (3.40) then cancels the explicit Reynolds stress terms, and the second integral can be expressed as

$$M_{nn33} = Y_{33} = 2K\alpha,$$

according to the definitions (3.16) and (3.18).

We expect effects of inhomogeneity to be largest for walls perpendicular to the magnetic field, because turbulence structures will be longer in the magnetic field direction. These walls are called Hartmann walls; they exhibit very step velocity gradients, and are therefor often responsible for a large part of the wall friction and heat transfer in a MHD channel flow. The wall-normal Reynolds stress will however be small near a wall. The first homogeneity approximation we made in Eq. (3.39) involved the term $\partial^2 \langle u_3 u_3' \rangle / \partial r_3^2$, which should be small compared to the other terms, at least near the Hartmann walls. As far as the scalar Joule dissipation is concerned, this suggests that the most important effects of inhomogeneity appear through the (spatially) inhomogeneous part of the Poisson Green function in the integrals of Eq. (3.40).

A proper account of the effects of walls and inhomogeneities should be a top priority for future modeling efforts; see Sec. 5.2 for a brief discussion.

3.5. Implementation in a commercial flow solver

The technical report included as **Paper 5** in this thesis describes an implementation of the MHD model equations in the commercial flow solver CFX 4.3. From the experience obtained so far, the MHD turbulence models appear to be numerically robust and well-behaved.

In implementing MHD model equations in a commercial flow solver, the biggest challenge is to make a numerically accurate implementation of the mean flow equations, and especially the computation of total current. Including the

magnetic sink terms in the turbulence equations is rather straightforward, and the α equation can usually be defined as a transported scalar. The α equation (3.27) is then complemented with convection and diffusion terms.

As mentioned above, no attempt has so far been made to model the near-wall effects. For high-Reynolds number implementations of the K- ε and Reynolds stress models, the wall boundary conditions are applied in the center of the first cell near the wall, and turbulence wall functions are used to account for what happens closer to the wall. The wall functions for mean velocity have not yet been modified to account for the effect of the magnetic field (although recent results by Alboussière and Lingwood [1] may be of interest). The treatment adopted for wall boundary conditions for the α equation is the same as for the K and Reynolds stress equations: we assume zero transport to the wall (i.e., $\partial/\partial n = 0$), and solve the equation as usual (with source terms in the first cell). This procedure gives a smooth behavior of α near the wall, and it is easily verified that the budget of α near the wall is indeed dominated by the source terms, and that transport is negligible.

CHAPTER 4

Concluding summary

In this thesis, conventional turbulence closures have been extended with an additional transported scalar, α , for modeling of MHD turbulence. The new scalar captures the anisotropy of length scales, which is a characteristic feature of MHD turbulence, and allows accurate modeling of the Joule dissipation. The concept has been used for both a three-equation "K- ε - α " model, and a full Reynolds stress or "RST- α " model.

Below follows a brief summary of the MHD source terms and model equations discussed in the thesis, and finally a summary of the appended papers.

4.1. The MHD turbulence closure

If n_i is a unit vector parallel with the magnetic field, the proposed Joule destruction terms in the K, ε , and Reynolds stress equations are, respectively,

$$\mu = \frac{2\sigma B^2}{\rho} K\alpha,\tag{4.1}$$

$$\mu_{\varepsilon} = C_{\varepsilon\alpha} \frac{2\sigma B^2}{\rho} \varepsilon \alpha, \tag{4.2}$$

$$\mu_{ij} = \frac{2\sigma B^2}{\rho} \left[G(\alpha, I_{na}) R_{ij} + \frac{H(\alpha)}{2} (n_i n_k R_{kj} + n_j n_k R_{ki}) \right], \tag{4.3}$$

where

$$G(\alpha, I_{na}) = \alpha + \frac{27}{20}\alpha^2(1-\alpha)\left(I_{na} + \frac{2}{3}\right),$$
 (4.4)

$$H(\alpha) = -\frac{27}{10}\alpha^2(1-\alpha),$$
 (4.5)

$$I_{na} \equiv \frac{n_i n_k R_{ki}}{K} - \frac{2}{3}.\tag{4.6}$$

The destruction terms (4.1) through (4.3) were first defined in **Paper 1**, while the scalar functions (4.4) and (4.5) shown here are those proposed in **Paper 2**.

For homogeneous turbulence, an evolution equation for α was developed from the governing equations (**Paper 2** and **Paper 4**). All terms require modeling, however. The proposed model transport equation for α is

$$\frac{\partial \alpha}{\partial t} + U_k \frac{\partial \alpha}{\partial x_k} - D_\alpha = P_\alpha + \Pi_\alpha + \pi_\alpha - \mu_\alpha, \tag{4.7}$$

where D_{α} is the diffusions term (see **Paper 5**)

$$D_{\alpha} = \begin{cases} \frac{\partial}{\partial x_{k}} \left(\frac{\nu_{T}}{\sigma_{\alpha}} \frac{\partial \alpha}{\partial x_{k}} \right) & (K - \varepsilon - \alpha \text{ model}) \\ \frac{\partial}{\partial x_{k}} \left(\frac{C_{s}}{\sigma_{\alpha}} \frac{K}{\varepsilon} R_{kj} \frac{\partial \alpha}{\partial x_{j}} \right) & (RST - \alpha \text{ model}) \end{cases}$$

$$(4.8)$$

 ν_T is here the turbulent viscosity (Eq. [2.41]), used in the standard K- ε model [21], and σ_{α} is a turbulent Prandtl number for α (we have used $\sigma_{\alpha} = 1$, which is the value generally used for the other turbulence quantities). The source terms in the α model equation are

$$P_{\alpha} = -\frac{1}{K} S_{im} R_{ki} \left[(G + \alpha) \delta_{mk} + H n_m n_k \right], \tag{4.9}$$

$$\Pi_{\alpha} = \alpha (1 - \alpha) \left[-\frac{9}{5} (1 - 3\alpha) - \frac{27}{5} \alpha \right] S_{ik} n_k n_i,$$
(4.10)

$$\pi_{\alpha} = \begin{cases} C_{\alpha 2} \frac{\varepsilon}{K} \left(\frac{1}{3} - \alpha \right) & \text{(Alt. 1)} \\ \frac{\varepsilon}{K} \max \left\{ C'_{\alpha 2} \alpha \; ; \; C_{\alpha 2} \left(\frac{1}{3} - \alpha \right) \right\} & \text{(Alt. 2)} \end{cases}$$

$$\mu_{\alpha} = C_{\alpha 1} \frac{2\sigma B^2}{\rho} \alpha^2. \tag{4.12}$$

The strain related terms P_{α} and Π_{α} were modeled in **Paper 4** (for the K- ε model, R_{ij} in P_{α} can be replaced by the Boussinesq hypothesis, Eq. [2.40]). The strain terms were found to have little effect on the turbulent kinetic energy in a channel flow with a transverse magnetic field, and can probably be neglected in most practical applications. The return-to-isotropy term π_{α} represents nonlinear angular energy transfer. The original model ("Alt. 1") was used in **Paper 1**, **Paper 3**, and in the flow solver implementation reported in **Paper 5**. The rather crude piecewise linear modification, "Alt. 2", was used in **Paper 7**. It was found that the modified behavior near the 2D limit ($\alpha = 0$) was important for obtaining the expected nonlinear energy decay observed in experiments (Alemany *et al.* [2]). The form of the magnetic destruction term μ_{α} was proposed in **Paper 1**, and supported by the linear rapid distortion analysis in **Paper 2**.

This thesis has not considered the modeling of near-wall effects, and the models have so far been used together with conventional high-Reynolds number closures, and standard wall functions. The wall boundary condition used for the α equation (applied in the first node) is the same as that generally used for K and the Reynolds stresses: the wall-normal gradient is set to zero, so that the solution is determined by the balance of the source terms.

The MHD model coefficients have varied as the work has progressed. The following values are currently recommended, based on the analysis in **Paper 7** (assuming the standard value $C_{\varepsilon 2} = 1.92$ in the ε equation):

$$\{ C_{\alpha 1}, C'_{\alpha 2}, C_{\alpha 2}, C_{\varepsilon \alpha} \} = \{ 2, 4.72, 0.4, 1.5 \}.$$
 (4.13)

For high interaction numbers (strong fields), the model then reproduces the energy and length scale evolution predicted by linear theory. When nonlinear effects

are of importance, it predicts energy decay and length scale evolution in agreement with experiments. The models coincide with the respective conventional models in the absence of a magnetic field.

4.2. Summary of papers

Paper 1. Ola Widlund, Said Zahrai, and Fritz H. Bark. Development of a Reynolds stress closure for modeling of homogeneous MHD turbulence. *Physics of Fluids*, 10(8):1987–1996, 1998.

A Reynolds stress closure is proposed for modeling of homogeneous MHD turbulence. The paper introduces the dimensionality anisotropy variable α_{μ} (called simply α in later work), and relates it to the Reynolds structure dimensionality tensor, Y_{ij} [31]. The new variable allows the scalar Joule dissipation to be expressed as

$$\mu(t) = 2 \frac{\sigma B^2}{\rho} \alpha_{\mu} K.$$

Based on scaling arguments, a phenomenological transport equation is proposed for α_{μ} , including a Joule destruction term a and return-to-isotropy term of Rotta type for nonlinear energy transfer. Model predictions are compared with Schumann's DNS data [34].

Paper 2. Ola Widlund, Said Zahrai, and Fritz H. Bark. Structure information in rapid distortion analysis and one-point modeling of axisymmetric magnetohydrodynamic turbulence. *Physics of Fluids*, 12(10):2609–2620, 2000.

An evolution equation for the dimensionality tensor Y_{ij} is derived, to replace the phenomenological equation for α used earlier; the analysis includes homogeneous mean velocity gradients, to support a future extension to general inhomogeneous flows. Rapid distortion theory (RDT) is applied to study the behavior of the different magnetic terms of the dimensionality and Reynolds stress tensor equations; a variety of different anisotropy states could be examined by letting magnetic forcing act on a number of initial spectral energy distributions obtained from axisymmetric strain. The properties and limitations of linear or bilinear invariant tensor models for the magnetic terms are evaluated. In the limit of large interaction number, where Joule dissipation dominates (linear decay), the resulting model equations have analytic solutions. Appropriate choice of one model coefficient produces the asymptotic energy decay $K \sim t^{-1/2}$ predicted earlier by linear theory (Lehnert [24], Moffatt [26]).

Paper 3. Ola Widlund and Göte Tallbäck. Modeling of anisotropic turbulent transport in simulations of liquid metal flows in magnetic fields. *3rd Int. Symposium on Electromagnetic Processing of Materials, EPM2000*, Nagoya, Japan, April 3-6, 2000.

This conference contribution reports how the MHD Reynolds stress model, and a simpler three-equation K- ε - α model, can be implemented in a commercial flow solver. Known limitations of the current models are discussed, especially concerning near-wall effects. The implemented equation for α includes strain terms documented in **Paper 4**. The full model implementation is documented in a technical report, available here as **Paper 5**.

Errata: The abstract promises comparison with experimental data, but the relevant 3D simulations were not finished in time for the proceedings. (The oral presentation included comparison with data of Tananaev [40]; see **Paper 5** for details.)

Paper 4. Ola Widlund. MHD turbulence modeling: Effects of mean strain on dimensionality anisotropy. (To be submitted.)

The evolution equation for the Y_{ij} tensor derived in **Paper 2** is used to formulate an equation for α . Models are proposed for two terms related to mean strain. One of the terms correspond to the production of turbulent kinetic energy, and the other is related to the rapid pressure—strain term in the Reynolds stress equations. A simulation of channel flow in a transverse magnetic field suggests that strain effects in the α equation are significant only in regions where the magnetic interaction parameter is small, and Joule dissipation is small compared to viscous dissipation. The net effect of the α strain terms on turbulent kinetic energy is therefor very small. In most practical MHD applications, it is probably appropriate to neglect effects of strain on dimensionality anisotropy, especially considering the algebraic complexity of the proposed model terms.

Paper 5. Ola Widlund. Implementation of MHD model equations in CFX 4.3. Technical report TRITA-MEK 2000:10, Dept. of Mechanics, KTH, Stockholm, 2000.

The report documents an implementation of MHD model equations in the commercial flow solver CFX 4.3. The implementation of the mean equations is accurate also for arbitrary non-orthogonal body-fitted multiblock grids. The new MHD turbulence closure is implemented as both a full Reynolds stress model, and a three-equation model of K- ε type. The properties of the model implementation are demonstrated in a simulation of a 3D channel flow with "M"-shaped velocity profiles. The implementation of the new MHD turbulence models appear to be well-behaved and numerically robust. The MHD model implementation can be used together with standard CFX modeling options, such as heat and mass transfer, multiphase and multicomponent flows.

Paper 6. Ola Widlund. Modeling anisotropic MHD turbulence in simulations of liquid metal flows. *4th International PAMIR Conference*, Presqu'île de Giens, France, 18-22 September, 2000.

The conference contribution discusses the asymptotic properties of the proposed turbulence closure, and presents a comparison with the experiment of Alemany *et al.* [2]. The principal differences between homogeneous and wall-bounded turbulence are discussed briefly.

Paper 7. Ola Widlund. Nonlinear effects in modeling of homogeneous MHD turbulence – Comparison with experiment. (To be submitted.)

The paper presents an analysis of the asymptotic properties of the turbulence closure for large times. For the case of intermediate interaction parameters, the analysis suggests that the model term originally proposed for the nonlinear energy transfer in the α equation should be modified, so that it vanishes in the 2D limit. A unique set of model coefficients could be determined, which makes

the model consistent with theory and experiments for interaction parameters N ranging from zero to infinity. The model coincides with the standard K- ε model when there is no magnetic field. In the linear regime of large N, it produces the $K \sim t^{-1/2}$ energy decay and length scale evolution predicted by linear theory. For intermediate interaction numbers (typically $N \sim 1$) where nonlinear effects are important, $K \sim t^{-1.7}$ and $L_{\parallel} \sim t^{0.65}$, in agreement with the classical experiments by Alemany et al. [2].

CHAPTER 5

Future challenges

We concluded with a discussion of remaining challenges for modeling of MHD turbulence in engineering applications.

5.1. Understanding nonlinear inertial effects

The magnetic model terms in the proposed models have been studied using rapid distortion theory. The return-to-isotropy term in the α equation is still phenomenological in nature, however, and we know very little about the underlying nonlinear inertial mechanism. Neither do we know much about how the magnetic field affects the nonlinear intercomponent energy transfer in the Reynolds stress equations.

In **Paper 7** it was argued that the return-to-isotropy term π_{α} in the α equation should be modified, so that the term decreases linearly to zero when we approach the 2D limit ($\alpha = 0$). The properties of such a model was evaluated using a crude piecewise linear model expression,

$$\pi_{\alpha} = \frac{\varepsilon}{K} \max \left\{ C'_{\alpha 2} \alpha ; C_{\alpha 2} (1/3 - \alpha) \right\}. \tag{5.1}$$

For large times, i.e., sufficiently small α , this term behaves as $\pi_{\alpha} = C'_{\alpha 2} \alpha \varepsilon / K$. The analysis showed that this behavior reflects the expected balance between angular energy transfer and Joule dissipation. The predicted decay of energy and length scale evolution is then consistent with expectations, and the model could be adjusted to reproduce the experimental results of Alemany *et al.*

The analysis in **Paper 7** did not consider the effect of the magnetic field on the triple correlations responsible for nonlinear energy transfer. Using DNS, Schumann found that the magnetic field reduces both the angular energy transfer rate, and the nonlinear slow pressure–strain interaction in the Reynolds stress equations [34]. One can argue that also viscous dissipation is affected, because nonlinear interaction is responsible for the transfer of energy from larger to smaller scales; Sreenivasan and Alboussière showed that the k^{-3} -spectra measured in many MHD turbulence experiments is consistent with reduced energy transfer to the dissipative scales [38].

Alemany et al. [2] have suggested that the nonlinear energy transfer rate in a magnetic field is reduced by a factor (1 + N), where $N = \sigma B^2 K/(\rho \varepsilon)$ is the interaction parameter. The nonlinear energy transfer rate is usually estimated as ε/K . Using Alemany's suggestion, the reduced transfer rate is then $f_N \varepsilon/K$,

with

$$f_N = \frac{1}{1+N}. (5.2)$$

The analysis in **Paper 7** supports the idea of Sreenivasan and Alboussière, that the "nonlinear" phase of decay (in which there is balance of angular energy transfer and Joule dissipation) is characterized by a constant value of the so-called true interaction parameter; In **Paper 7** this is defined as $N^* = \alpha N$. In the nonlinear regime of decay, α is small and presumably $N^* \sim const.$, so that $N \sim 1/\alpha$, and $f_N \sim \alpha$. This means that the original return-to-isotropy term π_{α} gets the desired asymptotic properties of (5.1), if we use the modified energy transfer rate, i.e.,

$$\pi_{\alpha} = C_{\alpha 2} f_N \frac{\varepsilon}{K} (1/3 - \alpha). \tag{5.3}$$

If we assume the same reduction is appropriate for the viscous dissipation terms, the viscous dissipation in the K equation would be replaced by a model term $\varepsilon_K = f_N \varepsilon$, and the destruction term in the ε equation becomes $\varepsilon_\varepsilon = C_{\varepsilon 2} f_N \varepsilon^2 / K$. Note that the closure variable ε would no longer directly represent the viscous dissipation of turbulent kinetic, but it would keep its role for estimates of time and length scales of the energy-containing eddies, K/ε and $K^{3/2}/\varepsilon$, respectively.

Although this model formulation is rather speculative in nature, we shall look at some very preliminary numerical results. We solve the equations for K, ε and α for a few different initial interaction parameters N_0 . Here $C_{\alpha 2}=1$ in (5.3); remaining model coefficients are the same as in **Paper 7**. According to (5.3), π_{α} depend on N, which changes with time; in Fig. 5.1 we have plotted $\pi_{\alpha}K/\varepsilon$ against α , with data from the simulations. The magnitude of π_{α} decreases with increasing N, but the approach towards the 2D limit ($\alpha = 0$) follows the same straight line. An consequence of the N dependence is that the time it takes to reach the nonlinear regime (constant N^*) depend on N_0 ; this is demonstrated in the left pane of Fig. 5.2. In the right pane of Fig. 5.2 the duration t_{lin} of the linear phase of decay is estimated and plotted against N_0 . The duration of the linear phase is described well by $t_{\text{lin}} \sim \tau N_0^{4/3}$, which is consistent with the estimates of both Alemany et al. [2], and Sreenivasan [38]. A preliminary analysis suggests that the viscous terms are negligible for large N, and that the asymptotic decay of energy is $K \sim t^{-1/(C_{\varepsilon\alpha}-1)}$. This gives $K \sim t^{-2}$ if $C_{\varepsilon\alpha} = 1.5$ (see **Paper 7**). For $C_{\varepsilon\alpha} = 1.59$ we get $K \sim t^{-1.7}$ (the result of Alemany et al.).

Schumann obtained very useful results from direct numerical simulations already in 1976; with the much more powerful computers available on our desk tops today, it should be possible to produce very useful data with relatively simple means. In a not too distant future, this may hopefully shed some light on the angular energy transfer mechanism, and the effect of the magnetic field on nonlinear energy transfer in general.

5.2. Including effects of walls and inhomogeneities

As discussed briefly in **Paper 6**, MHD turbulence in wall-bounded flows behave differently than homogeneous MHD turbulence. If a flow domain is bounded

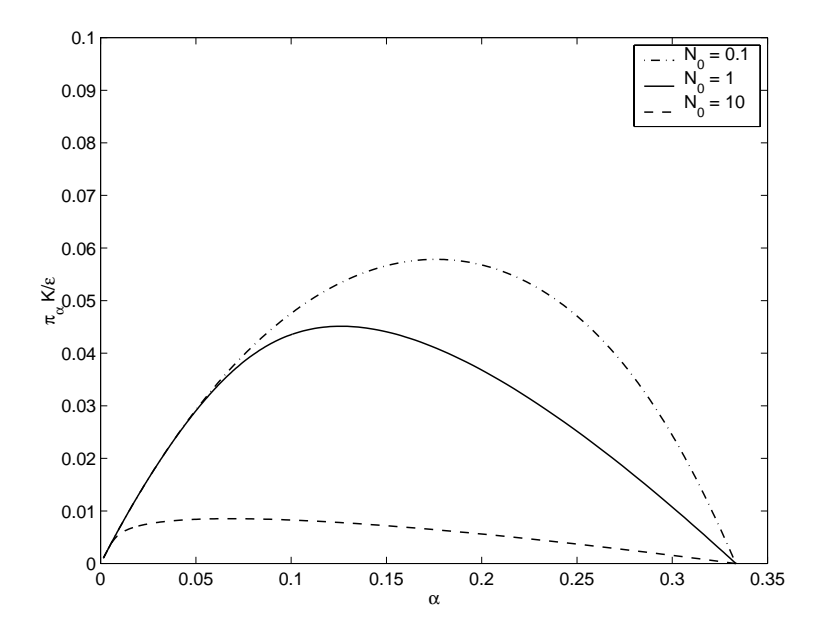


FIGURE 5.1 Plot of $\pi_{\alpha}K/\varepsilon$ versus α . Computed using Eq. (5.3), with data from the simulations $(C_{\alpha}2)$.

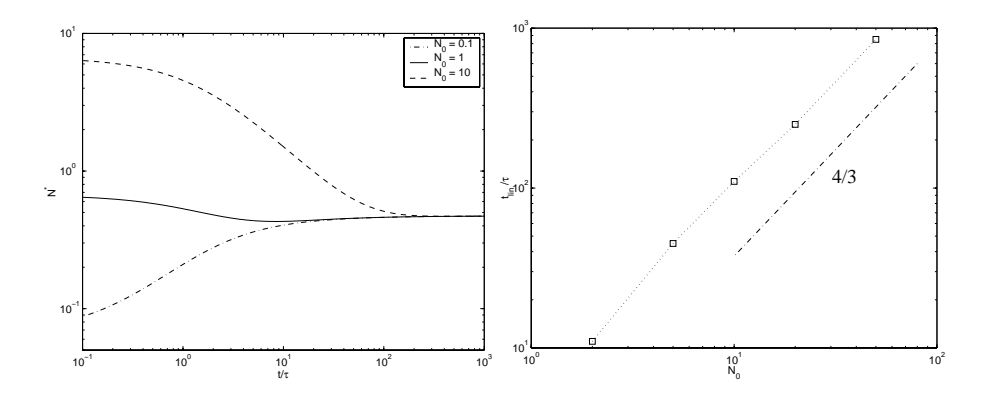


FIGURE 5.2 The left plot shows the evolution of the true interaction number. The right plot shows how the estimated duration of the linear decay (i.e., the time before $N^* \sim \text{const.}$) depend on N_0 . The dash-dotted line shows the power-law slope 4/3, for comparison.

by walls perpendicular to the magnetic field, the turbulence tend to become not only two-dimensional (long structures in the magnetic field direction), but also two-component (2C), i.e., with vanishing energy in the field-parallel stress component. The current models will not predict this particular feature of wall-bounded MHD flows.

Solid boundaries modify the solution not only through boundary conditions, but also through the fluctuating pressure, and the fluctuating electric potential.

The spectral analysis of Sec. 3.1 accounts only for the spatially homogeneous contribution to the fluctuating pressure and electric potential (see also Sec. 3.4).

The fluctuating pressure enters the Reynolds stress equations through the pressure-strain terms. These are responsible for transfer of energy between individual stress components, but has no net effect on turbulent kinetic energy. The pressure—strain terms are i.a. responsible for the damping of wall-normal Reynolds stresses near walls. For a Reynolds stress model to predict the development into a two-component state, the pressure–strain model terms [See Eq. (2.31) should be designed to promote damping of the wall-normal stress component (when the length scale of turbulence becomes comparable with the wall distance). Furthermore, all tensorial model terms must be realizable (see, e.g., [15], Sec. 3.6.4), so that they will not produce unphysical results (e.g. negative normal stresses) in the 2C limit. This includes not only the pressure-strain terms, but also the viscous dissipation tensor ε_{ij} , and the non-pressure part of the Joule dissipation tensor [see Eq. (2.32)]. Realizability generally requires the model tensor functions to be high-order in the Reynolds stress tensor. In addition, a realistic description of the wall damping requires that we include the extra length scale information available through α (and the magnetic field direction vector \mathbf{n}) in the modeling.

As discussed in Sec. 3.4, the fluctuating electric potential give rise to near-wall effects also in the scalar Joule dissipation of turbulent kinetic energy. In the equations for scalars like K, ε , and α , the near-wall effects can probably be accounted for by relatively simple damping functions. This may allow the development of a low-Reynolds number K- ε - α model, where equations are integrated down to the wall. In a high-Reynolds number model, the wall effects would instead be accounted for by modification of the wall functions (see, e.g., recent work by Alboussière and Lingwood [1]).

It appears to be very difficult to develop an MHD Reynolds stress model, which takes full account of wall effects, and allows transition to a two-component 2D state. Unless simplifications can be made, the complexity of the resulting model terms, and the modeling effort involved, is discouraging. In comparison, the inclusion of near-wall effects in a scalar K- ε - α model appears relatively straight-forward.

Efforts to model these wall effects would benefit greatly from direct numerical simulations (DNS) on channel flows. At least one such project is currently in preparation, within the group of Prof. These in Ilmenau, Germany.

5.3. Modeling of anisotropic turbulent transport

One experimentally verified feature of wall-bounded MHD flows is that the magnetic field will reduce the transport of a passive scalar (heat, species concentration) in the direction of the magnetic field (see, e.g., data of Kolesnikov and Tsinober [25]). This effect can be attributed to the elongation of length scales in the field direction, and the subsequent damping of wall-normal velocity fluctuations.

The ability of a Reynolds stress closure to predict this effect depends on how well the model can deal with damping of the field-parallel stress component. The

discussion in the previous section suggest it will be rather difficult to develop a Reynolds stress model with these properties. A more promising route may be to use a three equation K- ε - α model, and instead modify the Boussinesq and eddy diffusivity hypotheses to account for the effects of the magnetic field.

The original Boussinesq hypothesis, Eq. (2.40), relates the Reynolds stress anisotropy to the mean strain rate tensor. A modified expression should presumably depend also on α and the magnetic field direction vector \mathbf{n} , something like

$$-\left\langle u_i'u_j'\right\rangle = -\frac{2}{3}K\delta_{ij} + B_{ij}(S_{ij}, n_i, \alpha, K, \varepsilon, N, \cdots), \tag{5.4}$$

where B_{ij} is a traceless symmetric tensor function.

In order to obtain an anisotropic eddy diffusivity, the original isotropic expression (2.43) may be exchanged for

$$-\langle u_i'q'\rangle = G_{ik}(n_i, \nu_T, \sigma_Q, \alpha, N, \cdots) \frac{\partial Q}{\partial x_k},$$
 (5.5)

where G_{ij} is a symmetric tensor function.

It should be remembered that development of large anisotropies in MHD turbulence is accompanied by very strong Joule dissipation of turbulence; in many practical applications, turbulent transport may be small enough for effects of anisotropy to be insignificant.

Acknowledgments

I want to thank my supervisors, Prof. Fritz Bark and Doc. Said Zahrai, for their constructive ideas, support and encouragement. In particular I have enjoyed my numerous discussions with Said, often on subjects far remote from our common project. Thanks also to all my colleagues at the Department of Mechanics and the Faxén Laboratory, for good company and for generously sharing your knowledge.

This project was carried out within the Faxén Laboratory at the Royal Institute of Technology; the financial support of the Swedish National Board for Industrial and Technical Development (NUTEK) and the industrial sponsors within ABB is gratefully acknowledged. Special thanks to Göte Tallbäck and his colleagues at ABB Automation Systems AB in Västerås for many stimulating discussions, and continuing interest in my work.

Finally, I thank my mother and father, my brother and his family, and all my dear friends, new and old, for love and support at all times.

Bibliography

- T. Alboussière and R. J. Lingwood. A model for the turbulent Hartmann layer. Physics of Fluids, 12(6):1535-1543, 2000.
- [2] A. Alemany, R. Moreau, P. L. Sulem, and U. Frisch. Influence of an external magnetic field on homogeneous mhd turbulence. *Journal de Mécanique*, 28:277-313, 1979.
- [3] H. Alfvén. Existence of electromagnetic-hydrodynamic waves. Nature, 150(3805):405, 1942.
- [4] G. K. Batchelor. The Theory of Homogeneous Turbulence. Cambridge University Press, Cambridge, 1953.
- [5] H. Branover. Magnetohydrodynamic Flows in Ducts. Israel University Press, New York, 1978
- [6] U. Burr. Turbulente Transportvorgänge in magnetohydrodynamischen Kanalströmungen. PhD thesis, Forschungszentrum Karlsruhe, Karlruhe, Germany, 1998. Scientific report FZKA 6038.
- [7] C. Cambon, L. Jacquin, and J. L. Lubrano. Toward a new Reynolds stress model for rotating turbulence. Physics of Fluids A, 4(4):812–824, 1992.
- [8] Ph. Caperan and A. Alemany. Turbulence homogène m.h.d. a faible nombre de reynolds magnétique. Étude de la transition vers la phase quasi bidimensionnelle et charactérisation de son anisotropie. Journal de Mécanique théoretique et appliquée, 4(2):175-200, 1985.
- [9] P. Y. Chou. On velocity correlations and the solutions of the equations of turbulent fluctuation. Quart. of Appl. Math., 3(1):38-54, 1945.
- [10] B. J. Daly and F. H. Harlow. Transport equations in turbulence. Physics of Fluids, 13(11):2634-2649, 1970.
- [11] P. A. Davidson. The role of angular momentum in the magnetic damping of turbulence. Journal of Fluid Mechanics, 336:123-150, 1997.
- [12] Loup de la Montagne, 2000. Personal communication on the Ramalanger effect.
- [13] M. Faraday. Phil. Trans. Roy. Soc., page 163, 1832.
- [14] M. Hallbäck. Development of Reynolds Stress Closures of Homogeneous Turbulence through Physical and Numerical Experiments. Doctoral thesis, Royal Institute of Technology, Stockholm, Sweden, 1993.
- [15] M. Hallbäck, D. S. Henningson, A. V. Johansson, and P. H. Alfredsson, editors. Turbulence and Transition Modelling. ERCOFTAC Series. Kluwer Academic Publishers, Dordrecht, The Netherlands, 1996.
- [16] H.-C. Ji and R. A. Gardner. Numerical analysis of turbulent pipe flow in a transverse magnetic field. Int. Journal of Heat and Mass Transfer, 40(8):1839–1851, 1997.
- [17] N. Kasagi and M. Nishimura. Direct numerical simulation of combined forced and natural turbulent convection in a vertical plane channel. Int. J. Heat and Fluid Flow, 18(1):88–99, 1997.
- [18] S. Kenjereš and K. Hanjalić. On the implementation of effects of Lorentz force in turbulence closure models. Int. Journal of Heat and Fluid Flow, 21(3):329-337, June 2000.
- [19] J. Larmor. How could a rotating body such as the sun become a magnet? Engineering, 108:461, 1919.
- [20] B. E. Launder, G. J. Reece, and W. Rodi. Progress in the development of a Reynolds-stress turbulence closure. *Journal of Fluid Mechanics*, 68:537–566, 1975.

- [21] B. E. Launder and D. B. Spalding. The numerical computation of turbulent flows. Computer Methods in Appl. Mech. and Eng., 3:269-289, 1974.
- [22] A. F. Lehman, G. R. Tallbäck, and H. R. Hackl. Fluid flow control in continuous casting using various configurations of static magnetic fields. In *Proceedings of International Symposium on Electromagnetic Processing of Materials, Oct. 25-28, 1994*, pages 372–377, Nagoya, Japan, 1994. ISIJ.
- [23] B. Lehnert. On the behaviour of an electrically conductive liquid in a magnetic field. Ark. Fys., 5(5):69–90, 1952.
- [24] B. Lehnert. The decay of magneto-turbulence in the presence of a magnetic field and coriolis force. Quart. Appl. Math., 12(4):321-341, 1955.
- [25] O. Lielausis. Liquid-metal magnetohydrodynamics. Atomic Energy Review, 13(3):527–581, 1975.
- [26] H. K. Moffatt. On the suppression of turbulence by a uniform magnetic field. Journal of Fluid Mechanics, 28:571–592, 1967.
- [27] H. K. Moffatt. Magnetic field generation in electrically conducting fluids. Cambridge University Press, 1978.
- [28] R. Moreau. Magnetohydrodynamics. Kluwer Academic Publishers, Dordrecht, The Netherlands, 1990.
- [29] N. Nakauchi, H. Oshima, and Y. Saito. Two-dimensionality in low-magnetic Reynolds number magnetohydrodynamic turbulence subjected to a uniform external magnetic field and randomly stirred two-dimensional force. *Physics of Fluids A*, 4(12):2906–2914, dec 1992.
- [30] H. Noguchi, Y. Ohtsubo, and N. Kasagi. Dns database of turbulence and heat transfer. ftp://ftp.thtlab.t.u-tokyo.ac.jp/DNS, 1998.
- [31] W. C. Reynolds. Effects of rotation on homogeneous turbulence. In Proc. 10th Australasian Fluid Mechanics Conference, Melbourne, Australia, 1989. University of Melbourne.
- [32] W. C. Reynolds and S. C. Kassinos. One-point modelling of rapidly deformed homogeneous turbulence. Proceedings of the Royal Society of London, Series A, 451(1941):87–104, Oct 1995.
- [33] J. Rotta. Statistische Theorie nichthomogener Turbulenz. 1. Mitteilung. Zeitschrift für Physik, 129:547-572, 1951.
- [34] U. Schumann. Numerical simulation of transition from three- to two-dimensional turbulence under a uniform magnetic field. *Journal of Fluid Mechanics*, 74:31–58, 1976.
- [35] J. A. Shercliff. A Textbook of Magnetohydrodynamics. Pergamon Press, Oxford, 1965.
- [36] Y. Shimomura. Statistical analysis of magnetohydrodynamic shear flows at low magnetic Reynolds number. *Journal of the Physical Society of Japan*, 57(7):2365–2385, 1988.
- [37] J. Sommeria and R. Moreau. Why, how, and when, MHD turbulence becomes twodimensional. Journal of Fluid Mechanics, 118:507-518, 1982.
- [38] B. Sreenivasan and T. Alboussière. Evolution of a vortex in magnetic field. Eur. J. Mech. B - Fluids, 19:403-421, 2000.
- [39] K. Takatani, Y. Tanizawa, and M. Kawamoto. Mathematical model for fluid flow in a continuous casting mold with electromagnetic brake. In Proceedings of the Third Int. Symposium on Electromagnetic Processing of Materials, EPM2000, April 3-6, 2000, pages 91–96, Nagoya, Japan, 2000. ISIJ.
- [40] A. B. Tananaev. MHD Duct Flows. Atomizdat, 1979.
- [41] H. Tennekes and J. L. Lumley. A first course in turbulence. MIT Press, 1972.
- [42] O. Widlund, S. Zahrai, and F. H. Bark. Development of a Reynolds stress closure for modeling of homogeneous MHD turbulence. *Physics of Fluids*, 10(8):1987–1996, 1998.
- [43] H. A. Wouters, R. P. J. Duursma, A. A. Kamperman, and W. F. M. Damen. Modification of a turbulent two-phase flow by a magnetic field as applied to the continuous casting of steel. In Proceedings of the Third Int. Symposium on Electromagnetic Processing of Materials, EPM2000, April 3-6, 2000, pages 182–187, Nagoya, Japan, 2000. ISIJ.
- [44] O. Zikanov and A. Thess. Direct numerical simulation of forced MHD turbulence at low magnetic Reynolds number. *Journal of Fluid Mechanics*, 358:299–333, 1998.

Paper 1

DEVELOPMENT OF A REYNOLDS STRESS CLOSURE FOR MODELING OF HOMOGENEOUS MHD TURBULENCE

Ola Widlund¹, Said Zahrai², and Fritz H. Bark¹

¹Faxén Laboratory, Royal Institute of Technology, SE-100 44, Stockholm, Sweden ²ABB Corporate Research, SE-721 78, Västerås, Sweden

Abstract. A Reynolds stress closure is developed for homogeneous shearfree turbulence subjected to a strong magnetic field at low magnetic Reynolds numbers. A scalar dimensionality anisotropy parameter is introduced to carry information about the distribution of energy in spectral space. This information is vital in modeling MHD turbulence, as it determines both magnitude and anisotropy of the Joule dissipation tensor. The Joule dissipation tensor is modeled by a tensor function, which is bilinear in the Reynolds stress anisotropy and the unit direction vector of the magnetic field. The tensor function coefficients are second-order in the scalar dimensionality parameter. A phenomenological transport equation for the dimensionality parameter is proposed. The model is closed using the pressurestrain model of Sarkar, Speziale and Gatski and a magnetic destruction term in the standard dissipation equation. The purely magnetic linear problem contains no undetermined constants, while the complete model contains two constants. Model predictions for the case of decaying turbulence show very good agreement with direct numerical simulations.

Due to copyright restrictions, only the abstract is available online.

Published in Physics of Fluids, 10(8), 1998.

Paper 2

STRUCTURE INFORMATION IN RAPID DISTORTION ANALYSIS AND ONE-POINT MODELING OF AXISYMMETRIC MAGNETOHYDRODYNAMIC TURBULENCE

Ola Widlund¹, Said Zahrai², and Fritz H. Bark¹

¹Faxén Laboratory, Royal Institute of Technology, SE-100 44, Stockholm, Sweden ²ABB Corporate Research, SE-721 78, Västerås, Sweden

Abstract. It has recently been suggested that dimensionality information, as carried by the Reynolds dimensionality tensor, should be included in an extended Reynolds stress closure for modeling of magnetohydrodynamic (MHD) turbulence at low magnetic Reynolds numbers. This would enable more accurate modeling of the Joule dissipation, and capture the lengthscale anisotropies and tendencies towards two-dimensionality characteristic of MHD turbulence. In the present work, an evolution equation for the Reynolds dimensionality tensor is derived, based on the spectral formulation of the Navier-Stokes equations. Most of the terms in the equation require modeling. Rapid distortion theory (RDT) is applied to study the behavior of the different magnetic terms of the dimensionality and Reynolds stress tensor equations; a variety of different anisotropy states could be examined by letting magnetic forcing act on a number of initial spectral energy distributions obtained from axisymmetric strain. The properties and limitations of linear or bilinear invariant tensor models for the magnetic terms are evaluated. In the limit of large interaction numbers (where Joule dissipation dominates), the resulting model equations for the energy decay have analytic solutions. By choosing one model constant appropriately, these are made consistent with the asymptotic energy decay $K \sim t^{-1/2}$ predicted earlier by Moffatt. The long-term objective of these efforts is the development of an effective second-moment closure for engineering applications.

Due to copyright restrictions, only the abstract is available online.

Paper 3

MODELING OF ANISOTROPIC TURBULENT TRANSPORT IN SIMULATIONS OF LIQUID METAL FLOWS IN MAGNETIC FIELDS

Ola Widlund 1 and Göte Tallbäck 2

 $^1{\rm Fax\'{e}n}$ Laboratory, Royal Institute of Technology, Stockholm, Sweden $^2{\rm ABB}$ Automation Systems AB, Västerås, Sweden

Abstract. The paper deals with an extended Reynolds stress closure for modeling of turbulent transport in engineering MHD applications. The model was implemented in a commercial CFD code, and predictions were compared with experimental data. Properties and limitations of the model are discussed, especially in view of the extreme anisotropies encountered in MHD turbulence.

Due to copyright restrictions, only the abstract is available online.

Presented at 3rd International Symposium on Electromagnetic Processing of Materials, EPM2000, Nagoya, Japan, April 3-6, 2000.

Paper 4

4

MHD TURBULENCE MODELING: EFFECTS OF MEAN STRAIN ON DIMENSIONALITY ANISOTROPY

Ola Widlund

Faxén Laboratory Royal Institute of Technology SE-100 44, Stockholm, Sweden

Abstract. Widlund et al. have suggested to include an extra transported scalar, α , in one-point models of MHD turbulence. The new scalar is defined in terms of one single component (in the the direction of the magnetic field) of the Reynolds dimensionality tensor Y. It captures the length scale anisotropy characteristic of MHD turbulence, and allows accurate modeling of Joule dissipation of turbulence in a magnetic field. Earlier efforts have focussed on magnetic and nonlinear terms in the α transport equation; in the present work, an attempt is made to incorporate also effects of mean shear and strain. One of the new terms involves references to other components of the full tensor Y, which could only be resolved by assuming that Y is axisymmetric about the direction of the magnetic field. A simulation of channel flow in a transverse magnetic field suggests that strain effects in the α equation are significant only in regions where the magnetic interaction parameter is small, and Joule dissipation is small compared to viscous dissipation. The net effect of the α strain terms on turbulent kinetic energy is therefor very small. In most practical MHD applications, it is probably appropriate to neglect effects of strain on dimensionality anisotropy, especially considering the algebraic complexity of the proposed model terms.

1. Introduction

Widlund et al. [10, 11] have suggested that an extra transported variable, α , should be included in Reynolds stress transport (RST) and eddy viscosity closures for modeling of MHD turbulence. The extra scalar captures the length-scale anisotropy and tendency toward two-dimensionality, which is characteristic of MHD turbulence, and allows accurate modeling of magnetic effects on turbulence.

The new scalar is defined in terms of the normal component of the Reynolds dimensionality tensor \mathbf{Y} [5, 6] in the direction of the magnetic field. If \mathbf{n} is a unit vector parallel with the magnetic field, and K is the turbulent kinetic energy,

$$\alpha \equiv \frac{n_i n_j Y_{ji}}{2K}.\tag{1}$$

For homogeneous turbulence, the Joule dissipation of turbulent kinetic energy can then be expressed exactly as

$$\mu = 2 \frac{\sigma B^2}{\rho} \alpha K. \tag{2}$$

The dimensionality tensor **Y** carries information about the anisotropy of length scales of turbulence structures, and was introduced by Reynolds and coworkers to improve the modeling of rapidly rotating flows [5, 6]. Cambon *et al.* have worked with similar ideas, but using a slightly different formulation [1].

The phenomenological transport equation for α proposed in [10] for homogeneous turbulence was later confirmed by deriving an evolution equation for the full tensor **Y** [11]. These earlier efforts focussed on the magnetic and nonlinear terms in the α equation. In the present work we attempt to include model terms which describe the effects of mean velocity gradients (mean shear and strain) on α .

2. Theory

2.1. Governing equations. With spatial coordinates \mathbf{x} and time t, the Navier–Stokes equations for the instantaneous velocity field $u_i(\mathbf{x}, t)$ of an incompressible fluid are

$$\frac{\partial u_i}{\partial t} + u_j \frac{\partial u_i}{\partial x_j} = -\frac{1}{\rho} \frac{\partial p}{\partial x_i} + \nu \frac{\partial^2 u_i}{\partial x_j \partial x_j} + f_i, \tag{3}$$

$$\frac{\partial u_i}{\partial x_i} = 0, \tag{4}$$

where $p(\mathbf{x}, t)$ is the pressure field, ρ the fluid density, ν the kinematic viscosity, and f_i is the Lorentz force (per unit mass).

The Lorentz force f_i in (3) is governed by the non-relativistic Maxwell equations. If the magnetic Reynolds number is small (Rm_L \ll 1), convective disturbances to the magnetic field will be small compared to the external field **B**, and we can use the so-called quasistatic approximation (see [11] for details). Using lower-case letters to denote instantaneous values, we have

$$f_i \approx \frac{1}{\rho} \epsilon_{ikn} j_k B_n, \tag{5}$$

where the instantaneous electric current density j_i is given by Ohm's law,

$$j_i \approx \sigma(e_i + \epsilon_{ikn} u_k B_n). \tag{6}$$

and e_i is the electric field. The scalar electrostatic potential ϕ is defined by

$$e_i = -\frac{\partial \phi}{\partial x_i}. (7)$$

The current field is divergence free, so it follows from (6) that

$$\frac{\partial^2 \phi}{\partial x_i \partial x_i} \approx \epsilon_{ijk} \frac{\partial}{\partial x_i} (u_j B_k). \tag{8}$$

A Reynolds decomposition can be applied to split the instantaneous variables into mean and fluctuating parts [11]. If we consider the case of homogeneous turbulence, the equations for the fluctuating quantities can be Fourier transformed, allowing for homogeneous mean velocity gradients

$$U_{i,m}(t) = \frac{\partial U_i}{\partial x_m}.$$

In the spectral domain we can eliminate the fluctuating pressure from the equations, and find an explicit expression for the fluctuating Lorentz force (see [11], and Schumann [7]). The Fourier coefficients of velocity are then given by

$$\frac{d\hat{u}_i}{dt} = -U_{i,j}\hat{u}_j + 2\frac{k_i k_m}{k^2} U_{m,j}\hat{u}_j
-ik_j(\widehat{u_i'u_j'}) + i\frac{k_i k_m k_j}{k^2}(\widehat{u_m'u_j'}) - \nu k^2 \hat{u}_i - \frac{\sigma}{\rho} \frac{(\mathbf{B} \cdot \mathbf{k})^2}{k^2} \hat{u}_i,$$
(9)

complemented by an equation for the rate of change of the wave number of a component,

$$\frac{dk_i}{dt} = -U_{j,i}k_j. (10)$$

The spectral energy tensor is defined as the ensemble averaged second moments of $\hat{\mathbf{u}}$,

$$\hat{\Phi}_{ij}(\mathbf{k},t) = \langle \hat{u}_i(-\mathbf{k},t)\hat{u}_j(\mathbf{k},t)\rangle = \langle \hat{u}_i^*\hat{u}_j\rangle,\tag{11}$$

which correspond to the two-point velocity correlations in physical space. Here \hat{u}_i^* is the complex conjugate of \hat{u}_i . An evolution equation for $\hat{\Phi}_{ij}$ can be derived from (9), and from this we can formulate equations for several one-point turbulence quantities [11]. The turbulent kinetic energy, for example, is

$$K = \frac{1}{2} \int \hat{\Phi}_{nn} d^3 \mathbf{k},\tag{12}$$

given by

$$\frac{dK}{dt} = P_K - \varepsilon - \mu,\tag{13}$$

where the production and dissipation terms are

$$P_K = -U_{i,k} R_{ki}, (14)$$

$$\varepsilon = \nu \int k^2 \hat{\Phi}_{nn} d^3 \mathbf{k},\tag{15}$$

$$\mu = \frac{\sigma}{\rho} \int \frac{(\mathbf{B} \cdot \mathbf{k})^2}{k^2} \hat{\Phi}_{nn} d^3 \mathbf{k}. \tag{16}$$

The Reynolds stress tensor can be defined in the same way, as

$$R_{ij} = \int \hat{\Phi}_{ij} d^3 \mathbf{k}. \tag{17}$$

It is given by

$$\frac{dR_{ij}(t)}{dt} = P_{ij} + \Pi_{ij}^{(r)} + \Pi_{ij}^{(s)} - \varepsilon_{ij} - \mu_{ij},$$
(18)

with

$$P_{ij} = -U_{i,k}R_{kj} - U_{j,k}R_{ki}, (19)$$

$$\Pi_{ij}^{(r)} = 2U_{m,n} \int \left(\frac{k_i k_m}{k^2} \hat{\Phi}_{nj} + \frac{k_j k_m}{k^2} \hat{\Phi}_{in} \right) d^3 \mathbf{k}, \tag{20}$$

$$\Pi_{ij}^{(s)} = \int ik_m \left\{ \Delta_{in} \int \hat{T}_{mnj}^*(\mathbf{k}, \mathbf{k}') d^3 \mathbf{k}' - \Delta_{jn} \int \hat{T}_{mni}(\mathbf{k}, \mathbf{k}') d^3 \mathbf{k}' \right\} d^3 \mathbf{k},$$
(21)

$$\varepsilon_{ij} = 2\nu \int k^2 \hat{\Phi}_{ij} d^3 \mathbf{k}, \tag{22}$$

$$\mu_{ij} = 2\frac{\sigma}{\rho} \int \frac{(\mathbf{B} \cdot \mathbf{k})^2}{k^2} \hat{\Phi}_{ij} d^3 \mathbf{k}, \tag{23}$$

where P_{ij} is the turbulence production tensor, ε_{ij} is the viscous dissipation rate tensor, and μ_{ij} is the Joule dissipation tensor. The redistributive pressure–strain rate interaction falls naturally into three parts: a rapid part $\Pi_{ij}^{(r)}$, representing the mean deformation–turbulence interaction, a slow part $\Pi_{ij}^{(s)}$, representing nonlinear turbulence–turbulence interaction, and finally a magnetic part, which is here included in the Joule dissipation tensor.

The Joule dissipation of turbulent kinetic energy in (16) can be written as

$$\mu = \frac{\sigma B^2}{\rho} n_i n_j Y_{ji},\tag{24}$$

where \mathbf{n} is a unit vector parallel with the magnetic field, and \mathbf{Y} is the so-called dimensionality tensor introduced by Reynolds and co-workers [5, 6],

$$Y_{ij} = \int \frac{k_i k_j}{k^2} \hat{\Phi}_{ij}(\mathbf{k}, t) d^3 \mathbf{k}.$$
 (25)

Reynolds showed that **Y** contains information related to turbulent length scales in different directions. Based on (24), Widlund *et al.* [10] proposed a Reynolds stress transport (RST) model for MHD turbulence, which included an extra transport equation for a dimensionality anisotropy variable, α , defined as

$$\alpha \equiv \frac{n_i n_j Y_{ji}}{2K},\tag{26}$$

so that

$$\mu = 2 \frac{\sigma B^2}{\rho} \alpha K. \tag{27}$$

This expression for Joule dissipation is exact for homogeneous turbulence.

2.2. Transport equation for α . The main features of the phenomenological transport equation proposed for α in [10] were later confirmed, based on an equation derived for the complete tensor **Y** [11]. We have

$$\frac{dY_{ij}}{dt} = P_{ij}^Y + \Pi_{ij}^Y + \pi_{ij}^Y - \varepsilon_{ij}^Y - \mu_{ij}^Y, \tag{28}$$

where

$$P_{ij}^Y = -2U_{p,m} \int \frac{k_i k_j}{k^2} \hat{\Phi}_{mp} d^3 \mathbf{k}$$
 (29)

$$\Pi_{ij}^{Y} = -U_{n,j}Y_{ni} - U_{n,i}Y_{nj} + 2U_{m,n} \int \frac{k_i k_j k_m k_n}{k^4} \hat{\Phi}_{pp} d^3 \mathbf{k}$$
 (30)

$$\pi_{ij}^{Y} = \int ik_m \frac{k_i k_j}{k^2} \int \left(\hat{T}_{mpp}^*(\mathbf{k}, \mathbf{k}') - \hat{T}_{mpp}(\mathbf{k}, \mathbf{k}')\right) d^3 \mathbf{k}' \ d^3 \mathbf{k}$$
(31)

$$\varepsilon_{ij}^{Y} = 2\nu \int k_i k_j \hat{\Phi}_{nn} d^3 \mathbf{k}$$
 (32)

$$\mu_{ij}^Y = 2\frac{\sigma}{\rho} \int \frac{(\mathbf{B} \cdot \mathbf{k})^2}{k^2} \frac{k_i k_j}{k^2} \hat{\Phi}_{nn} d^3 \mathbf{k}.$$
 (33)

Like the Reynolds stress tensor \mathbf{R} , the dimensionality tensor has trace 2K, so that contraction of equation (28) yields an equation for turbulent kinetic energy. The different terms on the right-hand side of (28) have been grouped and labeled according to their physical origin, and the way they contribute to the turbulent kinetic energy. P_{ij}^Y represents turbulence production, as contraction yields two times the production of turbulent kinetic energy (14). The traceless term Π_{ij}^Y represents what we can call mean deformation energy transfer, and corresponds to the rapid pressure–strain term in the Reynolds stress equations. The nonlinear term π_{ij}^Y is also traceless, corresponding to slow pressure–strain in the Reynolds stress equations. ε_{ij}^Y and μ_{ij}^Y represent viscous and Joule dissipation, respectively.

Let $N_{ij} \equiv n_i n_j$. We take the time derivative of the definition (26), and insert (28) to obtain an evolution equation for α :

$$\frac{d\alpha}{dt} = P_{\alpha} + \Pi_{\alpha} + \pi_{\alpha} - \varepsilon_{\alpha} - \mu_{\alpha}, \tag{34}$$

where

$$P_{\alpha} = \frac{1}{2K} \left(N_{ik} P_{ki}^{Y} - 2\alpha P_{K} \right), \tag{35}$$

$$\Pi_{\alpha} = \frac{1}{2K} N_{ik} \Pi_{ki}^{Y},\tag{36}$$

$$\pi_{\alpha} = \frac{1}{2K} N_{ik} \pi_{ki}^{Y}, \tag{37}$$

$$\varepsilon_{\alpha} = \frac{1}{2K} \left(N_{ik} \varepsilon_{ki}^{Y} - 2\alpha \varepsilon \right), \tag{38}$$

$$\mu_{\alpha} = \frac{1}{2K} \left(N_{ik} \mu_{ki}^{Y} - 2\alpha \mu \right). \tag{39}$$

Earlier work [10, 11] described the modeling of the last three terms. The Joule destruction term μ_{α} was modeled with a simple linear expression, while the viscous term ε_{α} was absorbed in a "return-to-isotropy" model term, together with the nonlinear term π_{α} .

In the following we propose model expressions for the mean strain related terms P_{α} and Π_{α} .

3. Modeling

3.1. Modeling of P_{α} . The mean strain tensor $S_{ij} \equiv (U_{i,j} + U_{j,i})/2$ can replace $U_{i,j}$ in (29). The antisymmetric part, the mean rotation rate tensor $\Omega_{ij} \equiv (U_{i,j} - U_{j,i})/2$, is cancelled due to index symmetries of the integral. The production term P_{α} can be rewritten as

$$P_{\alpha} = \frac{1}{2K} \left(-2S_{ij}KF_{ji} - 2\alpha P_K \right), \tag{40}$$

where

$$F_{ij} = \frac{1}{K} N_{pq} \int \frac{k_p k_q}{k^2} \hat{\Phi}_{ij} d^3 \mathbf{k}. \tag{41}$$

The tensor F_{ij} appears also in the Joule dissipation tensor (23), which can be expressed as

$$\mu_{ij} = 2 \frac{\sigma B^2}{\rho} K F_{ij}. \tag{42}$$

Earlier papers [10, 11] proposed a bilinear tensor model for F_{ij} ,

$$F_{ij} = \frac{1}{K} \left(GR_{ij} + \frac{H}{2} [N_{ik}R_{kj} + N_{jk}R_{ki}] \right), \tag{43}$$

where G and H are scalar functions of α and tensor invariants. The same model can be reused here for P_{α} , without further assumptions. We use the third-order functions proposed in [11], as these behave well also near the 1D limit:

$$G(\alpha, I_{na}) = \alpha + \frac{27}{20}\alpha^2(1-\alpha)\left(I_{na} + \frac{2}{3}\right),$$
 (44)

$$H(\alpha) = -\frac{27}{10}\alpha^2(1-\alpha),\tag{45}$$

where $I_{na} = N_{ik}R_{ki}/K - 2/3$ is a tensor invariant. The behavior of (43) is discussed in more detail in [11].

We insert (43) into (40), together with the production of turbulent kinetic energy $P_K = -S_{ik}R_{ki}$, to get

$$P_{\alpha} = \frac{1}{2K} \left(-2GS_{ik}R_{ki} - 2HS_{im}N_{mk}R_{ki} - 2\alpha S_{ik}R_{ki} \right)$$

$$= -\frac{1}{K}S_{im}R_{ki} \left[(G + \alpha)\delta_{mk} + HN_{mk} \right].$$
(46)

3.2. Modeling of Π_{α} . We saw above that the single component of **Y** represented by the scalar α is enough to describe the effect of Joule dissipation. Unfortunately the other components of **Y** show up in the right-hand side of the α equation (34), through the mean deformation transfer term Π_{α} . The latter can be rewritten as

$$\Pi_{\alpha} = \frac{1}{K} \left(-U_{n,k} Y_{ni} N_{ik} + S_{in} A_{ni} \right), \tag{47}$$

where we have introduced the symmetric second-rank tensor

$$A_{ij} \equiv N_{nq} \int \frac{k_q k_n k_i k_j}{k^4} \hat{\Phi}_{pp} d^3 \mathbf{k}. \tag{48}$$

Note that $U_{i,j}$ in the last term of (47) has been replaced by S_{ij} , due to the index symmetry of **A**.

In the following we will assume that \mathbf{Y} is axisymmetric about the unit direction vector \mathbf{n} . This is a good approximation only when the magnetic effects are dominating, i.e., when the strain related terms are relatively weak. This is clearly a weakness in an attempt to model the strain terms. On the other hand, the assumption of axisymmetry about \mathbf{n} is consistent with the definition of α , which assumes there is a well-defined direction \mathbf{n} , presumably given by the orientation of the magnetic field.

According to invariant theory (see, e.g., [4]), any symmetric second-rank tensor D_{ij} which is axisymmetric about a vector \mathbf{n} can be expressed as

$$D_{ij} = d_1 \delta_{ij} + d_2 n_i n_j, \tag{49}$$

where d_1 and d_2 are scalar functions. **D** has only two independent principal components. As for the dimensionality tensor **Y**, its axial component is given by α , and we know the trace of **Y** is 2K. It is easily verified that the full axisymmetric tensor can then be expressed as

$$Y_{ij} = K(1 - \alpha)\delta_{ij} + K(3\alpha - 1)N_{ij}.$$
 (50)

The definition of \mathbf{A} (48) is rather similar to that of \mathbf{Y} , which suggest that the spectral information contained in the two tensors is related. We therefor assume that also \mathbf{A} is axisymmetric about \mathbf{n} , and that we can model \mathbf{A} in terms of α . The trace of \mathbf{A} is

$$A_{ii} = Y_{ik} N_{ki} = 2K\alpha. (51)$$

A dimensionally correct model expression is then

$$A_{ij} = 2K(f(\alpha)\delta_{ij} + [\alpha - 3f(\alpha)]N_{ij}), \tag{52}$$

where f is a scalar function of α .

When we insert (50) and (52) into (47), we get

$$\Pi_{\alpha} = -(1 - \alpha)U_{n,k}\delta_{ni}N_{ik} - (3\alpha - 1)U_{n,k}N_{ni}N_{ik}
+ 2f(\alpha)S_{in}\delta_{ni} + 2(\alpha - 3f(\alpha))S_{in}N_{ni}
= -6f(\alpha)S_{ik}N_{ki}
= g(\alpha)S_{ik}N_{ki}.$$
(53)

Here we have used the identities $\delta_{ik}N_{kj}=N_{ij}$, $N_{ik}N_{kj}=N_{ij}$, and $S_{ik}\delta_{ki}=S_{ii}=0$. The resulting expression is a scalar function of α , times the mean strain normal component in the direction of \mathbf{n} .

The rapid distortion analysis developed in the previous paper [11] can be reused here to study the behavior of Π_{α} in the axisymmetric case (see appendix for a description of the RDT equations). We assume an initially isotropic spectrum (with $\alpha = 1/3$), and let a magnetic forcing drive the spectrum towards the 2D limit, for which $\alpha = 0$, and "backwards" (although not physically realistic) towards the theoretical 1D limit, where $\alpha = 1$. This enables us to study Π_{α} (and $g(\alpha)$) for all permissible values of α . The solid line in Fig. 1 shows the RDT calculation of $\Pi_{\alpha}/S_{ik}N_{ki} = g(\alpha)$.

We would like a model expression for Π_{α} to be accurate for isotropic turbulence, and in the 2D limit, and as good as possible in between. We also wish the model to be correct in the 1D limit, to avoid unphysical values of α . This gives us three conditions for determining a model function $g(\alpha)$. With sufficient degrees of freedom, a model function could also be required to have accurate derivatives in one or two points, especially in the 2D limit, and in the isotropic state. Table 1 summarizes these conditions on $g(\alpha)$ and its derivative $g'(\alpha)$, with numerical values obtained from the RDT analysis.

The following fourth-order ansatz makes $g(\alpha) = 0$ in the 2D and 1D limits:

$$g(\alpha) = \alpha(1 - \alpha)(c_0 + c_1\alpha + c_2\alpha^2). \tag{54}$$

The remaining three conditions in Tab. 1 can be used to determine c_0 , c_1 and c_2 . A third-order model ($c_2 = 0$) can be designed to fix the value of g in the isotropic state, and fulfill *one* of the two derivative conditions. A second-order model ($c_1 = c_2 = 0$) is sufficient to fix the value of g at isotropy, but not to control the derivatives. This gives four alternative models for $g(\alpha)$, of different order, all of which give correct values of g in the three points in Tab. 1. Details of the models are listed in Tab. 2.

Table 1. Desired properties of the function $g(\alpha)$, and its derivate $g'(\alpha)$.

State	α	$g(\alpha)$	$g'(\alpha)$
2D	0	0	-14/5
Isotropic	1/3	-2/5	≈ 0.4286
1D	1	0	_

Model	$\{c_0,c_1,c_2\}$	Comment	
I	$\{-14/5, 5.29, -6.69\}$	4th order in α . Gradients correct	
		in 2D and isotropic states.	
IIa	$\{-14/5, -27/5, 0\}$	3rd order. Correct gradient in	
		2D limit.	
IIb	$\{-2.06, 0.77, 0\}$	3rd order. Correct gradient at	
		isotropy.	
III	$\{-9/5,0,0\}$	2nd order in α . No control of gra-	
		dients.	

Table 2. Desired properties of the function $g(\alpha)$, and its derivate $g'(\alpha)$.

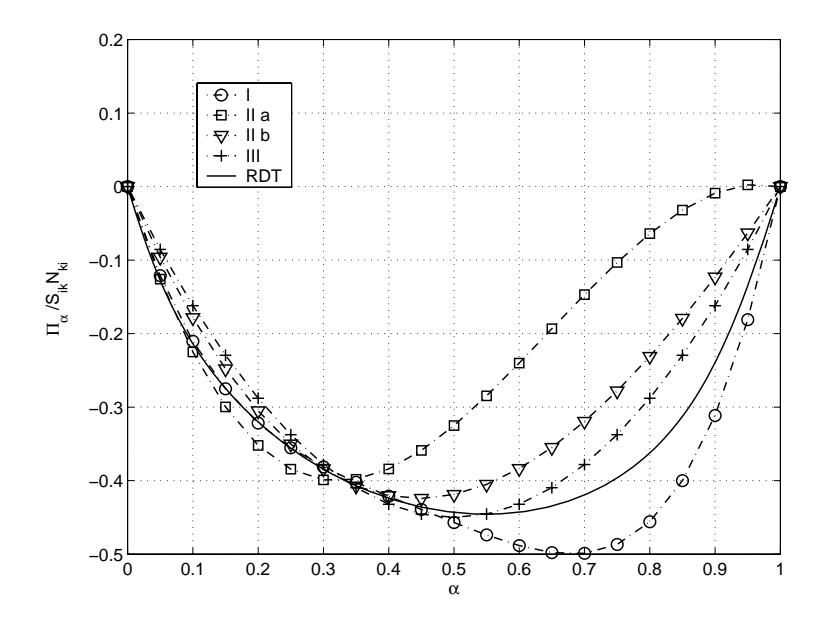


FIGURE 1. The four models in Tab. 2, compared with RDT results.

The four models are compared with RDT results in Fig. 1. The 2nd-order model probably gives the best overall performance. Only the 4th-order model is significantly better than the 2nd-order between the 2D and isotropic states, but at the cost of poor fit around $\alpha = 0.7$.

The 2nd and 3rd order models can all be parameterized in c_0 , which equals the derivate in the 2D limit, $c_0 = g'(0)$. We have

$$\Pi_{\alpha} = \alpha (1 - \alpha) \left[c_0 (1 - 3\alpha) - \frac{27}{5} \alpha \right] S_{ik} N_{ki}. \tag{55}$$

4. Results

We will illustrate the effect of the α strain terms in two simple channel flow examples. In both cases we have used a standard RST model [3], and an implementation of the MHD model equations in the commercial flow solver CFX 4.3 (see Widlund [9]).

4.1. Fully developed channel flow, without magnetic field. We consider the effect of the strain terms in a quadratic channel with fully developed flow (Re $\approx 10^5$), but without a magnetic field. The flow is in the x-direction, and we let **n** be in the transverse y-direction. Since there is no magnetic field, there is no physical reason for the dimensional changes to be aligned with **n**. The purpose of the test is to check the behavior of the model in regions of flow where the magnetic field is weak, or even absent; although the value of α does not affect the other equations in this case, we should still require that the model does not produce unphysical results, or cause a simulation to crash.

Figure 2 shows predicted profiles of α (top) and its source terms (bottom) in the center of the channel. The production term is positive near walls which are parallel with \mathbf{n} (Z/h=0), and negative near walls perpendicular to \mathbf{n} (Y/h=0). The production term P_{α} is balanced by the return term π_{α} , and the resulting value of α thus depends on the coefficient $C_{\alpha 2}$ in the return term. For the predictions in Fig. 2 we used $C_{\alpha 2}=1.0$, which gives $\alpha\approx0.5$ in the center of the channel. If instead $C_{\alpha 2}=0.2$, $\alpha\approx0.9$ in the channel center.

The transverse (and streamwise) mean strain normal components are zero in a fully developed channel flow, so that the modeled Π_{α} is zero when \mathbf{n} is in one of these directions. In the absence of a magnetic field, the orientation of the principal axes of the full tensor \mathbf{Y} would rather be determined by the mean velocity gradients, and the "pressure–strain" related term Π_{ij}^{Y} could be expected to play an important role, just as its counterpart in the Reynolds stress equations.

4.2. Channel flow with M-shaped velocity profile. Consider a 1 m long channel with flow in the x direction (see illustration in top-left pane of Fig. 3). The cross-section is 4×3 cm (in y and z directions, respectively). A transverse magnetic field is applied in the z direction, half-way along the channel. The length of the magnet is approximately 0.3 m. Based on channel half-width h = 0.02 m, the flow Reynolds number is $Re = 2 \cdot 10^5$, and the Hartmann number is Re = 700. The resulting bulk interaction parameter is Re = 2.45. This particular case has been studied experimentally by Tananaev [8], and has been subject to numerical simulations by Kenjereš & Hanjalić [2].

Figure 3 shows variable profiles of streamwise velocity, α , and budget of α source terms. The strain terms have an effect only near the wall. The change of α , and thus of the Joule dissipation, is about 10-15%. In the same region, however, the local interaction parameter can be shown to be well below one,

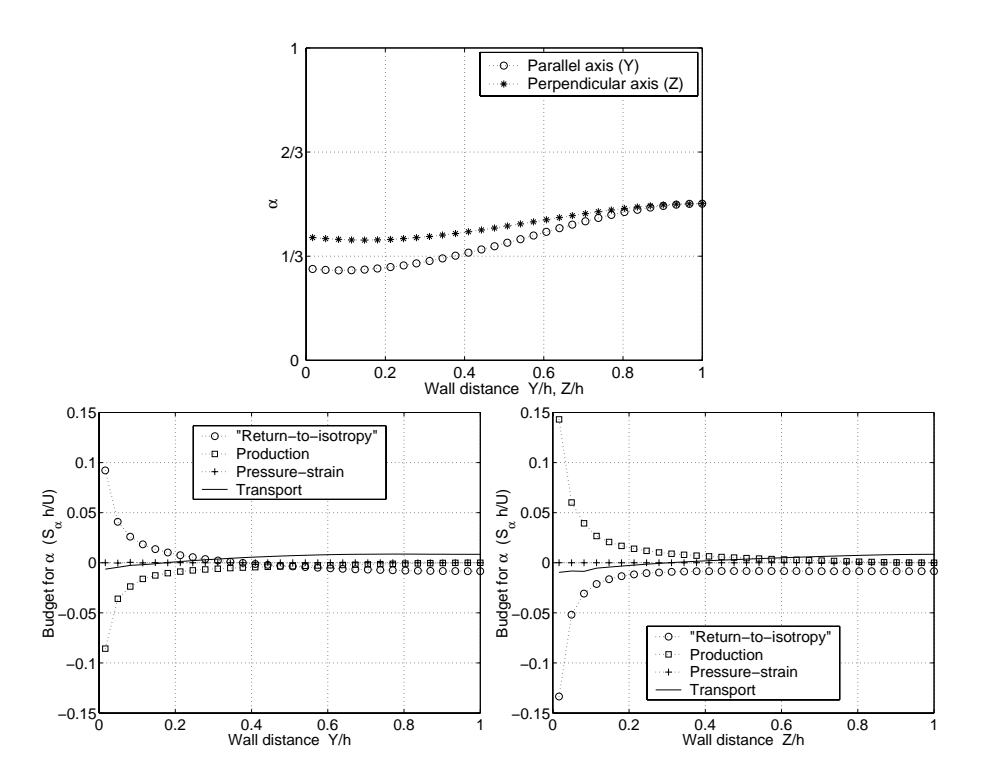


FIGURE 2. Fully developed quadratic channel flow, without magnetic field (Re \approx 1111). Channel half-width h, and mean velocity U. The unit direction vector ${\bf n}$ in the definition of α is in the transverse y direction. The plot at the top shows predicted profiles of α in the transverse directions, and plots below show the budget of α source terms.

and the viscous dissipation is 5-10 times larger than the Joule dissipation (not shown here; see [9] for details). The net effect of the α strain terms on turbulent kinetic energy is therefor very small.

As noted earlier, the modeled pressure–strain term (here model IIa of Tab. 2) is small in a developed channel flow, because the transverse normal component of mean strain is small. The MHD model coefficients in the simulation were $\{C_{\alpha 1}, C_{\alpha 2}, C_{\varepsilon \alpha}\} = \{0.86, 0.2, 0.5\}.$

5. Discussion and conclusions

The MHD turbulence models proposed by Widlund et al. [10, 11] include a transport equation for a dimensionality anisotropy variable, α . Apart from the magnetic and nonlinear effects discussed in earlier work, the α equation contains terms which describe the interaction with mean velocity gradients. The terms are related to the production of turbulent kinetic energy, and to the rapid pressure–strain rate correlation. For the case of homogeneous turbulence, these

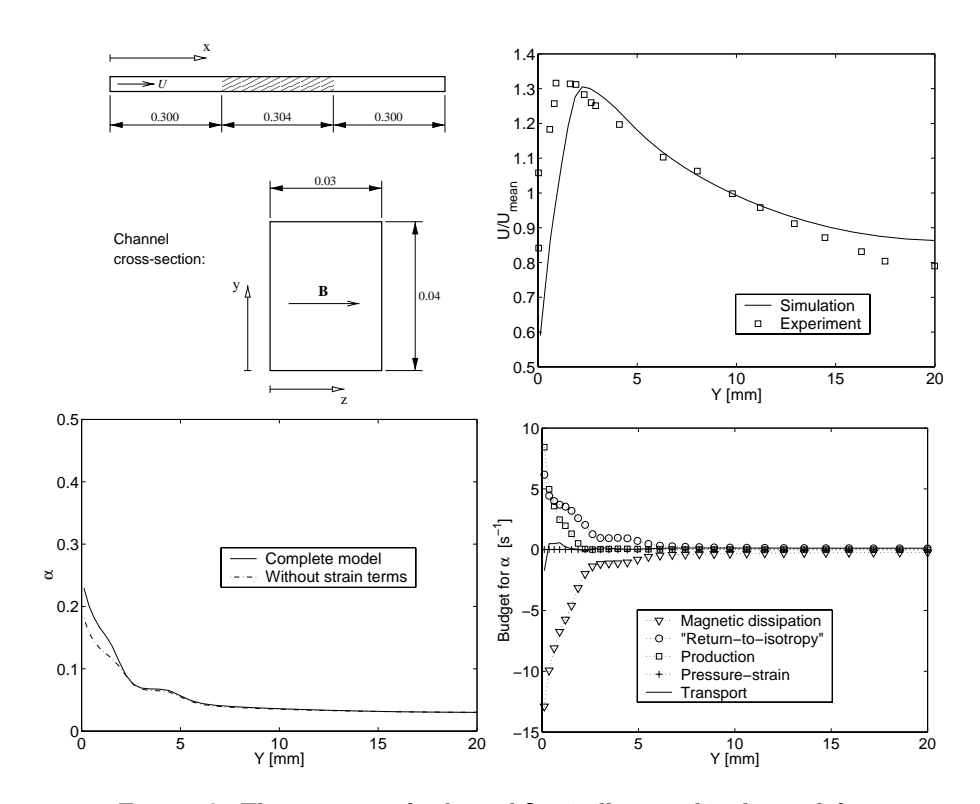


FIGURE 3. The geometry of a channel flow is illustrated in the top-left pane of the figure. The other panes show predicted variable profiles in the center of the magnet ($X=0.452~\mathrm{m},~Z=0.015~\mathrm{m}$). The top-right plot shows the M-shaped velocity profile. The lower-left plot shows predicted values of α , with and without the strain terms P_{α} and Π_{α} , and the lower-right shows a budget of α source terms in the same cross-section.

terms could be formulated based on the evolution equations derived for the full dimensionality tensor, \mathbf{Y} [11].

For modeling of the production term P_{α} , we could reuse the model tensor function developed in [10, 11] for modeling of the Joule dissipation tensor. No further assumptions were required.

The rapid pressure–strain term Π_{α} contains references to all components of the full \mathbf{Y} tensor, as well as to components of another second-rank tensor integral \mathbf{A} with similar structural information (presumably related to that in \mathbf{Y}). By assuming that both tensors are axisymmetric about the unit direction vector \mathbf{n} in the definition of α , the pressure–strain term could be modeled in terms of α and the axial component of the mean strain tensor. The assumption of axisymmetry about \mathbf{n} is a fair approximation when the effect of the magnetic field dominates

over mean strain effects. The axisymmetric rapid distortion equations described in [11] were used to study the properties of the exact term.

A consequence of the axisymmetry assumption is that only the axial mean strain normal component $S_{ij}n_jn_i$ enters the resulting model expression for the pressure–strain term Π_{α} . This component generally says very little about the mean velocity gradients. In a channel flow with a transverse magnetic field, for example, $S_{ij}n_jn_i$ is small, and we saw that the modeled Π_{α} is negligible. The part of \mathbf{Y} that would really interact with the mean velocity gradients in this situation, and contribute to Π_{α} , is the part which is not axisymmetric about \mathbf{n} . The proposed Π_{α} model term would be non-zero in expanding, or contracting flows. One example is the jets of liquid steel from the submerged inlet pipe in a continuous casting machine; with a transverse magnetic field, Π_{α} would presumably be negative. If we were to consider the purely hydrodynamic problem of axisymmetric flow expansion or contraction, e.g. in a wind tunnel contraction, and let \mathbf{n} be in the streamwise direction, the proposed model equation for α would probably predict the dimensional changes of the turbulence reasonably well.

A simulation of a channel flow with a transverse magnetic field showed that the strain terms have an effect only near the wall. The change of α , and thus of the Joule dissipation, is about 10-15%. The Joule dissipation is however much smaller than the viscous dissipation in this region, and the net effect on turbulent kinetic energy is therefor negligible.

To conclude, strain effects in the α equation appear to be significant only in regions where the interaction parameter is small, and Joule dissipation is small compared to viscous dissipation. In most practical MHD applications, it is probably appropriate to neglect effects of strain on dimensionality anisotropy, especially considering the algebraic complexity of the proposed model terms.

Appendix: Rapid distortion equations

For a detailed discussion, see Widlund et al. [11], or Schumann [7].

Assume that the magnetic interaction number is large $(N \gg 1)$, and that velocity gradients are small, so that the non-linear term and all terms containing $U_{i,j}$ can be neglected beside the magnetic and viscous terms. We further assume that the magnetic field is oriented in the x_3 -direction, so that the problem is axisymmetric about the z axis. The evolution of the spectral energy tensor is then described by

$$\frac{d}{dt}\hat{\Phi}_{ij}(\mathbf{k},t) = -2\nu k^2 \hat{\Phi}_{ij} - 2M \frac{k_3^2}{k^2} \hat{\Phi}_{ij}, \tag{56}$$

where $M = \sigma B^2/\rho$ (the inverse of the magnetic time scale). This is a linear system of uncoupled ordinary differential equations, which has the analytic solution

$$\hat{\Phi}_{ij}(\mathbf{k},t) = \hat{\Phi}_{ij}^{0}(\mathbf{k}) \exp\left[-2t\left(M\frac{k_3^2}{k^2} + \nu k^2\right)\right]. \tag{57}$$

We here assume the initial spectrum $\hat{\Phi}_{ij}^0(\mathbf{k})$ is isotropic,

$$\hat{\Phi}_{ij}^{0}(\mathbf{k}) = \frac{E(k)}{4\pi k^{2}} \left(\delta_{ij} - \frac{k_{i}k_{j}}{k^{2}} \right). \tag{58}$$

Introducing spherical coordinates, $\mathbf{k} = k(\sin\theta\cos\phi, \sin\theta\sin\phi, \cos\theta)$, all relevant one-point statistics and equation terms may now be obtained by spherical integration. It is convenient to separate out the radial integration over k; with axisymmetry about x_3 , this leaves only geometric tensor functions in θ to be evaluated.

The objective of the analysis is here to examine the behavior of certain tensor integrals for different shapes of the spectral energy distribution function, as characterized by $\alpha = Y_{33}/2K$. Regardless of initial energy distribution, the magnetic term in (56) will eventually drive the solution to a 2D state, for which the axial diagonal component $Y_{33} = 0$, so that $\alpha = 0$. We will here artificially extend the range of the analysis by allowing the magnetic deformation-rate parameter M in (56) to take negative values. This corresponds to an artificial forcing with the same structure as the magnetic force, but with opposite sign; the energy would grow exponentially, forcing the field to a 1D state with energy concentrated on the x_3 axis and $Y_{33} \to 2K$ ($\alpha = 1$).

The assumption that velocity gradients are small and can be excluded from (56) may seem to be in conflict with the objectives of the paper. Equation 57 is however used only to obtain axisymmetric spectral distributions with varying values of α . Different distortion mechanisms may well give energy spectra with the same α , but otherwise different properties. This is however not an issue here, since α is the only independent variable in the proposed model functions.

References

- [1] C. Cambon, L. Jacquin, and J. L. Lubrano. Toward a new Reynolds stress model for rotating turbulence. *Physics of Fluids A*, 4(4):812–824, 1992.
- [2] S. Kenjereš and K. Hanjalić. On the implementation of effects of Lorentz force in turbulence closure models. *Int. Journal of Heat and Fluid Flow*, 21(3):329–337, June 2000.
- [3] B. E. Launder, G. J. Reece, and W. Rodi. Progress in the development of a Reynolds-stress turbulence closure. *Journal of Fluid Mechanics*, 68:537–566, 1975.
- [4] J. L. Lumley. Stochastic Tools in Turbulence. Academic Press, New York, 1970.
- [5] William C. Reynolds. Effects of rotation on homogeneous turbulence. In Proc. 10th Australasian Fluid Mechanics Conference, Melbourne, Australia, 1989. University of Melbourne.
- [6] William C. Reynolds and S. C. Kassinos. One-point modelling of rapidly deformed homogeneous turbulence. Proceedings of the Royal Society of London, Series A, 451(1941):87–104, Oct 1995.

- [7] U. Schumann. Numerical simulation of transition from three- to twodimensional turbulence under a uniform magnetic field. *Journal of Fluid Mechanics*, 74:31–58, 1976.
- [8] A. B. Tananaev. MHD Duct Flows. Atomizdat, 1979.
- [9] O. Widlund. Implementation of MHD model equations in CFX 4.3. Technical Report TRITA-MEK 2000:10, Dept. of Mechanics, Royal Institute of Technology, Stockholm, Sweden, 2000. ISSN 0348-467X, ISRN KTH/MEK/TR-00/10-SE.
- [10] O. Widlund, S. Zahrai, and F. H. Bark. Development of a Reynolds stress closure for modeling of homogeneous MHD turbulence. *Physics of Fluids*, 10(8):1987–1996, 1998.
- [11] O. Widlund, S. Zahrai, and F. H. Bark. Structure information in rapid distortion analysis and one-point modeling of axisymmetric magnetohydrodynamic turbulence. *Physics of Fluids*, 12(10):2609–2620, 2000.

Paper 5

5

IMPLEMENTATION OF MHD MODEL EQUATIONS IN CFX 4.3

Ola Widlund

Faxén Laboratory Royal Institute of Technology Stockholm, Sweden

Abstract. This report documents an implementation of magnetohydrodynamic (MHD) model equations in the commercial flow solver CFX4.3. The implementation assumes a DC external magnetic field, which can be specified in user fortran, or read from a file. The code solves the Poisson equation for mean electrostatic potential. Great care has been taken to make the calculation of total electric current densities, and sources for the potential equations, accurate even on arbitrary non-orthogonal body-fitted multiblock grids. For modeling the effect of the magnetic field on turbulence, the implementation uses the MHD turbulence model proposed by Widlund et al. Both a full Reynolds stress model, and a three-equation model of $K-\varepsilon$ type are available. Commercial symbolic mathematics software was used to automate linearization, optimization and code generation for the often complex source terms in the turbulence model equations. The properties of the model implementation are demonstrated in a simulation of a 3D channel flow with "M"-shaped velocity profiles. The implementation of the new MHD turbulence models appear to be well-behaved and numerically robust. The MHD model implementation can be used together with standard CFX modeling options, such as heat and mass transfer, multiphase and multicomponent flows.

1. Introduction

This report documents the implementation of mean electromagnetic equations and magnetohydrodynamic (MHD) turbulence models in the commercial flow solver CFX 4.3.

The featured MHD turbulence models where developed by Widlund *et al.* [8, 7, 9] for modeling of Joule dissipation in simulations of continuous steel casting applications. The modeling approach is based on the formulation of a transport equation for a length scale anisotropy variable, α . The novel model can formulated either as a full Reynolds stress transport (RST) model, or as a three-equation K- ε - α model.

As for the mean equations, the external magnetic field is assumed to be steady, so that we need to solve only for the mean scalar electrostatic potential. We further assume the magnetic Reynolds number is low, so that the so-called quasistatic, or inductionless approximation is valid.

Also published as Technical Report TRITA-MEK 2000:10 (KTH, Stockholm, 2000).

There are several motives for this *CFX* implementation. First of all, we want to demonstrate that the new MHD turbulence models can be implemented in a commercial flow solver, and that the models are numerically robust and efficient enough to be useful for engineering MHD applications. Second, a complete 3D solver for complex geometries will be very useful in the work with validation of the new turbulence models. Finally, this work shows how existing in-house implementations of the mean equations in older versions of the code can be updated to work with complex multi-block non-orthogonal grids in *CFX* 4.3.

The following list summarizes the features of the MHD model implementation:

- User scalar equations for mean electrostatic potential EPOT (Φ) , and turbulence dimensionality anisotropy ALPHA (α) .
- Joule dissipation terms in both Reynolds stress, K, and ε equations, so that either the full RST MHD closure or the reduced three-equation K- ε - α closure can be used. Automatic detection of model type in user fortran.
- The mean strain terms in the α equation can be disabled.
- Mean electrostatic potential and total electric current densities are computed accurately even on multiblock non-orthogonal grids.
- The external magnetic field can be specified as constant and uniform in the command file, read from a separate text file, or specified in user fortran.
- Total current density and Lorentz force components are stored in user scalars for post-processing.
- Under-relaxation of Lorentz forces in the mean momentum equations (supported by standard command file options in *CFX* 4.3).
- Walls can be either non-conducting, or given a fixed electric potential.
- The electrical boundary conditions in flow inlets and outlets can be modified with options in the command file.
- The location of a zero reference point for electric potential can be specified in the command file.
- A number of MHD model options and model parameters are read from the end of the *CFX* command file when a simulation is started. This reduces the need for recompilation of the fortran source code.

The report is structured as follows: Section 2 introduces the governing equations, and the model equations. Section 3 describes how the model equations are discretized and implemented in the code. Some of the results obtained with the code so far are described in Section 4. Section 5 contains discussion and conclusions. Appendix A describes the various CFX and specific MHD model options specified in the CFX command file, while Appendix B provides details about the fortran routines used in the implementation. Appendix C lists a MAPLE script for linearization and coding of source terms, and App. D is a listing of a sample command file.

2. Theory and model equations

2.1. Governing equations. With spatial coordinates \mathbf{x} and time t, the Navier–Stokes equations for the instantaneous velocity field $u_i(\mathbf{x}, t)$ of an incompressible fluid are

$$\frac{\partial \rho u_i}{\partial t} + u_j \frac{\partial \rho u_i}{\partial x_j} = -\frac{\partial p}{\partial x_i} + \frac{\partial}{\partial x_j} \left(\mu \frac{\partial u_i}{\partial x_j} \right) + f_i, \tag{1}$$

$$\frac{\partial u_i}{\partial x_i} = 0, (2)$$

where $p(\mathbf{x}, t)$ is the pressure field, μ is the (molecular) dynamic viscosity ¹, and f_i is a body force (per unit volume). In the MHD problem at hand, the body force f_i in (1) corresponds to the magnetic Lorentz force.

The fluid is subjected to an external magnetic field, with magnetic flux density **B** (here in vector notation). The fluid flow will induce electrical currents in the fluid, and these in turn give rise to an induced magnetic field, which can be regarded as a perturbation of the external field. The relative size of this perturbation is governed by the dimensionless magnetic Reynolds number

$$Rm_L \equiv \eta \sigma u L, \tag{3}$$

where η is magnetic permeability, σ electrical conductivity, and u and L are characteristic velocity and length scales, respectively. In most industrial and laboratory flows, the magnetic Reynolds number is very low, $\mathrm{Rm}_L \ll 1$. The flow-induced magnetic field perturbations are then negligible beside the external field. Using this so-called quasistatic approximation, the non-relativistic Maxwell equations yield

$$\mathbf{f} \approx \mathbf{j} \times \mathbf{B}.$$
 (4)

The instantaneous electric current \mathbf{j} is given by Ohm's law,

$$\mathbf{j} \approx \sigma(\mathbf{e} + \mathbf{u} \times \mathbf{B}),$$
 (5)

where **e** is the electric field. The scalar electrostatic potential ϕ is defined by

$$\mathbf{e} = -\nabla \phi. \tag{6}$$

In the absence of free charges, the current field is divergence free. If the conductivity σ is assumed constant, the divergence of Ohm's law (5), together with (6), therefore yields

$$\nabla^2 \phi \approx \nabla \cdot (\mathbf{u} \times \mathbf{B}). \tag{7}$$

¹Not to be confused with the Joule dissipation μ introduced later

2.2. Reynolds averaged equations. A Reynolds decomposition is applied to split the instantaneous variables into mean and fluctuating parts. The mean of a quantity v is here defined as the ensemble average over an infinite number of realizations v_n ,

$$\langle v \rangle = \lim_{N \to \infty} \frac{1}{N} \sum_{n=1}^{N} v_n. \tag{8}$$

We use capital letters for mean values, and primes to denote fluctuating parts. The velocity is, for example, expressed as the sum $U_i + u'_i$, where U_i is the mean velocity, and u'_i is the velocity fluctuations. By definition the mean value of the fluctuation is zero.

Ensemble averaging of (1) and (2) gives the Reynolds averaged Navier–Stokes (RANS) equations, or the mean momentum equations,

$$\frac{\partial \rho U_i}{\partial t} + U_j \frac{\partial \rho U_i}{\partial x_j} = -\frac{\partial P}{\partial x_i} + \frac{\partial}{\partial x_j} \left(\mu \frac{\partial U_i}{\partial x_j} + \rho \left\langle u_i' u_j' \right\rangle \right) + F_i, \tag{9}$$

$$\frac{\partial U_i}{\partial x_i} = 0. ag{10}$$

Here F_i is the mean Lorentz force; see Sec. 2.3 below.

After Reynolds averaging, the transport equation for the mean Q of a passive scalar q = Q + q' is

$$\frac{\partial \rho Q}{\partial t} + U_j \frac{\partial \rho Q}{\partial x_j} = \frac{\partial}{\partial x_j} \left(\Gamma_Q \frac{\partial Q}{\partial x_j} + \rho \langle u_i' q' \rangle \right) + S_Q, \tag{11}$$

where S_Q is a volume source of the scalar, and Γ_Q is the molecular diffusivity of the scalar.

Turbulent velocity fluctuations contribute to the transport of the mean quantities through the turbulent Reynolds stresses $\rho \langle u'_i u'_j \rangle$ in (9), and the turbulent Reynolds flux $\rho \langle u'_i q' \rangle$ in (11), respectively. These turbulent correlations must be provided by a turbulence model of some kind (see Sec. 2.4).

2.3. Mean electromagnetic equations. We perform a Reynolds decomposition also of the Maxwell equations (4) through (7). The mean Lorentz force F_i in (9) is thus given by

$$\mathbf{F} = \mathbf{J} \times \mathbf{B}.\tag{12}$$

The mean electric current density is

$$\mathbf{J} = \sigma(-\nabla\Phi + \mathbf{U} \times \mathbf{B}). \tag{13}$$

The divergence of (13), together with the continuity condition $\nabla \cdot \mathbf{J} = 0$, yields

$$\nabla \cdot (\sigma \nabla \Phi) = \nabla \cdot (\sigma \mathbf{U} \times \mathbf{B}). \tag{14}$$

For constant conductivity σ , this reduces to the familiar Poisson equation

$$\nabla^2 \Phi = \nabla \cdot (\mathbf{U} \times \mathbf{B}). \tag{15}$$

The Lorentz force \mathbf{F} can be computed, if we first solve (14) with appropriate boundary conditions. If \mathbf{n} is an inward unit normal at the boundary, (13) yields the Neumann boundary condition

$$\frac{\partial \Phi}{\partial n} = -\frac{J_n}{\sigma} + \mathbf{n} \cdot (\mathbf{U} \times \mathbf{B}),\tag{16}$$

where $J_n = \mathbf{J} \cdot \mathbf{n}$ is the current into the domain. A non-conducting wall has zero normal current at the wall, $J_n = 0$. For a stationary wall with no-slip velocity boundary conditions, the boundary condition for Φ is then simply

$$\frac{\partial \Phi}{\partial n} = 0. \tag{17}$$

The formal solution to (14) with only Neumann boundary conditions contains an undetermined constant term. The electric potential must therefor be specified explicitly in at least one point in the domain. Alternatively, a fixed electric potential can be specified at one or more walls.

- **2.4. Conventional turbulence models.** The complete set of transport equations must be closed by providing models for the Reynolds stress and flux terms $\rho \langle u_i' u_j' \rangle$ and $\rho \langle u_i' q' \rangle$ appearing in the mean momentum and scalar equations (9) and (11). Common models can be put into two broad classes; eddy viscosity models, and Reynolds stress transport (RST) models. The most common eddy viscosity model is the K- ε model.
- **2.4.1.** Second moment RST model. A full Reynolds stress closure features transport equations for each of the six independent components of the Reynolds stress tensor $R_{ij} \equiv \langle u'_i u'_j \rangle$, complemented by a transport equation for scalar viscous dissipation, ε . The turbulent transport in the mean momentum equation (9) is thus accounted for without further modeling.

The Reynolds flux term in the scalar equation is usually modeled as

$$-\langle u_i'q'\rangle = \frac{C_s}{\sigma_Q} \frac{K}{\varepsilon} R_{ij} \frac{\partial Q}{\partial x_j},\tag{18}$$

where C_s is a model constant, and σ_Q is the turbulent Prandtl number for the scalar [1]. The use of the Reynolds stresses in this model makes the turbulent diffusion anisotropic. The transport equation (11) for the mean Q of a passive scalar becomes

$$\frac{\partial \rho Q}{\partial t} + U_j \frac{\partial \rho Q}{\partial x_j} - \frac{\partial}{\partial x_i} \left(\left[\Gamma_Q \delta_{ij} + \rho \frac{C_s}{\sigma_Q} \frac{K}{\varepsilon} R_{ij} \right] \frac{\partial Q}{\partial x_j} \right) = S_Q. \tag{19}$$

If we neglect molecular diffusion, the turbulence model equations are

$$\frac{\partial \rho R_{ij}}{\partial t} + U_k \frac{\partial \rho R_{ij}}{\partial x_k} - \frac{\partial}{\partial x_k} \left(\rho \frac{C_s}{\sigma_{RS}} \frac{K}{\varepsilon} R_{kl} \frac{\partial R_{ij}}{\partial x_l} \right) = \rho \left(P_{ij} + \Pi_{ij}^{(s)} + \Pi_{ij}^{(r)} - \varepsilon_{ij} \right) + S_{ij}^{RS},$$
(20)

$$\frac{\partial \rho \varepsilon}{\partial t} + U_{j} \frac{\partial \rho \varepsilon}{\partial x_{j}} - \frac{\partial}{\partial x_{j}} \left(\rho \frac{C_{s}}{\sigma_{\varepsilon}} \frac{K}{\varepsilon} R_{jk} \frac{\partial \varepsilon}{\partial x_{k}} \right) = \rho \left(C_{\varepsilon 1} \frac{\varepsilon}{K} P_{ii} / 2 - C_{\varepsilon 2} \frac{\varepsilon^{2}}{K} \right) + S_{\varepsilon}.$$
(21)

In the Reynolds stress equation (20), only the production term P_{ij} is exact, and all other terms require modeling. With the most common model (Launder, Reece & Rodi [3]), we have

$$P_{ij} \equiv -R_{ik} \frac{\partial U_j}{\partial x_k} - R_{jk} \frac{\partial U_i}{\partial x_k}, \tag{22}$$

$$\Pi_{ij}^{(s)} = -C_1 \frac{\varepsilon}{K} \left(R_{ij} - \frac{2}{3} K \delta_{ij} \right), \tag{23}$$

$$\Pi_{ij}^{(r)} = -\gamma \left(P_{ij} - \frac{2}{3} P_{kk} \delta_{ij} \right), \tag{24}$$

$$\varepsilon_{ij} = \frac{2}{3} \varepsilon \delta_{ij}. \tag{25}$$

Here (23) and (24) represent slow and rapid pressure–strain, while (25) is viscous dissipation. S_{ij}^{RS} is a source term due to the body force in the Navier–Stokes equations. The first two model terms in the right-hand side of the ε equation (21) represent production and viscous dissipation, respectively, while S_{ε} is a source term. The Reynolds stress model above has model constants $C_{\varepsilon 1}$, $C_{\varepsilon 2}$, C_{1} , C_{1} , C_{2} , C_{3} , C_{4} , C_{5} , C_{5} , and C_{5} .

Wall boundary conditions for the discretized equations are generally applied using wall functions. The mean velocity and the value of ε are then prescribed some distance from the wall, within the logarithmic region of the boundary layer. The Reynolds stress equations are solved assuming the wall-normal gradient is zero, and the source terms are evaluated in a way consistent with the wall law.

2.4.2. Eddy viscosity models. In eddy viscosity models, the Reynolds stresses are modeled using the so-called Boussinesq hypothesis, relating Reynolds stress anisotropy to the mean strain tensor:

$$-\rho \left\langle u_i' u_j' \right\rangle = -\frac{2}{3} \rho K \delta_{ij} + \mu_T S_{ij} \tag{26}$$

where μ_T is the turbulent viscosity, $K \equiv \langle u_i' u_i' \rangle / 2$ is the turbulent kinetic energy, and

$$S_{ij} \equiv \frac{1}{2} \left(\frac{\partial U_i}{\partial x_j} + \frac{\partial U_j}{\partial x_i} \right) \tag{27}$$

is the mean strain tensor.

The two-equation K- ε model contains transport equations for the turbulent kinetic energy K, and the viscous dissipation rate ε . The turbulent viscosity in (26) is given by a constitutive relationship,

$$\mu_T = C_\mu \rho \frac{K^2}{\varepsilon},\tag{28}$$

where C_{μ} is a model constant.

If (26) is inserted in (9), the mean momentum equation becomes

$$\frac{\partial \rho U_i}{\partial t} + U_j \frac{\partial \rho U_i}{\partial x_j} = -\frac{\partial P}{\partial x_i} + \frac{\partial}{\partial x_j} \left([\mu + \mu_T] \frac{\partial U_i}{\partial x_j} \right) + F_i. \tag{29}$$

In analogy with (26), we have the eddy diffusivity hypothesis which expresses the Reynolds flux as

$$-\rho \langle u_i' q' \rangle = \frac{\mu_T}{\sigma_Q} \frac{\partial Q}{\partial x_i},\tag{30}$$

where σ_Q is a turbulent Prandtl number. The mean scalar transport equation then takes the form

$$\frac{\partial \rho Q}{\partial t} + U_j \frac{\partial \rho Q}{\partial x_j} - \frac{\partial}{\partial x_j} \left(\left[\Gamma_Q + \frac{\mu_T}{\sigma_Q} \right] \frac{\partial Q}{\partial x_j} \right) = S_Q. \tag{31}$$

Neglecting molecular diffusion, the model transport equations for K and ε are (Launder & Spalding, [4])

$$\frac{\partial \rho K}{\partial t} + U_j \frac{\partial \rho K}{\partial x_j} - \frac{\partial}{\partial x_j} \left(\frac{\mu_T}{\sigma_K} \frac{\partial K}{\partial x_j} \right) = \rho \left(P_K - \varepsilon \right) + S_K, \tag{32}$$

$$\frac{\partial \rho \varepsilon}{\partial t} + U_j \frac{\partial \rho \varepsilon}{\partial x_j} - \frac{\partial}{\partial x_j} \left(\frac{\mu_T}{\sigma_{\varepsilon}} \frac{\partial \varepsilon}{\partial x_j} \right) = \rho \left(C_{\varepsilon 1} \frac{\varepsilon}{K} P_K - C_{\varepsilon 2} \frac{\varepsilon^2}{K} \right) + S_{\varepsilon}. \tag{33}$$

Here P_K is the turbulence production, which is modeled using the eddy viscosity hypothesis (26),

$$P_K \equiv \frac{P_{ii}}{2} \approx \frac{\mu_T}{\rho} S_{ij} S_{ji}. \tag{34}$$

 S_K and S_{ε} are source terms due to the body force in the Navier–Stokes equations (1). C_{μ} , $C_{\varepsilon 1}$, $C_{\varepsilon 2}$, σ_K and σ_{ε} are model constants.

In the standard high-Reynolds number version of the K- ε model, the treatment of wall boundary conditions is the same as for the Reynolds stress model (see above).

2.5. Models for MHD turbulence. The MHD turbulence models proposed by Widlund *et al.* [8, 7, 9] extend the conventional turbulence closures with a transport equation for a dimensionality anisotropy variable, α . The new scalar is then used to model Joule dissipation source (sink) terms for the K, ε and Reynolds stress equations. The model concept can be used either as a three equation K- ε - α model, or as a full Reynolds stress model.

The dimensionality anisotropy variable is defined in terms of the component of the Reynolds dimensionality tensor, Y_{ij} , which is parallel with the magnetic field. If n_i is a unit vector parallel with the magnetic field,

$$\alpha \equiv \frac{n_i n_j Y_{ji}}{2K}.\tag{35}$$

With this definition, the expression for scalar Joule dissipation of turbulent kinetic energy is exact for homogeneous turbulence,

$$\mu \equiv 2 \frac{\sigma B^2}{\rho} \alpha K. \tag{36}$$

The dimensionality tensor \mathbf{Y} was first introduced by Reynolds and co-workers to improve modeling of rapidly rotating turbulence [5]. Like the Reynolds stress tensor \mathbf{R} , \mathbf{Y} is a symmetric tensor with trace 2K, so that $0 \le \alpha \le 1$. For isotropic turbulence, $\alpha = 1/3$. The effect of a magnetic field is to decrease α towards the limit of 2D turbulence, where $\alpha = 0$. A low value of α means that the turbulent structures are very long in the direction of the magnetic field. In contrast, a value close to unity means that the structures are flat, and short in the direction of the field.

An exact equation for α can be derived from the Navier–Stokes equations [9], but all terms in the equation require modeling. The model equation for α implemented in this work can be written on the generic form (11), with a source term

$$S_{\alpha}/\rho = P_{\alpha} + \Pi_{\alpha}^{(r)} + \pi_{\alpha} - \mu_{\alpha}, \tag{37}$$

where

$$P_{\alpha} = -2G \frac{R_{ij}S_{ji}}{K} - 2H \frac{n_{i}n_{j}R_{jk}S_{ki}}{K} + \alpha \frac{R_{ij}S_{ji}}{K},$$
 (38)

$$\Pi_{\alpha}^{(r)} = 2\alpha \left(-\frac{3}{2}\alpha^2 + \frac{29}{10}\alpha - \frac{7}{5} \right) n_i n_j S_{ji},$$
(39)

$$\pi_{\alpha} = C_{\alpha 2} \frac{\varepsilon}{K} \left(\frac{1}{3} - \alpha \right), \tag{40}$$

$$\mu_{\alpha} = 2C_{\alpha 1} \frac{\sigma B^2}{\rho} \alpha^2. \tag{41}$$

The first two terms, (38) and (39), represent the effect of mean strain (production and rapid pressure–strain, respectively). π_{α} is a return-to-isotropy term, due to non-linear energy transfer, while μ_{α} is the Joule destruction term. S_{ij} is the mean strain tensor, and G and H are model functions defined below.

The modeling of the mean strain terms P_{α} and $\Pi_{\alpha}^{(r)}$ relies on the assumption that the full dimensionality tensor **Y** is axisymmetric about the magnetic field (see [9]). This is probably a rather poor assumption in regions where the magnetic field is weak, but there the value of α is not important. Wherever magnetic effects are strong, the strain terms are likely to play little role; considering

their algebraic complexity they can probably be neglected in most cases, to save computation time.

The current version of the MHD model assumes the underlying conventional turbulence model is of high-Reynolds number type, with wall function boundary conditions. The wall boundary conditions for the discretized α equation are defined in analogy with those normally used for K and the Reynolds stresses. The equation is dominated by a balance of its source terms near walls, and transport is negligible. We therefor assume zero normal gradient in the first cell $(d\alpha/dn=0)$, and evaluate the source terms as usual. There is currently no low-Re version of the MHD model.

Magnetic destruction terms for K, ε and the Reynolds stresses are put in the source terms of the respective equations (32), (33)/(21), and (20). We have (see [8, 9])

$$S_K/\rho = -\mu = -2\frac{\sigma B^2}{\rho}\alpha K,\tag{42}$$

$$S_{\varepsilon}/\rho = -\mu_{\varepsilon} = -2C_{\alpha 2} \frac{\sigma B^2}{\rho} \alpha \varepsilon, \tag{43}$$

$$S_{ij}^{(RS)}/\rho = -\mu_{ij} = -2\frac{\sigma B^2}{\rho} \left(GR_{ij} + \frac{H}{2} \left[n_i n_k R_{kj} + n_j n_k R_{ki} \right] \right),$$
 (44)

where

$$G(\alpha, I_{na}) = \alpha + \frac{27}{20}\alpha^2(1-\alpha)\left(I_{na} + \frac{2}{3}\right),$$
 (45)

$$H(\alpha) = -\frac{27}{10}\alpha^2(1-\alpha),\tag{46}$$

$$I_{na} \equiv \frac{n_i n_k R_{ki}}{K} - \frac{2}{3}.\tag{47}$$

3. Model implementation

3.1. Electric potential equation. The generic user scalar transport equation available in CFX can be reduced to a Poisson equation by defining the scalar as quasistatic (to disable the transient term) and disabling the convection term (one option in selecting differencing scheme). With the eddy diffusivity hypothesis, the resulting model equation for mean electric potential then takes the form

$$-\frac{\partial}{\partial x_{j}} \left(\left[\Gamma_{\Phi} + \frac{\mu_{T}}{\sigma_{\Phi}} \right] \frac{\partial \Phi}{\partial x_{j}} \right) = S_{\Phi}. \tag{48}$$

To obtain the desired results, we must cancel the turbulent contribution to the total diffusivity in (48). We do this by setting the total diffusivity explicitly in the user subroutine USRDIF. The actual value used is unimportant, but the same value must of course be used when the source term S_{Φ} is computed. Here we use the value for the electric conductivity specified in the command file, $\Gamma_{\Phi} = \sigma$.

For consistency with (15), the source term S_{Φ} in (48) must be

$$S_{\Phi} = -\nabla \cdot (\Gamma_{\Phi} \mathbf{U} \times \mathbf{B}). \tag{49}$$

When (48) is integrated over a control volume, we use Gauss' theorem to rewrite the volume integral of the source as a surface integral,

$$\int S_{\Phi} dV = -\int \nabla \cdot (\Gamma_{\Phi} \mathbf{U} \times \mathbf{B}) dV$$
$$= -\int \Gamma_{\Phi} (\mathbf{U} \times \mathbf{B}) \cdot d\mathbf{A}.$$

In its discretized form, this is a sum over the faces f of a grid cell,

$$\int S_{\Phi} dV = S_{\Phi} V_{cell}$$

$$= -\sum_{f} \Gamma_{\Phi} (\mathbf{U}_{f} \times \mathbf{B}_{f}) \cdot \mathbf{A}_{f},$$

so that

$$S_{\Phi} = -\frac{1}{V_{cell}} \sum_{f} \Gamma_{\Phi} (\mathbf{U}_f \times \mathbf{B}_f) \cdot \mathbf{A}_f.$$
 (50)

Here \mathbf{U}_f and \mathbf{B}_f are interpolated values of \mathbf{U} and \mathbf{B} at the faces, and \mathbf{A}_f is the outward normal area vector of the face. This approach guarantees conservation of source current, and it is consistent with the calculation of total current density described in Sec. 3.2.

Walls are generally assumed to be non-conducting, in which case zero normal flux boundary conditions should be specified for electrostatic potential. Alternatively, a fixed potential is specified at the wall. If only zero flux boundary conditions are used, the electrostatic potential is not uniquely defined. The potential must be known in some point in the domain. An MHD model option can be read from the command file to define Cartesian coordinates for a reference point in the domain where the electrostatic potential is forced to zero (see App. A.2).

All inlet boundaries in CFX use Dirichlet boundary conditions for user scalars. The same is true if we have inflow through pressure and mass flow boundaries. Unless we want these boundaries to have fixed potentials, the behavior can be modified with MHD model options read from the command file, causing the flow boundaries to behave as if they were electrically insulating (see App. A.2). This is achieved by evaluating the source term (50) with $\mathbf{U} \times \mathbf{B} = 0$ on cell faces at the flow boundaries, and setting the corresponding diffusion coefficient to zero when the potential equation is solved.

3.2. Total current density and Lorentz force. The total current density is

$$\mathbf{J} = -\sigma \nabla \Phi + \sigma \mathbf{U} \times \mathbf{B}. \tag{51}$$

The two terms on the right-hand side are of the same order, and the total current density is often a small difference between them. Near an isolated wall, for example, the two terms must balance almost completely for the wall-normal current to be zero. A second-order accurate calculation of the potential gradient in a cell P can be interpreted as the average of the first-order gradients evaluated at the cell faces. To achieve the required accuracy of the total current density, it is essential that we compute the $\mathbf{U} \times \mathbf{B}$ term in a similar manner. It should therefor be computed as the average of $(\mathbf{U} \times \mathbf{B})_f$ at the cell faces.

To describe the calculation of the $\mathbf{U} \times \mathbf{B}$ term for general body-fitted grids, we need to discuss briefly the general non-orthogonal coordinate system used in CFX.

We first introduce the Cartesian physical space coordinates x^i , and the general non-orthogonal computational space coordinates ξ^i . The computation space system is such that grid cells have unit volume and edges of unit length in terms of computational coordinates. The two systems are related through the Jacobian matrix J^i_j , and the inverse Jacobian matrix \bar{J}^i_j ,

$$J_j^i \equiv \frac{\partial x^i}{\partial \xi^j},\tag{52}$$

$$\bar{J}_{j}^{i} \equiv \frac{\partial \xi^{i}}{\partial x^{j}}.$$
 (53)

We also define the Jacobian determinant

$$|J| \equiv \det\left(J_j^i\right). \tag{54}$$

In any point in the curvilinear coordinate system (ξ^i) , we can define two frames of basis vectors:

$$\mathbf{e}_{(i)} = \frac{\partial \mathbf{x}}{\partial \xi^i}$$
 (tangent to coordinate curves), (55)

$$\mathbf{e}^{(i)} = \frac{\partial \xi^i}{\partial \mathbf{x}}$$
 (normal to coordinate surfaces). (56)

These are the *covariant* and *contravariant* basis vectors, respectively. Any Cartesian vector $\mathbf{V} = (V_i)$ has two sets of components with respect to these basis vectors:

$$\mathbf{V} = V^{\prime i} \mathbf{e}_{(i)} = V^{\prime}{}_{i} \mathbf{e}^{(i)}, \tag{57}$$

where V'^i and V'_i are the contravariant and covariant components of \mathbf{V} , respectively. The two sets of basis vectors are dual to each other, which means that

$$\mathbf{e}^{(i)} \cdot \mathbf{e}_{(j)} = \delta^i_j. \tag{58}$$

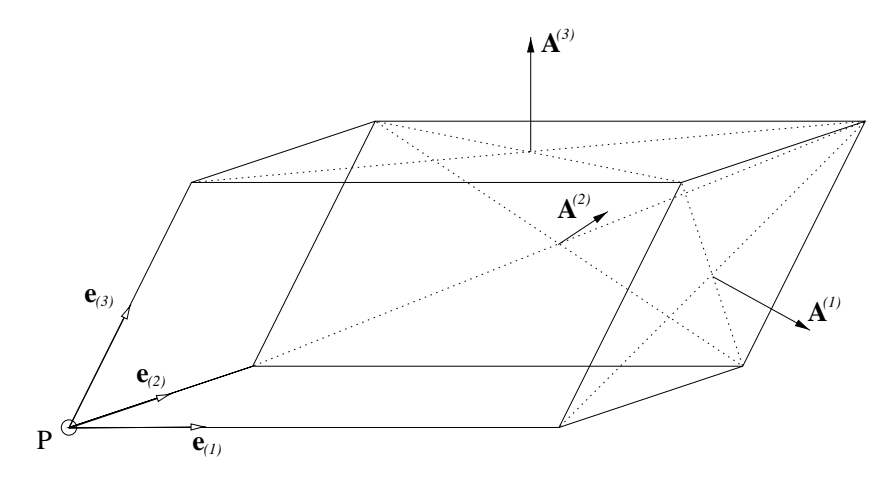


FIGURE 1. The covariant basis vectors in a point P generates a parallelepiped. Area vector are normal to the faces, with magnitude equal to the face area.

¿From (57) it then follows that the scalar product of a basis vector with the Cartesian vector produces the corresponding components,

$$V^{i} = \mathbf{V} \cdot \mathbf{e}^{(i)}, \tag{59}$$

$$V_i' = \mathbf{V} \cdot \mathbf{e}_{(i)}. \tag{60}$$

The two sets of basis vectors can be given a geometric interpretation. Let Ω be denote a parallelepiped generated by the covariant basis vectors $\mathbf{e}_{(i)}$. Let $\mathbf{A}^{(i)}$ be area vectors, i.e., vectors normal to the faces of Ω with magnitude equal to the area of the faces. See Fig. 1. Area vectors are given by

$$\mathbf{A}^{(1)} = \mathbf{e}_{(2)} \times \mathbf{e}_{(3)}, \quad \mathbf{A}^{(2)} = \mathbf{e}_{(3)} \times \mathbf{e}_{(1)}, \quad \mathbf{A}^{(3)} = \mathbf{e}_{(1)} \times \mathbf{e}_{(2)},$$
 (61)

and the volume of Ω is

$$vol(\Omega) = \mathbf{e}_{(1)} \cdot \mathbf{e}_{(2)} \times \mathbf{e}_{(3)} = |J|. \tag{62}$$

This is often called the infinitesimal volume element; in CFX the notation $\sqrt{g} = vol(\Omega) = |J|$ is used.

¿From the above we can express the contravariant basis vectors in terms of the area vectors and the infinitesimal volume element,

$$\mathbf{e}^{(i)} = \frac{\mathbf{A}^{(i)}}{|J|}.\tag{63}$$

In CFX, both face area vector $\mathbf{A}^{(f)}$ (positively oriented in computational space) and the facial volume element \sqrt{g}_f is stored, so the contravariant basis vector normal to each face f is given by (63),

$$\mathbf{e}^{(f)} = \frac{\mathbf{A}^{(f)}}{\sqrt{g}_f}.\tag{64}$$

The covariant basis vector at a cell face is given by the vector between the cell centers P and Q on either side,

$$\mathbf{e}_{(f)} = d\mathbf{x}_f = \mathbf{x}_Q - \mathbf{x}_P \tag{65}$$

(assuming Q is located towards positive computational coordinates, relative to P).

Let us now return to the calculation of the $\mathbf{U} \times \mathbf{B}$ term in (51). For a more compact notation, let

$$\mathbf{Z} = \mathbf{U} \times \mathbf{B}.\tag{66}$$

Using the weight factors stored in CFX, we interpolate **U** and **B** to cell faces, and compute \mathbf{Z}_f at cell faces. The contravariant component in the face normal direction is

$$Z'_{(f)} = \mathbf{Z} \cdot \mathbf{e}_{(f)} = \mathbf{Z} \cdot d\mathbf{x}_f. \tag{67}$$

The vector \mathbf{Z}_P in the center of cell P is now redefined as the average of the contravariant components at the cell faces,

$$\mathbf{Z}_{P} = \sum_{f} W_{P}^{(f)} Z_{(f)}' \mathbf{e}^{(f)}$$
 (68)

$$= \sum_{f} W_{P}^{(f)} Z_{(f)}' \mathbf{A}^{(f)} / \sqrt{g}_{f}. \tag{69}$$

The weight factor in the averaging is one half, $W_P^{(f)} = 1/2$.

In the special case where the grid is orthogonal, the contravariant and covariant basis vectors are parallel, $\mathbf{e}_{(i)} \parallel \mathbf{e}^{(i)}$. ¿From (63) and (58) then follows that

$$\mathbf{e}_{(f)} = \frac{\sqrt{g}_f}{A_f^2} \mathbf{A}^{(f)},\tag{70}$$

where $A_f = |\mathbf{A}^{(f)}|$ is the face area. If this inserted in (67) and (68), we get

$$\mathbf{Z}_{P} = \sum_{f} W_{P}^{(f)} \hat{Z}^{(f)} \mathbf{A}^{(f)} / A_{f}^{2}, \tag{71}$$

where $\hat{Z}^{(f)} = \mathbf{Z}_f \cdot \mathbf{A}^{(f)}$ is the normal flux component we used for computing the source term for the electrostatic potential equation. This was stored in memory, and can be reused for computing the total current in the orthogonal case.

To compute the total current density, we also need to compute the gradient of electrostatic potential. We use the built-in CFX subroutine GRADS for this. This routine however does not compute the correct gradient in cells adjacent to wall boundaries. The gradients in cells next to walls, inlets, pressure boundaries and massflow boundaries are therefor recomputed after the call to GRADS (see App. B.10). If the MHD model options for insulated inlets/outlets are invoked, this affects both the calculation of potential gradient, and the $\mathbf{U} \times \mathbf{B}$ term at

the boundaries, in a way consistent with zero total current through the flow boundary (see App. B).

With total current density computed with (51), the mean Lorentz force is given by $\mathbf{F}_L = \mathbf{J} \times \mathbf{B}$. *CFX* supports under-relaxation of body forces in the command file. The Lorentz forces can be switched off completely with a MHD model option read from the command file.

3.3. Dimensionality anisotropy. In the CFX implementation, α is assigned a user scalar equation of the generic form (11). Source terms are linearized so that, for the source in a cell P, the source term for a scalar Q can be written

$$S = S_U + S_P Q_P. (72)$$

Source terms proportional to the variable itself should be put in S_P if they are negative, since they will then enhance the diagonal dominance of the solution matrix and improve convergence and robustness.

The symbolic mathematics engine MAPLE V was used to manipulate the source terms, and translate the model expressions presented above into fortran source code (see App. C). This procedure reduces the risk for programming errors, and simplifies debugging. The procedure was as follows:

- 1. The source term model expression is expanded into component form and simplified.
- 2. The resulting expressions are evaluated term by term, sorting them into S_U or S_P . A proportional term is put into S_P if it is guaranteed to be negative, and into S_U otherwise. The sign of the term is determined by MAPLE, assuming that K and ε are positive, α is between zero and one, and all other variables and constants are real.
- 3. Names of variables and parameters are substituted for those used in CFX, and the expressions for S_U and S_P are automatically optimized and translated into fortran source code.
- 4. The automatically generated source code is included in the appropriate user fortran routine.

The mean velocity gradients used in P_{α} and $\Pi_{\alpha}^{(r)}$ are computed using the built-in CFX subroutine GRADV. As far as we can tell, the gradients obtained next to the walls are consistent with those used to compute the turbulence production and pressure–strain terms in the standard turbulence equations. If the user has selected the K- ε model, the Reynolds stresses in P_{α} and $\Pi_{\alpha}^{(r)}$ are substituted by the Boussinesq hypothesis (26). The two strain terms contain the unit direction vector of the magnetic field, \mathbf{n} , which is undefined if $\mathbf{B} = 0$. In this case, the code uses $\mathbf{n} = \mathbf{e}_z$ to avoid numerical errors. Note however, that if there is no preferred direction of length scale anisotropy, the only physically relevant value for α would be the isotropic value of 1/3. The mean strain terms P_{α} and $\Pi_{\alpha}^{(r)}$ can be switched off with an MHD model option in the command file, to reduce the computational effort.

3.4. Turbulence equations. The fortran code for the source terms in the turbulence equations is automatically generated, with the same procedure described above for the source terms of the α equation.

All magnetic source terms in the standard turbulence equations can be switched off with an MHD model option in the command file.

4. Results

4.1. Calculation of currents on non-orthogonal grids. The calculation of total current on non-orthogonal grids is demonstrated in the following simple 2D case. The electric potential and total current are computed in a box with side L, with fixed zero potential boundary conditions on all sides. We assume a uniform velocity field through the domain, from left to right, and solve only the electric potential equation. The magnetic field distribution is cone shaped, localized inside a circle of radius 0.14L, and the field orientation is perpendicular to the plane. This induces currents $\sigma \mathbf{U} \times \mathbf{B}$ directed downwards inside the magnetic field, and a counteracting electric potential which causes the currents to close outside the magnetic field.

In Fig. 2 we compare results computed on one uniform rectangular grid, and one non-orthogonal grid with badly distorted grid cells. Both grids have 50×50 grid cells. The distortion and the uneven distribution of grid cells cause a slight asymmetry of both electric potential and current distribution on the non-orthogonal grid, but the results are otherwise consistent. In contrast, the lower right plot shows what happens if we compute the total current on the skewed grid as if it was rectangular. The accuracy of the term $\mathbf{U} \times \mathbf{B}$ is then very poor, and we get a large false horizontal current component inside the magnetic field.

The non-orthogonal grid above was constructed of two 50×25 blocks. This enabled us to use the same simple test case to verify that the algorithms for electrostatic potential and total current work for multiblock grids with orientation changes at block boundaries.

4.2. Channel flow with "M" profiles. The following simulation of a channel flow considers the same geometry as the mercury experiment by Tananaev [6] (also studied numerically by Kenjereš and Hanjalić [2]). The flow is subjected to a localized transverse magnetic field, as illustrated in Fig. 3 (the region of the magnetic field is shaded). In terms of the channel half-width h=0.020 m, the channel Reynolds number is $\text{Re}=Uh/\nu=2\cdot 10^5$, the Hartmann number $\text{Ha}=\sqrt{\sigma/(\rho\nu)}Bh=700$, and the interaction number $N=\text{Ha}^2/\text{Re}=2.45$.

The most striking effect of the magnetic field is the development of an "M"-shaped velocity profile. This is caused by the distribution of mean Lorentz forces in the entry to the magnet, and it is enhanced further in the magnet exit.

The Joule dissipation of turbulence in the magnetic field reduces the turbulent viscosity, but the reduction of turbulence is visible only as a secondary effect on the mean velocity profiles. Unless we have measured turbulent statistics to

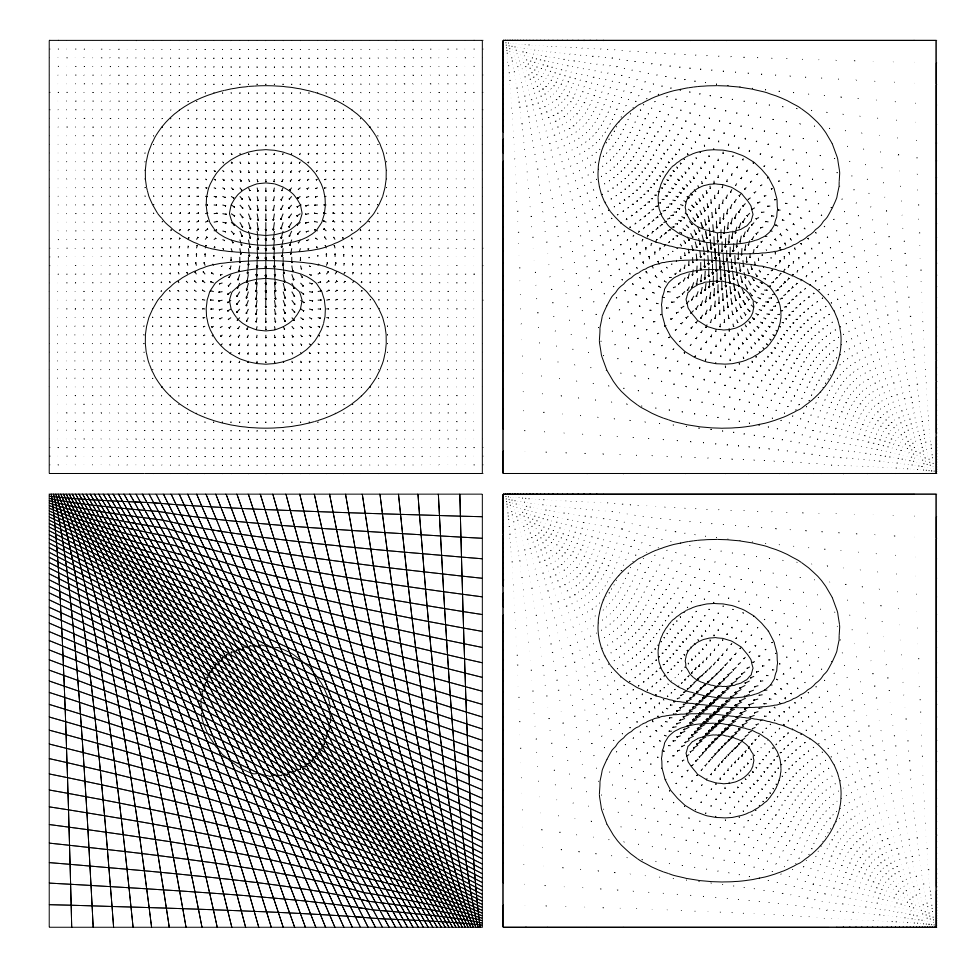


FIGURE 2. The top two figures show contours of electrostatic potential and vectors of total current for a uniform rectangular grid (left), and a non-orthogonal grid (right). The non-orthogonal grid and the region of the magnetic field is shown in the lower left plot. The lower right plot, finally, shows what happens if we try to compute the total current as if the grid was rectangular (assuming contravariant and covariant basis vectors are parallel). Note that the current here has a false horizontal component inside the magnetic field.

compare with, the dominating effect of the mean Lorentz forces makes this experimental configuration a less than ideal test case for MHD turbulence models. Nevertheless, it serves here as an illustration of how the MHD model implementation works, and a chance to look at the behavior of the MHD turbulence models in a wall-bounded 3D flow.

The number of grid cells used in the channel cross-section was 59×39 (largest in the y direction), and 65 in the streamwise direction. The grid was stretched

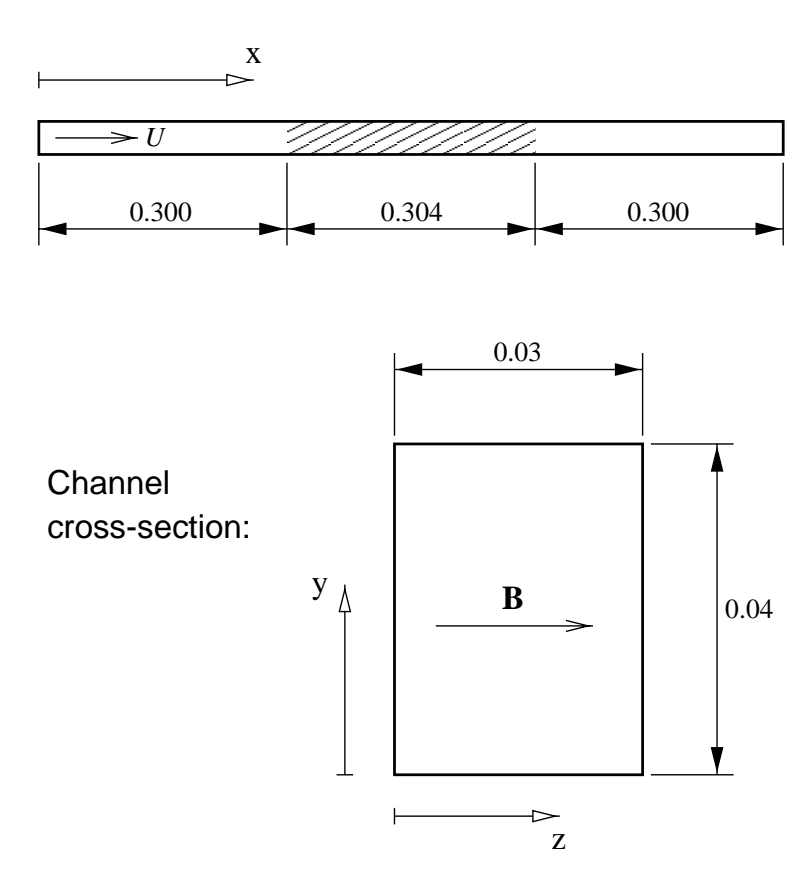


Figure 3. Geometry of the channel flow.

to give the highest resolution close to walls, and in the entry and exit of the magnet.

All walls were assumed non-conducting, and the inlet and downstream pressure boundary defined as electrically insulated. We used standard turbulent wall functions, with y^+ in the range 50 to 80 inside the magnet.

Four different simulations were performed, with different turbulence models. See Table 1. In all cases, the model constants were $\{C_{\alpha 1}, C_{\alpha 2}, C_{\varepsilon \alpha}\} = \{0.866, 0.2, 0.5\}.$

Figure 4 shows the velocity profile in the center of the channel, and in the center of the magnet. The width of the wall jet predicted by the MHD models is in good agreement with experiments. With the standard K- ε model, turbulent diffusion is over predicted, and the velocity peak is "smeared out". All simulations locate the velocity peak too far from the wall. Assuming the experimental data is reliable, there is currently no obvious explanation for this. The trend is the same for both MHD models and the standard K- ε . It may be a result of the standard wall functions we used in the simulation. We are also aware

Case	Model	Description
A	K - ε - α	Three-equation MHD model (no strain terms in α
		equation).
В	RST- α	MHD Reynolds stress model (no strain terms in α
		equation).
C	RST- $\alpha(S)$	Complete MHD Reynolds stress model, including
		strain terms in α equation.
D	Std K - ε	Standard model (no MHD terms).

Table 1. Description of channel flow simulations.

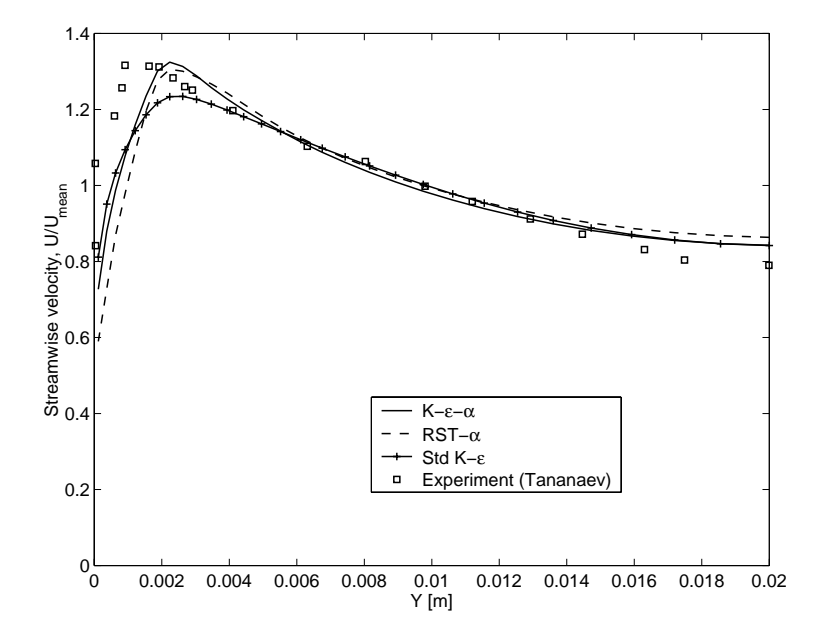


FIGURE 4. Mean velocity profiles in the center of the magnet. Lines show model predictions, and square symbols show experimental data (Tananaev [6]) for comparison.

that certain inhomogeneous contributions to the Joule dissipation near walls are currently not accounted for in the MHD models. Figure 5 shows vectors of total current, and contours of electric potential, in the entry of the magnet. Figure 6 shows contours of the x-component of the Lorentz force in the same region, together with the mesh. The grid resolution in the streamwise direction is rather poor, and one might suspect that the strong gradients of total current and Lorentz forces in the entry of the magnet are not resolved properly, and that this could be a source of error. However, a test with three times more grid cells in the streamwise direction in the entry of the magnet did not affect the location of the velocity maximum.

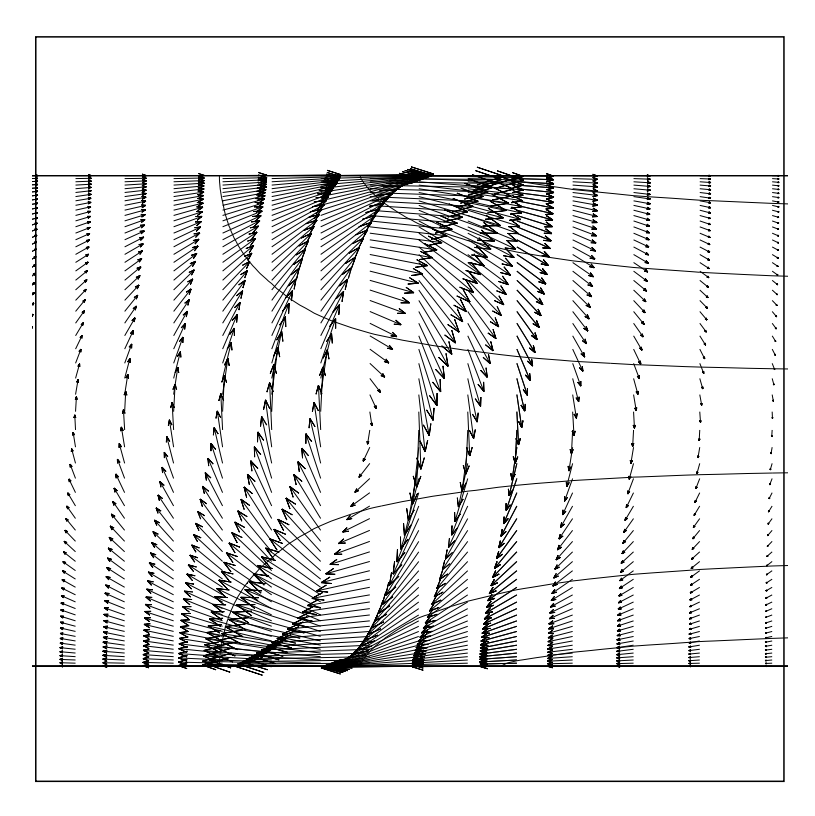


FIGURE 5. Vectors of total current, and contours of electric potential in the entry of the magnet $(K-\varepsilon-\alpha \text{ model})$.

Figure 7 shows K, ε and μ in the center of the magnet, as predicted by the K- ε - α model. The results with the standard K- ε model are shown for comparison. In the core flow, the MHD model predicts K and ε values about two orders of magnitude smaller than the standard model, but close to the wall the difference is small. This is because the turbulence production and viscous dissipation dominates over Joule dissipation close to the wall. A local interaction number $N_{loc} = \sigma B^2 K/(\rho \varepsilon)$ is of order 10 or larger outside the velocity peak, but drops off to below unity when we approach the wall (not shown here).

Figure 8 compares predictions of turbulent kinetic energy in the center of the magnet, as predicted by the different models (Tab. 1). We see it makes little difference whether we include the strain terms in the α equation, or neglect them (models RST- α (S) and RST- α , respectively). As expected, all MHD models predict lower energy than the standard K- ε model, but there is also a significant difference between the three equation K- ε - α and the RST- α models. The difference between the two is that the production term in a Reynolds stress model is exact, but it is modeled using the Boussinesq hypothesis in the K- ε model. The Boussinesq hypothesis relates the Reynolds stress anisotropy to the mean strain

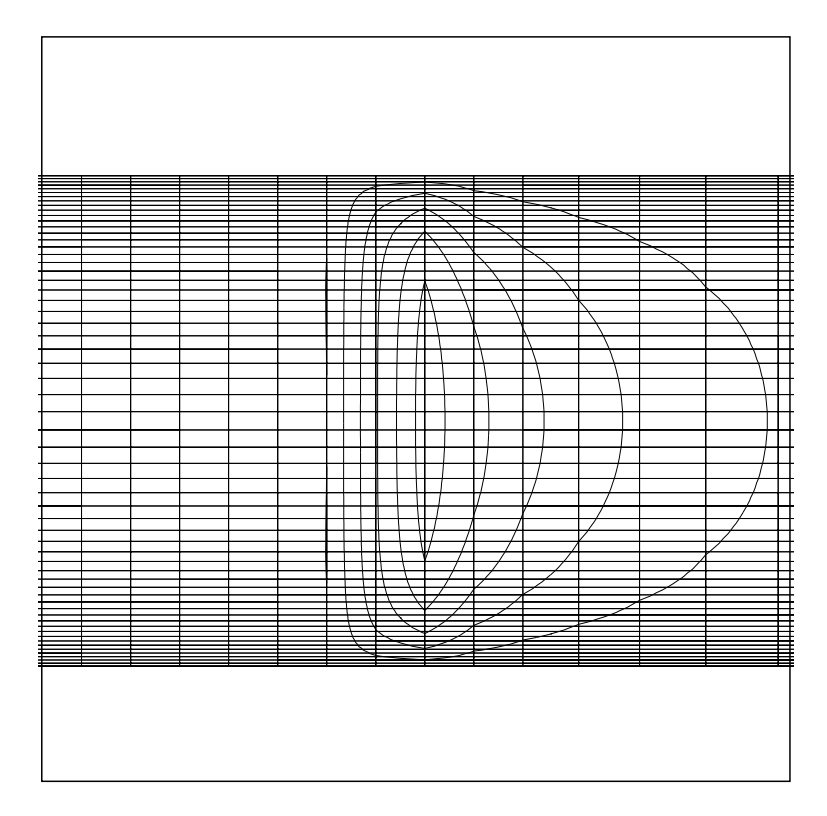


FIGURE 6. Contours of Lorentz force, together with the mesh in the same plane, in the entry of the magnet $(K-\varepsilon-\alpha \text{ model})$.

tensor. This is often a good approximation in ordinary shear flows, but in MHD flows it neglects the effect of Joule dissipation on the stress anisotropy.

The Reynolds stresses predicted by the RST- α model in the center of the magnet are plotted in Fig. 9 (normalized with the turbulent kinetic energy). The plotted cross-section is in the mid plane of the channel (z=0.015), so the only non-zero shear stress is $\langle u'v' \rangle$. The effect of the anisotropic Joule dissipation dominates in the center of the channel, which causes the component $\langle w'w' \rangle$ parallel with the magnetic field to be larger than the other normal stresses. This behavior is typical for Joule dissipation of homogeneous turbulence, for which the current model works well. In wall-bounded flows, however, the model neglects certain inhomogeneous contributions to the Joule dissipation tensor, and to the pressure–strain terms in the Reynolds stress equations. The effect of these contribution would presumably be to redistribute energy from the field-parallel component into the other components, to force the turbulence field towards a 2D and two-component (2C) state.

The left pane in Fig. 10 shows the profile of α predicted by the different models in the center of the magnet, while the right pane shows the budget of α

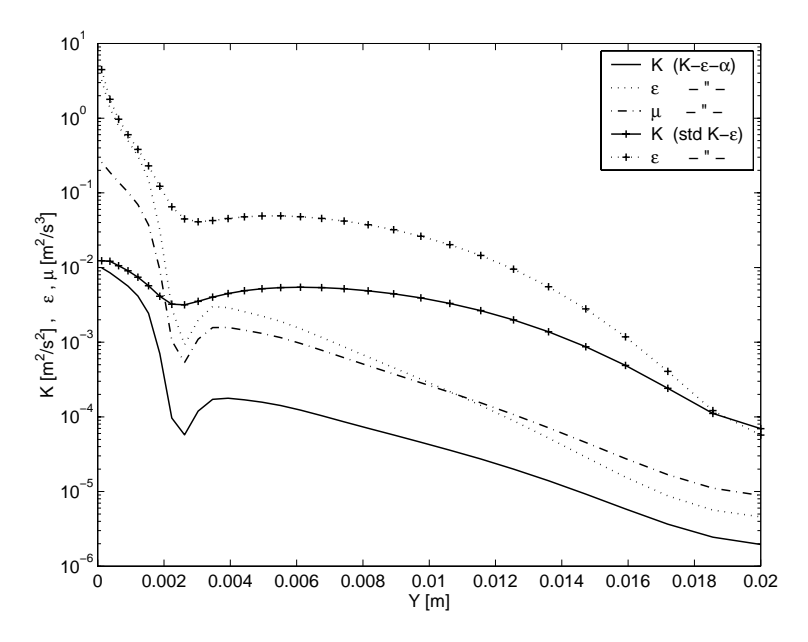


FIGURE 7. Turbulent kinetic energy, viscous and Joule dissipation in the center of the magnet, as predicted with the K- ε - α model. Predictions with the standard K- ε model are shown for comparison.

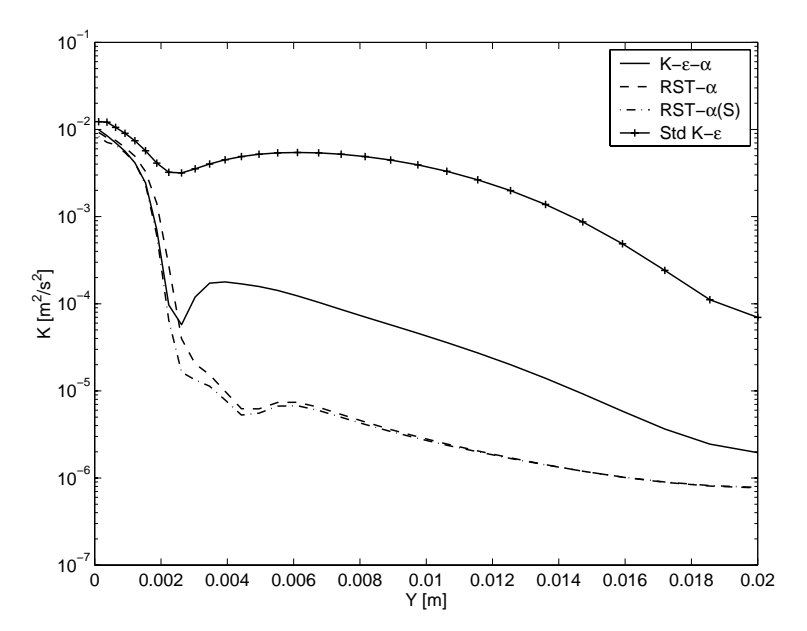


FIGURE 8. Predictions of turbulent kinetic energy with different turbulence models (center of magnet).

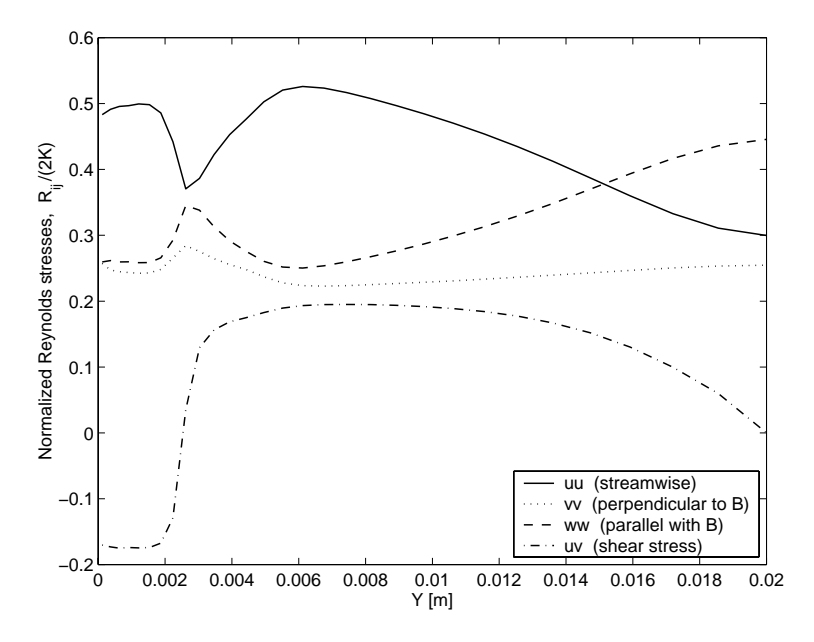


FIGURE 9. Profiles of normalized Reynolds stresses in the center of the magnet.

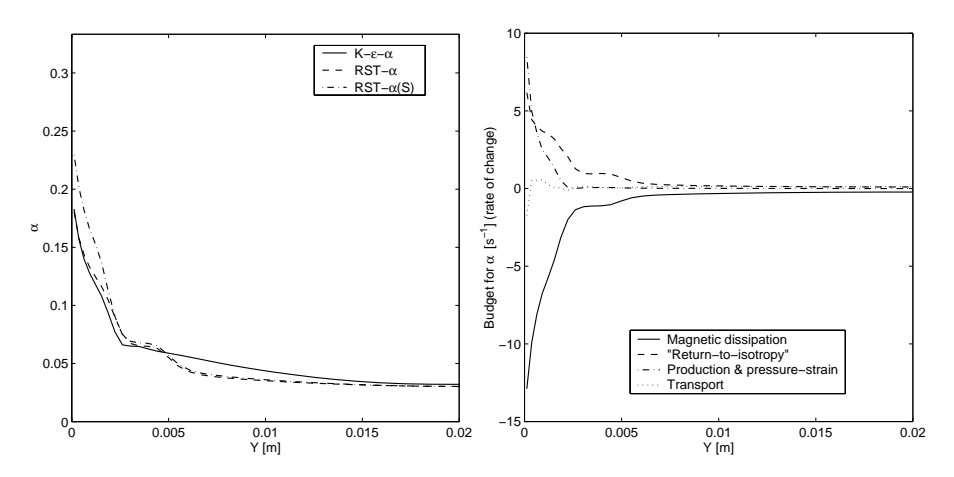


FIGURE 10. Left: Profiles of α in the center of the magnet. Right: Budget of α in the same cross-section (RST- α (S) model).

production and dissipation in the case of the RST- α model. The strain terms in the α equation give a significant positive contribution to α only near the wall. The right plot shows that the source and sink terms dominate over transport near the wall. This behavior is similar to that of the turbulent kinetic energy and the Reynolds stresses, and thus supports our choice of zero normal flux boundary conditions in the first node near walls.

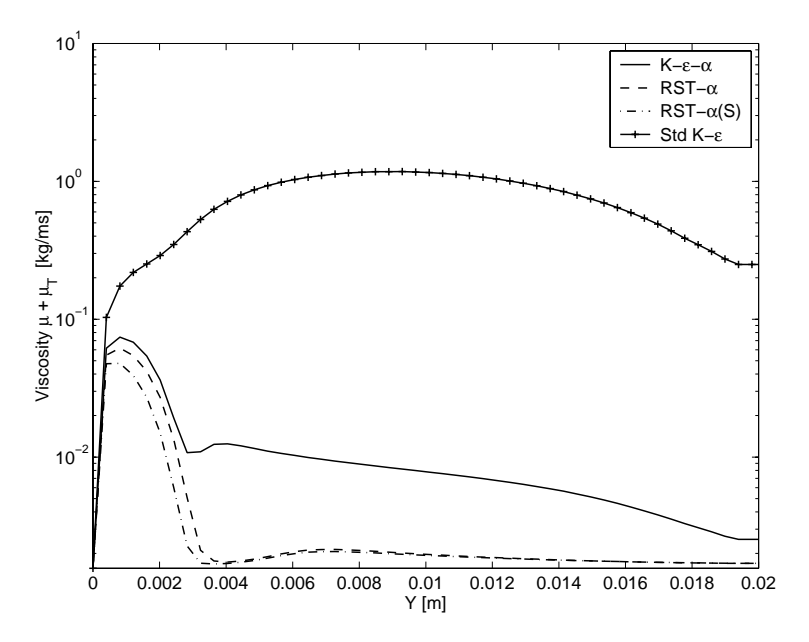


FIGURE 11. Predicted effective viscosities, $\mu + \mu_T$, in the exit of the magnet. The baseline of the plot represents the value of the molecular viscosity.

Figure 11, finally, shows profiles of effective viscosity, $\mu + \mu_T$, in the exit of the magnet, as predicted with the different models. Note that the baseline of the figure represents the molecular viscosity. The difference between predictions with the RST models and the K- ε - α was discussed earlier (see Fig. 8).

5. Discussion and outlook

This report documents an implementation of mean electromagnetic equations, Lorentz forces, and MHD turbulence models in the commercial code *CFX*4.3.

¿From a numerical point of view, the most difficult part of this effort is not, as one might think, the implementation of the new turbulence models. Instead the challenge is to solve the equation for electrostatic potential, and compute the total current density with sufficient accuracy, especially on general non-orthogonal grids.

We used the symbolic mathematics tool MAPLE V to manipulate, simplify and linearize all source terms for the turbulence equations, and to translate them directly into into fortran source code for the *CFX* subroutines. This minimizes the risk for programming errors, and simplifies validation and debugging. The procedure will also simplify future modifications, and evaluation of alternative models.

Both the Reynolds stress and eddy viscosity versions of the implemented MHD turbulence models appear to be very robust and well-behaved. Apart from the

extra work required for solving one more equation, the rate of convergence seem to be no worse for the MHD models, than for the standard models.

The current versions of the MHD turbulence models were developed to perform well for homogeneous turbulence, in the absence of walls. In order to simplify the model expressions, some inhomogeneous contributions to fluctuating pressure and fluctuating electric potential were neglected. Some of the missing terms are analogous to the wall reflection terms in the rapid pressure—strain model by Launder, Reece and Rodi [3]. This is the Reynolds stress model used in *CFX*, but the wall reflection terms are not implemented. For ordinary shear flows, the neglected terms are usually important only near walls. In MHD flows, however, the turbulence tends to be two-dimensional, so that turbulent structures grow very large in one direction. When the length of these structures becomes the same order as the distance to the nearest wall, we can expect the neglected inhomogeneous terms to be important. They will hence be important even in the core of an MHD channel flow, if the length scale anisotropy is sufficiently developed.

The missing inhomogeneous terms should certainly contribute to the Joule dissipation terms in the scalar K and ε equations, but their effect is perhaps more obvious in the Reynolds stress equations. Here they should contribute to the Joule dissipation tensor, and to the rapid and slow pressure–strain terms. For a wall perpendicular to the magnetic field, their net effect would be to redistribute energy from the wall-normal component (parallel with the field), to the other components. This means that the Reynolds stress component parallel with magnetic field will be damped, so that we approach a turbulent state which is two-component (2C) as well as 2D. This a feature typical for wall-bounded MHD flows, and different from the behavior of homogeneous turbulence. The channel flow simulation discussed in Sec. 4.2 (especially Fig. 9) illustrated the inability of the current MHD Reynolds stress model to predicted the damping of the field-parallel stress component.

Including the inhomogeneous contributions in the scalar K and ε (and α) equations is probably relatively straightforward. Including them in the Reynolds stress equations is much more difficult. The simple Launder, Reece and Rodi model only works well for relatively small stress anisotropies. Since all terms are linear, they will produce unphysical results even for rather moderate anisotropies. To deal with the situation, completely new and algebraically complex higher-order model terms would have to be developed, including also dimensionality information. The main reason we want accurate predictions of Reynolds stresses, is to model anisotropic diffusion, using Eq. (18). Considering the difficulties with a full Reynolds stress model, a more effective approach is probably to use a three-equation K- ε - α , with an algebraic model for modeling of Reynolds stresses and anisotropic diffusion.

In future work, the present model implementation will be used to study the effect of the different MHD model constants, and

to compare model predictions with experiments reported in literature. Unfortunately turbulence statistics are very difficult to measure, and not often reported in the literature. This makes validation of MHD turbulence models very difficult. Direct numerical simulations (DNS), and large eddy simulations (LES) may play an important role here.

References

- [1] B. J. Daly and F. H. Harlow. Transport equations in turbulence. *Physics of Fluids*, 13(11):2634–2649, 1970.
- [2] S. Kenjereš and K. Hanjalić. On the implementation of effects of Lorentz force in turbulence closure models. *Int. Journal of Heat and Fluid Flow*, 21(3):329–337, June 2000.
- [3] B. E. Launder, G. J. Reece, and W. Rodi. Progress in the development of a Reynolds-stress turbulence closure. *Journal of Fluid Mechanics*, 68:537–566, 1975.
- [4] B. E. Launder and D. B. Spalding. The numerical computation of turbulent flows. *Computer Methods in Appl. Mech. and Eng.*, 3:269–289, 1974.
- [5] William C. Reynolds. Effects of rotation on homogeneous turbulence. In Proc. 10th Australasian Fluid Mechanics Conference, Melbourne, Australia, 1989. University of Melbourne.
- [6] A. B. Tananaev. MHD Duct Flows. Atomizdat, 1979.
- [7] O. Widlund and G. Tallbäck. Modeling of anisotropic turbulent transport in simulations of liquid metal flows in magnetic fields. In *Proceedings* of the Third Int. Symposium on Electromagnetic Processing of Materials, EPM2000, April 3-6, 2000, pages 97–102, Nagoya, Japan, 2000. ISIJ.
- [8] O. Widlund, S. Zahrai, and F. H. Bark. Development of a Reynolds stress closure for modeling of homogeneous MHD turbulence. *Physics of Fluids*, 10(8):1987–1996, 1998.
- [9] O. Widlund, S. Zahrai, and F. H. Bark. Structure information in rapid distortion analysis and one-point modeling of axisymmetric magnetohydrodynamic turbulence. *Physics of Fluids*, 12(10):2609–2620, 2000.

Appendix A. Using the MHD model in CFX

In order to use this MHD model implementation, the first step is of course to include all the necessary MHD fortran routines, and the *CFX* user fortran routines, and make sure that latter contain the proper calls to the MHD routines. If the magnetic field should be defined in user fortran, the routine MHDBXT should be updated accordingly. Even if MHDBXT is not used, it should be included in the compilation.

Most of the modeling can then be controlled from the CFX command file. Section A.1 describes the necessary CFX options in the command file, while Sec. A.2 describes the special MHD model options read from the end of the command file.

A.1. CFX options in the command file. *CFX* user subroutines must be specified, as follows:

```
>>USER FORTRAN
USRSRC
USRBF
USRINT
USRWTM
USRDIF
```

The first three perform calls to specific MHD routines, which do the actual work. The user can add his/her own stuff in any of the routines.

The following user scalar variable names must be defined. The names are important, but the order is not.

>>VARIABLE NAMES

```
USER SCALAR1
               'EPOT'
USER SCALAR2
               'ALPHA'
USER SCALAR3
               'USRD B_X'
USER SCALAR4
              'USRD B_Y'
USER SCALAR5
              'USRD B_Z'
USER SCALAR6
              'USRDCC J_X'
USER SCALAR7
               'USRDCC J_Y'
USER SCALAR8
               'USRDCC J_Z'
USER SCALAR9
               'USRDCC S_MAG'
USER SCALAR10 'USRDCC S_RET'
USER SCALAR11 'USRDCC S_PRD'
USER SCALAR12 'USRDCC S_PST'
```

The last seven are stored only for post-processing, and the code could easily be rewritten to save storage space.

The differencing scheme for EPOT must be set to "NO CONVECTION", to disable the convection term. If the simulation is transient, also the transient term must be disabled by defining EPOT as "quasistatic". Example:

```
>>MODEL DATA

>>DIFFERENCING SCHEME

EPOT 'NO CONVECTION'

>>PHYSICAL PROPERTIES

>>TRANSIENT PARAMETERS

>>FIXED TIME STEPPING

TIME STEPS 30*0.010

>>QUASISTATIC VARIABLES

EPOT
```

Fluid viscosity and density should be specified as usual. Note however that exactly the same values must be specified for the corresponding MHD model options (see next section)! It is recommended to set the scalar diffusivity of ALPHA equal to the viscosity. The value specified for EPOT is unimportant, as it is overridden by the value of the MHD model option COND read from the end of the command file (see next section).

```
#CALC
     DENS = 13550.0;
     VISC = 0.00156;
     COND = 1.05E+6;
 #ENDCALC
/* ----- */
   >>FLUID PARAMETERS
     VISCOSITY
                 #VISC
     DENSITY
                 #DENS
   >>SCALAR PARAMETERS
     >>DIFFUSIVITIES
       EPOT
                #COND
       ALPHA
                #VISC
```

The MHD model implementation supports both the RST model, and the high-Re K- ε model. The code automatically recognizes which one is used. The turbulent Prandtl number for ALPHA is set to 1.0, same as for the Reynolds stresses.

```
>>TURBULENCE PARAMETERS

>>TURBULENCE MODEL

TURBULENCE MODEL 'DIFFERENTIAL STRESS'

/* TURBULENCE MODEL 'K-EPSILON' */

>>TURBULENT PRANDTL NUMBER

ALPHA 1.0
```

The body forces can be underrelaxed from within the command file, if it helps convergence. If turbulence equations are underrelaxed, it makes sense to use the same under-relaxation for ALPHA. Note that no under-relaxation should be used for EPOT, as it makes convergence slower than it needs to be. It is recommended to allow a fairly large number of sweeps for both pressure and EPOT equations (and a small value of the reduction factor), as this is noted to improve the rate of convergence.

```
>>SOLVER DATA
  >>PROGRAM CONTROL
    MAXIMUM NUMBER OF ITERATIONS
                                   1200
    MASS SOURCE TOLERANCE 1.0E-6
  >>UNDER RELAXATION FACTORS
    U VELOCITY
                  0.4
    V VELOCITY
                  0.4
    W VELOCITY
                  0.4
                  0.2
    BFX
    BFY
                  0.2
    BFZ
                  0.2
    K
                  0.3
    EPSILON
                  0.3
    ALPHA
                  0.3
    EPOT
                  1.0
                            /* NOTE! */
  >>SWEEPS INFORMATION
    >>MAXIMUM NUMBER
      EPOT
                  50
      PRESSURE
                 200
  >>REDUCTION FACTORS
    EPOT
               0.10
    PRESSURE
               0.10
```

Flow boundary conditions are set as usual. The inlet Dirichlet boundary condition for EPOT (default treatment for scalars) can be overridden using MHD model options for insulated inlets and outlets (see next section).

```
>>MODEL BOUNDARY CONDITIONS
  >>SET VARIABLES
    PATCH NAME 'OUT'
    PRESSURE 5000.0
  >>SET VARIABLES
    PATCH NAME 'IN'
    NORMAL VELOCITY
                               1.15
    K
                               2.0E-5
    EPSILON
                               9.9E-6
    EPOT
                               0.0
    ALPHA
                               0.333
```

ALPHA should have zero normal flux at walls. This is the default treatment for all scalars in *CFX*, so the specification in the example below is redundant. The same is true for EPOT and non-conducting walls, but in some situations one might want to set EPOT to a fixed potential, as for the wall "W_HIGH" in the example below.

```
>>WALL BOUNDARY CONDITIONS
PATCH NAME 'W_LOW'
EPOT FLUX 0.0
ALPHA FLUX 0.0
>>WALL BOUNDARY CONDITIONS
PATCH NAME 'W_HIGH'
EPOT 0.0
ALPHA FLUX 0.0
```

A complete sample command file is found in App. D.

A.2. MHD model options. The *CFX* frontend stops reading the command file when it reaches the stop command,

```
>>STOP
```

This allows us to control certain features of the MHD model implementation, by specifying a number of MHD model options at the end of the *CFX* command file.

Table 2 is a description of scalar model parameters that can be set. The model option is written on one line, and its new value on the following. The following lines, for example, sets the viscosity, electric conductivity and density to that of mercury:

```
COND
1.05E+6
DENS
13550.0
VISC
0.00156
```

Table 3 shows a list of option for defining the external magnetic field. The following lines, for example, indicate that a magnetic field is specified in user fortran (MHDBXT), but it should be multiplied by two:

```
B_FORT
BSCALE
2.0
```

Table 4 describes model options used to modify the solution of the EPOT and ALPHA equations. The following example prevents currents through inlets and outlets, specifies a zero reference point for the EPOT equation (in the origin), and disables the mean strain terms in the ALPHA equation:

Table 2. A list of scalar model parameters, set using MHD model options read from the end of the command file.

Model parameter	Description
PERM	Magnetic permeability, μ_m [Vs/Am].
COND	Electrical conductivity, σ [$\Omega^{-1}m^{-1}$].
DENS	Fluid density, $\rho [kg/m^3]$.
VISC	Fluid dynamic viscosity, μ [$kg/m/s$].
CA1	MHD model constant, $C_{\alpha 1}$.
CA2	MHD model constant, $C_{\alpha 2}$.
CA3	MHD model constant, $C_{\alpha 3}$ (currently not used).
CA4	MHD model constant, $C_{\alpha 4}$ (currently not used).
CEA	MHD model constant, $C_{\varepsilon\alpha}$.
CAMOD	Moderator coefficient for Joule dissipation source
	terms in turbulence equations (CAMOD=1 by de-
	fault).
CLF	Moderator coefficient for Lorentz force in mean mo-
	mentum equations (CLF=1 by default).
ALPHA	Constant initial value for ALPHA (default is AL-
	PHA=0.33).

Table 3. Model options for defining the external magnetic field.

Model option	Description
B0 Sets a uniform magnetic field, with all three cor	
	nents given on the following line.
B_FORT	The magnetic field is specified in subroutine MHD-
	BXT (must be supplied by the user.
B_FILE	The magnetic field should be read from file 'B.dat'
	in the problem directory. (See next option.)
XYZ	Causes the code to print a file 'xyz.dat' in the prob-
	lem directory, containing XYZ coordinates of all cell
	centers. The magnetic field in 'B.dat' should be in
	this order.
BSCALE	The magnetic field read from file, or defined in
	MHDBXT, is multiplied by this factor before use.
	(BSCALE=1.0 by default.)

INSULATED_INLETS
INSULATED_OUTLETS
EPOT_REFERENCE_POSITION
0.0 0.0 0.0
NO_STRAIN_IN_ALPHA

Table 4 .	Model options for	modifying	the solution	of the l	EPOT :	and
ALPHA e	equations.					

Model option	Description
INSULATED_INLETS	Causes inlet and outlet patches, respec-
INSULATED_OUTLETS	tively, to be electrically insulated. (Af-
	fects the source term and solution ma-
	trix in the EPOT equation, and the cal-
	culation of total current.)
NO_STRAIN_IN_ALPHA	DISABLES the strain-related model
	terms in the ALPHA equation. The
	terms are algebraically complex, and re-
	quires calculation of mean velocity gra-
	dients. The model terms give inaccu-
	rate results outside the magnetic field,
	and slows down the calculation. The
	effect of the terms appears to be small
	inside a magnetic field.
EPOT_REFERENCE_POSITION	The next line should contain the XYZ
	coordinates for a point where EPOT
	will be forced to zero. This is necessary
	unless a fixed value of EPOT is speci-
	fied on any of the boundaries (otherwise
	EPOT is undefined!).

Appendix B. Documentation of fortran source code

Table 5 shows a list of fortran subroutines. The grouping and indentation is used as a rough illustration of dependencies and calling order. All routines starting with "USR" are standard *CFX* user subroutines, while those starting with "MHD" are used only for implementation of the MHD models.

The *CFX* routines USRINT, USRBF and USRSRC contain only calls to the corresponding routines MHDINT, MHDBF and MHDSRC, respectively. The remaining routines are discussed individually below.

The common block UC_MHD is used to simplify the transfer of common variables and model parameters between the subroutines of the model implementation. Most of the parameters are initialized in the subroutine MHDINT (based on MHD model options read at the end of the *CFX* command file), although some of the parameters are given useful defaults in the block data subprogram MHD_DATA. The parameters carried in the common block are listed in Table 6.

Table 5. List of fortran subroutines, grouped and indented to show calling order.

Subroutines		5	Purpose		
USRINT				(Call MHDINT.)	
	MHDINT		VT	Read MHD model options from the end of the	
				CFX command file. Initialize model parameters.	
				Call MHDBXT, if magnetic field is defined in user	
				fortran.	
•		MI	HDBXT	Definition of magnetic field in all nodes (op-	
				tional).	
US	RBF	7		(Call MHDBF.)	
	MI	IDB	F	Compute total current density and Lorentz force.	
		MI	HDJSC	Compute contravariant component of $\mathbf{U} \times \mathbf{B}$ at	
				cell faces (for body-fitted grids).	
		MI	HDGEP	Compute gradient of EPOT.	
			MHDGE2	Recompute EPOT gradient in a single cell next	
				to a boundary.	
US	RDI	F		Set diffusivity for EPOT equation explicitly.	
US	RW	ГΜ		Set turbulent wall multiplier for EPOT explicitly,	
				to override turbulent wall function.	
US	RSR			(Call MHDSRC.)	
	MI	HDS:	RC	Compute source terms for scalar and turbulence	
				equations.	
		MI	HDJSF	Compute normal flux components of $\mathbf{U} \times \mathbf{B}$ on	
				all cell faces.	
		MI	HDSEP	Compute source term for the EPOT equation.	
				Modify matrix coefficients at certain boundaries.	
MF	MHD_DATA		A	BLOCK DATA subprogram. Assigns default val-	
				ues for some parameters in the UC_MHD common	
				block.	

B.1. MHDINT. Called from USRINT. Reserves permanent workspace for currents at cell faces (computed in MHDJSF and MHDJSC), checks which turbulence model is used, and initializes common block pointers to user scalars.

Reads a number of MHD model options from the end of the command file, starting after the CFX ">>STOP" command. See App. A.2 for a description of model options.

Depending on model options, the magnetic field is either specified as constant and uniform, read from the file "B.dat" in the problem directory, or a call is made to the subroutine MHDBXT. One option causes the routine to print Cartesian

Table 6. Contents of UC_MHD common block.

Parameter	Type	Description
PERM	real	Magnetic permeability, μ_m [Vs/Am].
COND	real	Electrical conductivity, $\sigma [\Omega^{-1}m^{-1}]$.
DENS	real	Fluid density, ρ [kg/m^3].
VISC	real	Fluid dynamic viscosity, μ [$kg/m/s$].
CA1	real	MHD RST model constant, $C_{\alpha 1}$.
CA2	real	MHD RST model constant, $C_{\alpha 2}$.
CA3	real	MHD RST model constant, $C_{\alpha 3}$ (currently not used).
CA4	real	MHD RST model constant, $C_{\alpha 4}$ (currently not used).
CEA	real	MHD RST model constant, $C_{\varepsilon\alpha}$.
CAMOD	real	Moderator coefficient for Joule dissipation
		source terms in turbulence equations (CAMOD=1
		by default).
CLF	real	Moderator coefficient for Lorentz force
		in mean momentum equations (CLF=1 by default).
ISCL	integer	Variable number for SCAL array (from GETVAR).
IEP	integer	Scalar number for EPOT variable (from GETSCA).
IALPHA	integer	Scalar number for ALPHA variable (from
		GETSCA).
IB(1:3)	integer	Scalar numbers for stored B -field components.
IJ(1:3)	integer	Scalar numbers for stored total current components.
IJSF	integer	Pointer to facial currents in WORK array.
INDEPR	integer	INODE number for EPOT zero reference point.
LINSIN	logical	Logical TRUE to avoid currents through INLET
		boundaries.
LINSPR	logical	Logical TRUE to avoid currents through PRES-
		SURE boundaries.
LINSMF	logical	Logical TRUE to avoid currents through MASS-
		FLOW boundaries.
LEPREF	logical	Logical TRUE if an EPOT zero reference points is
		defined.
LNOSTR	logical	Logical TRUE to disable mean strain terms in AL-
		PHA equation.
LRSM	logical	Logical TRUE indicates that the Reynolds stress
		model is used. If FALSE, we assume the high-Re
		K - ε model is specified.

coordinates for all nodes to a file "xyz.dat", in the order B-field values should appear in "B.dat".

In case all inlets, outlets and walls are non-conducting, there is an option for specifying the coordinates of a zero reference point for the electrostatic potential EPOT. If the given point is not in the flow domain, the center of the first block is used instead.

B.2. MHDBXT. Called from MHDINT. This routine can be used to specify the magnetic field in all nodes, e.g. as function of position. Even if the routine is not used, a dummy version should still be available at compilation time. The following example sets a uniform field B=1 in the z direction.

```
SUBROUTINE MHDBXT(XP,YP,ZP,SCAL,IBX,IBY,IBZ,BSCALE,BMAX
                        , NNODE, NPHASE, NSCAL)
C
С
      Routine for specification of external B-field.
С
      DIMENSION
           SCAL (NNODE, NPHASE, NSCAL)
           ,XP(NNODE),YP(NNODE),ZP(NNODE)
С
C-
С
С
      B-field should be specified below for all nodes, e.g.
С
      as a function of node coordinates XP, YP and ZP!
C
C
      Maximum norm of B should be stored in BMAX!
C
      DO 100 INODE=1, NNODE
C
         BX = 0.0
         BY = 0.0
         BZ = 1.0
C
         SCAL(INODE, 1, IBX) = BX
         SCAL(INODE, 1, IBY) = BY
         SCAL(INODE,1,IBZ)=BZ
         BMAX=MAX(BMAX,SQRT(BX**2+BY**2+BZ**2))
C
 100 CONTINUE
      RETURN
      END
```

The factor BSCALE can be specified in the command file, so that the magnitude of the magnetic field can be scaled without recompiling the fortran routines.

- **B.3. USRDIF.** Explicitly sets the total diffusivity for the EPOT equation equal to the electric conductivity COND stored in the UC_MHD common block. This is necessary to override the turbulent diffusivity added by *CFX*. (Note that the diffusivity can be scalar or tensorial, depending on what turbulence model is used.)
- **B.4. USRWTM.** For the EPOT equation, sets the turbulent wall multiplier TMULT for each wall boundary node to

$$TMULT = \frac{COND}{YWALL},$$
(73)

where COND is the electric conductivity, and YWALL the distance to the first node. This overrides the effect of the turbulent wall function in *CFX*, and ensures natural wall boundary conditions for the EPOT equation.

B.5. MHDSRC. Called from USRSRC, for both ICALL=1 and ICALL=2.

For the EPOT equation, and if ICALL=1, MHDJSF is called to compute normal flux components of the term $\sigma(\mathbf{U} \times \mathbf{B})$ on all cell faces. Then MHDSEP is called to compute the source term for EPOT. MHDSEP is called also if ICALL=2, for modification of SU, SP, and AM to account for boundary conditions.

MHDSRC further computes magnetic source terms for all turbulence equations, including ALPHA. The magnetic source terms in all turbulence equations are multiplied by the factor CAMOD. By default CAMOD=1, but by setting it to zero with the MHD model options in the command file, all magnetic source terms are disabled.

If the mean strain terms in the ALPHA equation are to be computed, the mean velocity gradients are computed with the *CFX* routine GRADV. The different ALPHA source term contributions are currently stored in user scalars (see Sec. 2.5):

$$S_MAG = -\mu_{\alpha}, \tag{74}$$

$$S_RET = \pi_{\alpha}, \tag{75}$$

$$S_{-}PRD = P_{\alpha}, \tag{76}$$

$$S_PST = \Pi_{\alpha}^{(r)}. \tag{77}$$

B.6. MHDJSF. Called from MHDSRC. Computes and stores the normal flux components $\sigma(\mathbf{U} \times \mathbf{B})_f \cdot \mathbf{A}_f$ on all cell faces.

In the interior of the flow domain, facial values of \mathbf{U} and \mathbf{B} are interpolated using the CFX weight factors WFACT. We assume no-slip boundaries, so that $\mathbf{U} = 0$ on all walls. The relevant velocity at inlet, pressure and massflow boundaries are taken from the dummy nodes at the boundary. If the command file

options for insulted boundaries are specified, however, the normal flux is set to zero at the respective boundaries.

B.7. MHDSEP. Called from MHDSRC for both ICALL=1 and ICALL=2.

If ICALL=1, MHDSEP loops over all cells and computes the source term for EPOT from the facial source currents computed in MHDJSF.

If ICALL=2, and if the relevant insulated boundary option is specified, the matrix coefficient AM in the direction of the boundary is set to zero in all active cells adjacent to the boundary.

If a zero reference point for EPOT is specified, MHDSEP sets SU=0 for this node, SP to a large negative number, and all its matrix coefficients to zero. This forces EPOT to zero in the node.

B.8. MHDBF. Called from USRBF. Computes the total current density and the Lorentz force in all cells. The total current density is stored in user scalars. The total current density is given by

$$\mathbf{J} = -\sigma \nabla \Phi + \sigma \mathbf{U} \times \mathbf{B}. \tag{78}$$

In the first part of the routine, MHDGEP is called to compute the gradient of EPOT. For the $\mathbf{U} \times \mathbf{B}$ term to behave well together with the gradient term, we need to compute $\mathbf{U} \times \mathbf{B}$ in the cell center as the average of the contravariant components on the faces of the cell. The procedure is similar to that used for body forces in CFX, to make these compatible with gradients of pressure.

If the grid is rectangular, the contravariant components of $\mathbf{U} \times \mathbf{B}$ can be expressed in terms of the normal flux components already computed by MHD-JSF for the EPOT source terms. Note, however, that MHDJSF is called from MHDBF on the first iteration, if it is a restart from an existing dump file. This is because the momentum equations are the first variables in the outer iteration, and no call has yet been made to MHDJSF from MHDSRC.

If the grid is body-fitted (and presumed non-orthogonal), we call MHDJSC to compute and store the contravariant components of $\mathbf{U} \times \mathbf{B}$ on the faces.

The Lorentz force is multiplied by the factor CLF before it is added to the body force array. By default CLF=1, but by setting it to zero with the MHD model option in the command file, the Lorentz force can be disabled.

- **B.9.** MHDJSC. Called from MHDBF. Computes and stores the contravariant components of $\mathbf{U} \times \mathbf{B}$ on the faces. (These components overwrite the normal flux components previously stored by MHDJSF.) The general approach, and the treatment of boundary conditions, is similar to that in MHDJSF (see App. B.6).
- **B.10.** MHDGEP and MHDGE2. Called by MHDBF. Calls the *CFX* routine GRADS to compute the gradients of EPOT. The gradients must however be modified in the cells adjacent to walls, inlets, pressure and massflow boundaries. The main reason for this is that the normal gradient at walls is incomplete, as the wall gradient of a scalar usually depends on a turbulent wall function.

The modification at boundaries is made in two steps. First, the gradient in cells adjacent to wall, inlet, pressure and massflow boundaries are marked as undefined, by setting its x component to a large dummy value (larger than 10^{10}). In the next step, we loop again over cells adjacent to the different boundary types. The new gradient in the node P is defined as

$$\left(\frac{\partial \Phi}{\partial \mathbf{x}}\right)_P = \frac{1}{V_P} \sum_f \Phi_f \mathbf{A}_f,\tag{79}$$

where V_P is the cell volume, Φ_f the value of EPOT at the cell faces f, and \mathbf{A}_f is the face area vectors. This equation follows from the generalized Gauss law (see the CFX manual, Sec. 13.2). If the gradient is already defined (will happen if the cell is adjacent to more than one boundary), the contribution from the current boundary is modified with the appropriate value of EPOT at the current face.

The calculation of the gradient (79) in an individual cell is performed in the routine MHDGE2, which is called from MHDGEP with the appropriate EPOT value for the current boundary face.

The EPOT value for a face at a wall is taken from the active cell. This corresponds to the desired zero normal gradient at the wall. The default behavior for an inlet boundary is to take the EPOT value from the boundary node, where the boundary conditions are stored. If the insulated inlet option is active, the value is instead taken from the active cell (zero normal gradient). The default behavior for pressure and massflow boundaries is to use the EPOT value from the dummy node. The value in the dummy node is equal to the value in the active cell on outflow (Neumann boundary conditions), but equal to the Dirichlet condition specified at the patch in case of inflow. If the insulated outlet option is active, the value in the active node is used instead (zero normal gradient).

Appendix C. MAPLE script for generating source terms

Below is a listing of a MAPLE script for generating the fortran source for the source terms in the ALPHA equation. A similar procedure is used for the source terms in the Reynolds stress equations.

```
scalfunc:={G=alpha-3*alpha^2*f1/2/2*(Ina+2/3),}
          H=3*alpha^2*f1/2,
          aN=CA3*(-alpha+4*alpha^2-3*alpha^3)
                 +13/10*alpha^2-3/10*alpha^3 }:
name subs: =\{R.1.1=UU, R.2.2=VV, R.3.3=WW,
          R.1.2=UV, R.2.3=VW, R.1.3=WU}:
fortsubs:={R.1.1=RS[INODE, IPH, 1], R.2.2=RS[INODE, IPH, 2],
          R.3.3=RS[INODE, IPH, 3], R.1.2=RS[INODE, IPH, 4],
          R.2.3=RS[INODE, IPH, 5], R.1.3=RS[INODE, IPH, 6],
          alpha=ALPHA,
          n.1=DUV[1],n.2=DUV[2],n.3=DUV[3],
          K=TE[INODE, IPH], eps=ED[INODE, IPH], ttuinv=TTUINV,
          Ug11=UGRX, Ug12=UGRY, Ug13=UGRZ,
          Ug21=VGRX, Ug22=VGRY, Ug23=VGRZ,
          Ug31=WGRX,Ug32=WGRY,Ug33=WGRZ}:
EVMsubs: = \{seq(seq(R.i.j=2/3*K*delta[i,j]-nuT*(Ug[i,j]+Ug[j,i]) \}
           ,j=i..3),i=1..3)}:
#-----
# Define tensors and tensorial groups
#-----
R:=array(symmetric,1..3,1..3):
n:=array(1..3,[n1,n2,n3]):
Ug:=array(1..3,1..3):
#-----
# Set variable properties for linearization:
# - Diagonal R_ij: > 0
# - Off-diagonal R_ij: REAL
# - Kinetic energy: K>0
# - Dissipation: eps>0
# - Alpha: 0<=alpha<=1
# - direction unit vector, all components: -1 <= n_k <= 1
# - CMU and CA3 >0
#-----
for i from 1 to 3 do
  assume (n. i > = -1, n. i < = 1);
  for j from i to 3 do
      if (i=j) then
         assume(R.i.j>0);
         assume(R.i.j,real);
      fi;
      R[i,j]:=R.i.j;
  od;
od;
for i from 1 to 3 do
  for j from 1 to 3 do
      assume(Ug.i.j,real);
      Ug[i,j]:=Ug.i.j;
  od;
od;
assume(alpha>=0,alpha<=1);
```

```
assume(K>0);
assume (TELIM>0);
assume(eps>0);
assume(EDLIM>0);
assume(CA3>0);
assume(CMU>0);
a:=evalm(sumt(R[i1,i2]/K-2/3*delta[i1,i2],0,2)):
Ina_:=simplify(sumt(n[s1]*n[s2]*a[s2,s1],2,0)):
InaRST:=expand(subs(K=TELIM,Ina_)):
InaEVM:=simplify(subs(nuT=CMU*K^2/EDLIM,subs(EVMsubs,Ina_))):
# Derived tensors, groups and invariants
#-----
# Production term, P_alpha
#-----
prod1:=sumt(-2*G*Ug[s1,s2]*R[s1,s2],2,0):
prod2:=sumt(-H*Ug[s1,s2]*n[s1]*n[s3]*R[s3,s2],3,0):
prod3:=sumt(-H*Ug[s1,s2]*n[s2]*n[s3]*R[s3,s1],3,0):
prodK:=sumt(-Ug[s1,s2]*R[s1,s2],2,0):
Prod:=simplify((prod1+prod2+prod3-2*alpha*prodK)/(2*TELIM)):
# Production term in eddy viscosity model:
     prod1 & prodK: subs K=0 to cancel K-term
     (drops out due to continuity)...
#-----
prod1EVM:=subs(K=0, subs(EVM subs, prod1)):
prod2EVM:=subs(EVMsubs,prod2):
prod3EVM:=subs(EVMsubs,prod3):
prodKEVM:=subs(K=0, subs(EVM subs, prodK)):
ProdEVM: =simplify(subs(nuT=CMU*K^2/EDLIM,
  (prod1EVM+prod2EVM+prod3EVM-2*alpha*prodKEVM)/(2*K))):
#-----
# Pressure-strain term, Pi_alpha:
#-----
Pi_{:=}simplify(sumt(2*(aN-alpha)*Ug[s1,s2]*n[s1]*n[s2],2,0)):
# Compute source terms and print fortran to file
# Linear terms put in SP if always negative. Otherwise in SU.
#-----
writeto('alpha_source.f');
#-----
# Production term:
#-----
x:=expand(subs(Ina=InaRST, subs(scalfunc, Prod))):
# Prepare linearization of source term...
su0:=coeff(x,alpha,0):
sp0:=expand(simplify((x-su0)/alpha)):
# -- Only negative linear part in SP, rest in SU...
# -- Check whether polynomial, or product/nil...
```

```
if (whattype(sp0)='+') then
  sp:=select(t->is(t<=0),sp0):
  su:=su0+alpha*remove(t->is(t<=0),sp0):
  if (is(sp0 \le 0)) then
      sp:=sp0:
  else
      su:=su0+alpha*sp0:
  fi:
fi:
# -- Simplify...
su:=simplify(su):
sp:=simplify(sp):
lprint('C -----'):
lprint('C Production (RST version)'):
lprint('C -----'):
fortran([SU[INODE,IPH]=SU[INODE,IPH]+DENS*VOL(INODE)*subs(fortsubs,su),
     SP[INODE, IPH] = SP[INODE, IPH] + DENS * VOL(INODE) * subs(fortsubs, sp)],
             optimized):
#-----
# Production term in EV model:
#-----
x:=expand(subs(Ina=InaEVM, subs(scalfunc, ProdEVM))):
# Prepare linearization of source term...
su0:=coeff(x,alpha,0):
sp0:=expand(simplify((x-su0)/alpha)):
# -- Only negative linear part in SP, rest in SU...
# -- Check whether polynomial, or product/nil...
if (whattype(sp0)='+') then
  sp:=select(t->is(t<=0),sp0):
  su:=su0+alpha*remove(t->is(t<=0),sp0):
else
  if (is(sp0 \le 0)) then
      sp:=sp0:
  else
      su:=su0+alpha*sp0:
  fi:
fi:
# -- Simplify...
su:=simplify(su):
sp:=simplify(sp):
lprint('C -----'):
lprint('C
            Production (EVM version)'):
lprint('C -----'):
fortran([SU[INODE,IPH]=SU[INODE,IPH]+DENS*VOL(INODE)*subs(fortsubs,su),
     SP[INODE, IPH] = SP[INODE, IPH] + DENS * VOL(INODE) * subs(fortsubs, sp)],
             optimized):
#-----
# Pressure-strain term:
#-----
x:=expand(subs(scalfunc,Pi_)):
```

```
# Prepare linearization of source term...
su0:=coeff(x,alpha,0):
sp0:=expand(simplify((x-su0)/alpha)):
# -- Only negative linear part in SP, rest in SU...
# -- Check whether polynomial, or product/nil...
if (whattype(sp0)='+') then
  sp:=select(t->is(t<=0),sp0):
   su:=su0+alpha*remove(t->is(t<=0),sp0):
   if (is(sp0 \le 0)) then
       sp:=sp0:
   else
       su:=su0+alpha*sp0:
   fi:
fi:
# -- Simplify...
su:=simplify(su):
sp:=simplify(sp):
lprint('C -----'):
lprint('C Pressure-strain interaction'):
lprint('C -----'):
fortran([SU[INODE, IPH] = SU[INODE, IPH] + DENS*VOL(INODE)*subs(fortsubs, su),
      SP[INODE, IPH] = SP[INODE, IPH] + DENS * VOL(INODE) * subs(fortsubs, sp)],
              optimized):
writeto(terminal);
```

Appendix D. Listing of sample command file

```
>>CFX4
 >>SET LIMITS
   TOTAL INTEGER WORK SPACE 14000000
   TOTAL CHARACTER WORK SPACE 1500
   TOTAL REAL WORK SPACE 90000000
   MAXIMUM NUMBER OF BLOCKS 10
   MAXIMUM NUMBER OF PATCHES 50
   MAXIMUM NUMBER OF INTER BLOCK BOUNDARIES 20
 >>OPTIONS
   TURBULENT FLOW
   TRANSIENT FLOW
   USER SCALAR EQUATIONS 12
 >>USER FORTRAN
   USRSRC
   USRBF
   USRINT
   USRW TM
   USRDIF
 >>VARIABLE NAMES
   USER SCALAR1 'EPOT'
   USER SCALAR2 'ALPHA'
   USER SCALAR3 'USRD B_X'
```

```
USER SCALAR4 'USRD B_Y'
   USER SCALAR5 'USRD B_Z'
   USER SCALAR6 'USRDCC J_X'
   USER SCALAR7 'USRDCC J_Y'
   USER SCALAR8 'USRDCC J_Z'
   USER SCALAR9 'USRDCC S_MAG'
   USER SCALAR10 'USRDCC S_RET'
   USER SCALAR11 'USRDCC S_PRD'
   USER SCALAR12 'USRDCC S_PST'
   END
/* --- Parameters --- */
   #CALC
    DENS = 13550.0;
     VISC = 0.00156;
     COND = 1.05E+6;
   #ENDCALC
/* ---- */
>>MODEL DATA
 >>DIFFERENCING SCHEME
   EPOT 'NO CONVECTION'
 >>PHYSICAL PROPERTIES
   >>TRANSIENT PARAMETERS
    >>FIXED TIME STEPPING
      TIME STEPS 30*0.010
     >>QUASISTATIC VARIABLES
      EPOT
   >>FLUID PARAMETERS
     VISCOSITY #VISC
     DENSITY
               #DENS
     F.ND
   >>SCALAR PARAMETERS
     >>DIFFUSIVITIES
      EPOT #COND
ALPHA #VISC
   >>TURBULENCE PARAMETERS
     >>TURBULENCE MODEL
       TURBULENCE MODEL 'DIFFERENTIAL STRESS'
/*
        TURBULENCE MODEL 'K-EPSILON' */
     >>TURBULENT PRANDTL NUMBER
       ALPHA 1.0 /* Same as for Reynolds stresses */
>>SOLVER DATA
 >>PROGRAM CONTROL
   MAXIMUM NUMBER OF ITERATIONS 1200
   ITERATIONS OF TURBULENCE EQUATIONS 3
   PRESSURE REFERENCE POSITION 0.452 0.02 0.015
   MASS SOURCE TOLERANCE 1.0E-6
 >>UNDER RELAXATION FACTORS
   U VELOCITY 0.4
```

```
V VELOCITY 0.4
   W VELOCITY 0.4
   BFX
               0.2
              0.2
   BFY
   BFZ
              0.2
               0.3
   EPSILON
              0.3
   UU
               0.3
   ٧V
               0.3
   WW
               0.3
   UV
               0.3
   VW
               0.3
   WU
               0.3
   ALPHA
              0.3
                       /* NOTE! */
   EPOT
               1.0
 >>SWEEPS INFORMATION
   >>MAXIMUM NUMBER
    EPOT
              50
     PRESSURE 200
 >>REDUCTION FACTORS
   EPOT 0.10
   PRESSURE 0.10
>>MODEL BOUNDARY CONDITIONS
 >>SET VARIABLES
   PATCH NAME 'OUT'
   PRESSURE 5000.0
 >>SET VARIABLES
   PATCH NAME 'IN'
   NORMAL VELOCITY
                          1.15
                          2.0E-5
   EPSILON
                          9.9E-6
   EPOT
                          0.0
   ALPHA
                          0.333
/* - - - - - - */
 >>WALL BOUNDARY CONDITIONS
   PATCH NAME 'W_LOW'
   EPOT FLUX 0.0
   ALPHA FLUX O.O
 >>WALL BOUNDARY CONDITIONS
   PATCH NAME 'W_HIGH'
   EPOT FLUX 0.0
   ALPHA FLUX O.O
 >>WALL BOUNDARY CONDITIONS
   PATCH NAME 'W_SOUTH'
   EPOT FLUX 0.0
   ALPHA FLUX 0.0
 >>WALL BOUNDARY CONDITIONS
   PATCH NAME 'W_NORTH'
   EPOT FLUX 0.0
   ALPHA FLUX 0.0
```

```
/* - - - - - - - */
>>OUTPUT OPTIONS
 >>PRINT OPTIONS
   >>WHAT
     NO VARIABLES
    WALL PRINTING
   >>WHEN
    FINAL SOLUTION
>>STOP
\% - - - MHD model options follow - - - - - - - - -
%
%
\mbox{\ensuremath{\mbox{\%}}} On a COMPAQ mahine, the components of vectors must lie
% within these marks:
%
COND
1.05E+6
PERM
1.25664E-6
DENS
13550.0
VISC
0.00156
CEA
1.5
EPOT_REFERENCE_POSITION
   0.452 0.020 0.015
INSULATED_INLETS
INSULATED_OUTLETS
NO_STRAIN_IN_ALPHA
B_FORT
BSCALE
1.35
```

Paper 6

MODELING ANISOTROPIC MHD TURBULENCE IN SIMULATIONS OF LIQUID METAL FLOWS

Ola Widlund

Faxén Laboratory Royal Institute of Technology SE-100 44, Stockholm, Sweden

1. Introduction

Electrostatic magnetic fields are used in continuous casting of steel to brake and control the mean flow of liquid metal in the mould. The magnetic field also causes magnetic Joule dissipation of turbulence, thus affecting turbulent transport of heat and mass. Numerical simulations of this and other turbulent MHD flows generally suffer from the inability of conventional turbulence models (like the $K-\varepsilon$ model, or a full Reynolds stress closure) to deal with the large anisotropies of length scales encountered in MHD turbulence. To improve the situation, it has been suggested to include information about length-scale anisotropy in an extended Reynolds stress model for MHD applications (Widlund et al. [6]).

The so-called dimensionality tensor, Y_{ij} , was first introduced by Reynolds [4] to help describe the effect of rapid rotation on turbulence. While the Reynolds stress tensor R_{ij} accounts for the kinetic energy of fluctuations in different directions, the dimensionality tensor carries information about the length scales in different directions. The latter information seems vital for a correct description of Joule dissipation. The scalar Joule dissipation rate can, for example, be exactly expressed in terms of the component of the dimensionality tensor which is parallel with the magnetic field,

$$\mu = \frac{1}{2}\mu_{nn} = \frac{\sigma B^2}{\rho} n_i n_j Y_{ji},\tag{1}$$

where n_i is a unit direction vector of the magnetic field.

A conventional Reynolds stress transport (RST) model includes transport equations for the six independent Reynolds stresses and the scalar viscous dissipation rate. Inspired by (1), an RST model has been extended with a model transport equation for a dimensionality anisotropy variable α , defined as

$$\alpha \equiv \frac{n_i n_j Y_{ji}}{2K}.$$
 (2)

The anisotropic Joule dissipation tensor is then modeled with an invariant tensor function in \mathbf{R} and α . An exact transport equation for α can be derived from

Presented at 4th International PAMIR Conference, Presqu'île de Giens, France, September 18-22, 2000.

the Navier–Stokes equations, including magnetic and inertial effects, as well as effects of mean shear and strain. All terms in the equation require modeling, however.

The complete model has been implemented in the commercial CFD solver CFX4 [5]. Predictions show qualitative agreement with available experiments for the energy dissipation, and the elongation of turbulence structures. They also demonstrate known limitations with the current model implementation, when it comes to predicting extreme Reynolds stress anisotropies in wall bounded flows.

In Section 2 we highlight properties of the model for the homogeneous case, and compare predictions with the classical experiment of Alemany *et al.* [1]. In Section 3 we briefly discuss effects of inhomogeneity in wall bounded flows. These effects are currently not captured by the model.

2. Homogeneous turbulence

2.1. Model equations. Assume Cartesian coordinates oriented so that the magnetic field vector is in the x_3 -direction, i.e. $\mathbf{B} = B\mathbf{e}_3$. For the case of homogeneous shear-free MHD turbulence, initially axisymmetric about the magnetic field vector, there is only two independent Reynolds stress components, R_{11} and R_{33} , and the turbulent kinetic energy is $K = (2R_{11} + R_{33})/2$. If we introduce a magnetic time scale $\tau = \rho/(2\sigma B^2)$, the Reynolds stress closure proposed by Widlund *et al.* [6] reduces to

$$\frac{dK}{dt} = -\varepsilon - \frac{1}{\tau} \alpha K, \tag{3}$$

$$\frac{d\varepsilon}{dt} = -C_{\varepsilon 2} \frac{\varepsilon^2}{K} - \frac{C_{\varepsilon \alpha}}{\tau} \alpha \varepsilon, \tag{4}$$

$$\frac{d\alpha}{dt} = C_{\alpha 2} \frac{\varepsilon}{K} \left(\frac{1}{3} - \alpha \right) - \frac{C_{\alpha 1}}{\tau} \alpha^2, \tag{5}$$

$$\frac{dR_{33}}{dt} = \pi_{33} - \frac{2}{3}\varepsilon - \frac{G(\alpha, R_{33}/K) + H(\alpha)}{\tau}R_{33}.$$
 (6)

An equation for R_{11} is redundant, as it can be computed from K and R_{33} . In (6), π_{33} is a component of a return-to-isotropy model for slow pressure—strain, and the anisotropy of the Joule dissipation is governed by the functions G and H; see [6] for details.

The K equation is exact, as the Joule dissipation term follows from the definition of α . In contrast, both destruction terms in the ε equation (4) are model terms, with model constants $C_{\varepsilon 2}$ and $C_{\varepsilon \alpha}$, respectively. The last term in (5) represents destruction of α due to the magnetic field, driving the equation towards the 2D limit ($\alpha = 0$). The first term in (5) is a linear return-to-isotropy term of Rotta-type, which governs a return to the isotropic state when there is no magnetic field. In the homogeneous case, the properties of the model are determined by the coupled non-linear system of scalar ODE:s for K, ε and α (decoupled from stress anisotropy). In the absence of magnetic field, (3) and (4) form the familiar two-equation $K-\varepsilon$ model. There are analytic solutions for K and ε in this case. For large times $K(t) \sim t^{-n}$, where $n \equiv 1/(C_{\varepsilon^2} - 1)$. The standard value $C_{\varepsilon^2} = 1.92$ gives $n \approx 1.09$, in good agreement with experiments on grid generated turbulence.

In the limit of large interaction numbers $(N \equiv \sigma B^2 K/(\rho \varepsilon) \gg 1)$, Joule dissipation dominates and the decay is controlled by the K and α equations. Analytic power law solutions can be found also for this case [7], and $K(t) \sim t^{-n}$ with $n \equiv 1/C_{\alpha 1}$. By choosing $C_{\alpha 1} = 2$ the model is made consistent with the asymptotic decay rate $K \sim t^{-1/2}$ found earlier by Moffatt [3]. The integral length scale $L \sim K^{3/2}/\varepsilon$ goes as $t^{(C_{\varepsilon\alpha}-3/2)/C_{\alpha 1}}$, so that the length scale is unaffected if $C_{\varepsilon\alpha} = 3/2$. Furthermore, $\alpha(t) \sim t^{-1}$ for large t. Comparison with earlier work suggests that $\alpha \sim (L/L_{\parallel})^2$, so that this is consistent with $L_{\parallel} \sim t^{1/2}$ if L changes slowly [2].

The situation is more complicated for intermediate interaction numbers. As explained in spectral terms by Alemany *et al.* [1], we will eventually reach a balance between Joule dissipation and nonlinear angular energy transfer. Angular energy transfer is represented in the α equation (5) by the "return-to-isotropy" term,

$$\pi_{\alpha} = C_{\alpha 2} \frac{\varepsilon}{K} \left(1/3 - \alpha \right). \tag{7}$$

The behavior of (7) near $\alpha=0$ is very important for large times. One can argue that the spectral triad interactions responsible for the angular energy transfer should vanish in the limit of 2D turbulence, where all the energy is concentrated in the wave number plane $k_{\parallel}=0$. This means that π_{α} should be zero for $\alpha=0$. In contrast, the linear model term (7) has its maximum value for $\alpha=0$. We would like to use a value of $C_{\varepsilon\alpha}$ close to 3/2 to get a slow evolution of the length scale L, but then (7) causes a faster energy decay than we would expect ($\sim t^{-4}$ for large times). In the following we use $C_{\varepsilon\alpha}=3/2$, with a small value of $C_{\alpha 2}$ in (7) to postpone the adverse effect on the energy decay.

It would be fairly easy to construct a higher-order model term for π_{α} , which is zero in both the isotropic and 2D states. A detailed analysis shows that the desired asymptotic development of both energy and length scales can then be obtained by adjusting the *slope* of π_{α} near $\alpha = 0$.

2.2. Comparison with experiment. The experiments by Alemany *et al.* measured the r.m.s. velocity parallel with the magnetic field, u_{\parallel} , and the parallel integral scale, l_{\parallel} . The MHD turbulence model, on the other hand, features the independent variables R_{33} , K, ε and α ; only R_{33} can be compared directly with the measured u_{\parallel}^2 . We therefor assume that a turbulent length scale L and a parallel length scale L_{\parallel} can be related to the closure variables through

$$L = A \frac{K^{3/2}}{\varepsilon}, \qquad \alpha = \alpha_{iso} \left(\frac{L}{L_{\parallel}}\right)^{2},$$
 (8)

where A is a constant of order one, and $\alpha_{iso} = 1/3$ the isotropic value of α .

Alemany et al. performed experiments with and without magnetic field, and for three different mean velocities, U = [5, 10, 20] cm/s. Without magnetic field, we should find good agreement between the standard K- ε model and experiments if the Reynolds number is high enough. This appears to be the case only for U = 20 cm/s; for the lower velocities the length scale development is slower than predicted by the model and conventional theory. The comparison below is made only for U = 20 cm/s.

Like Alemany et al., we present the results with the non-dimensional time scale $Z-Z_0=tU/M$, where M=2 cm is the mesh size, $Z_0=4$ is the location of the effective origin, and t is real time in the simulation. Initial conditions were computed from measured data in $Z-Z_0=2$, corresponding to a time t_1 in the simulations. An ODE solver was then run forwards and backwards in time, so we could check the model behavior near the effective origin. The measured u_{\parallel}^2 at $t=t_1$ was used for the initial R_{33} . The Reynolds stress anisotropy is small and does not affect results much; we computed K assuming $R_{11}=0.85R_{33}$. L_{\parallel} was taken from the measured l_{\parallel} . The turbulent length scale L had to be estimated; we used a value $L_1=0.25$ cm that makes L approximately equal to L_{\parallel} in the effective origin. Initial values for ε and α were computed using relations (8), with a constant A=0.23 adjusted to match the measured energy decay. The model coefficients used in the simulation were $\{C_{\varepsilon 2}, C_{\alpha 1}, C_{\alpha 2}, C_{\varepsilon \alpha}\} = \{1.92, 2, 0.4, 1.5\}$ (see discussion above).

Results are showed in Fig. 1. The agreement between model predictions and measurements is good. Note especially that the decay of α predicted by the model reproduces the divergence of the two length scales; faster growth of the parallel scale, and slower of the turbulent length scale. A detailed analysis of the model equations shows that the model variables have power-law behavior determined by the model coefficients. We therefor expect that the coefficients may be given values of rather general validity.

3. Additional effects in wall-bounded flows

In contrast to homogeneous turbulence, wall bounded turbulence in a magnetic field tend to become not only two-dimensional (long structures in the magnetic field direction), but also two-component, i.e., with vanishing energy in the field-parallel stress component. For a couple of reasons, the current model will not predict this particular feature of wall-bounded MHD flows.

The MHD model has been derived in Fourier space, where the Poisson equations for fluctuating pressure and fluctuating electrostatic potential can be used to eliminate these variables from the analysis. This however accounts only for the homogeneous parts of the solutions to the Poisson equations. The inhomogeneous contributions are of importance when the turbulence length scales become of the same order as the wall distance.

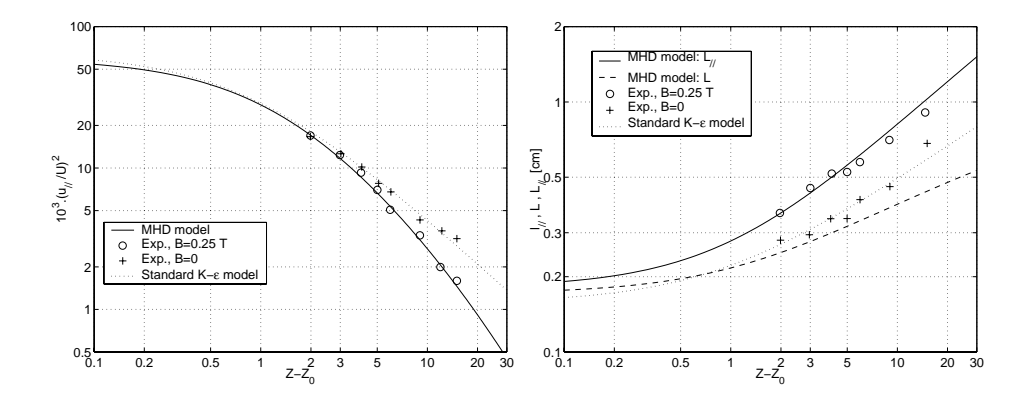


FIGURE 1. Comparison of model predictions and experimental data by Alemany *et al.* ($U=20~{\rm cm/s}$). Left pane: Decay of field-parallel Reynolds stress. Right pane: Development of computed length scales (see text). Predictions with standard $K-\varepsilon$ model and experimental data for B=0 are shown for comparison.

We note the following:

- 1. There should be a near-wall correction to the scalar Joule dissipation, to account for the inhomogeneous contribution to the fluctuating potential.
- 2. In a Reynolds stress closure, the pressure–strain rate correlation is responsible for redistribution of energy between stress components. The pressure–strain terms are i.a. responsible for the damping of wall-normal Reynolds stresses near walls. The magnetic part of the pressure–strain correlation is included in the Joule dissipation tensor, but only the homogeneous effects are accounted for in the present model.
- 3. The so-called slow and rapid pressure–strain terms are part of the conventional Reynolds stress closure. Most commercial implementations of these models *also* neglect the inhomogeneous contributions to fluctuating pressure in models for pressure–strain.
- 4. The linear models for the viscous dissipation and pressure–strain tensors used in the most common Reynolds stress models are not "realizable", i.e., they produce unphysical results in the limit of two-component turbulence. In fact, they give reasonable accuracy only for moderate anisotropies.

The last item could be addressed with high-order models available in the literature, but at the cost of algebraic complexity. The other items are perhaps more intricate, and characteristic of local one-point modeling. The turbulent pressure–strain correlation is non-local by nature. Any description of it in terms of local one-point statistics is therefor unlikely to be universal, but may depend on geometry and other properties of the flow.

Only the first item applies to a three-equation K- ε - α model. This kind of model, on the other hand, assumes isotropic turbulent diffusion, and uses the

Boussinesq hypothesis (relating stress anisotropy to mean strain) for modeling of the production term. A possible route to an effective engineering model could be to model anisotropic diffusion and stress anisotropy using the anisotropy information available in α .

References

- [1] A. Alemany, R. Moreau, P. L. Sulem, and U. Frisch. Influence of an external magnetic field on homogeneous mhd turbulence. *Journal de Mécanique*, 28:277–313, 1979.
- [2] P. A. Davidson. The role of angular momentum in the magnetic damping of turbulence. *Journal of Fluid Mechanics*, 336:123–150, 1997.
- [3] H. K. Moffatt. On the suppression of turbulence by a uniform magnetic field. *Journal of Fluid Mechanics*, 28:571–592, 1967.
- [4] William C. Reynolds. Effects of rotation on homogeneous turbulence. In *Proc. 10th Australasian Fluid Mechanics Conference*, Melbourne, Australia, 1989. University of Melbourne.
- [5] O. Widlund and G. Tallbäck. Modeling of anisotropic turbulent transport in simulations of liquid metal flows in magnetic fields. In *Proceedings* of the Third Int. Symposium on Electromagnetic Processing of Materials, EPM2000, April 3-6, 2000, pages 97–102, Nagoya, Japan, 2000. ISIJ.
- [6] O. Widlund, S. Zahrai, and F. H. Bark. Development of a Reynolds stress closure for modeling of homogeneous MHD turbulence. *Physics of Fluids*, 10(8):1987–1996, 1998.
- [7] O. Widlund, S. Zahrai, and F. H. Bark. Structure information in RDT analysis and one-point modeling of axisymmetric MHD turbulence. *Physics* of Fluids, 12(10):2609–2620, 2000.

Paper 7

NONLINEAR EFFECTS IN MODELING OF HOMOGENEOUS MHD TURBULENCE – COMPARISON WITH EXPERIMENT

Ola Widlund

Faxén Laboratory Royal Institute of Technology SE-100 44, Stockholm, Sweden

Abstract. The dynamical properties of the MHD turbulence model proposed by Widlund et al. are studied for the case of homogeneous decaying turbulence. The proposed model is a Reynolds stress closure, extended with a transport equation for a dimensional anisotropy variable, α , which carries information about length scale anisotropy. The analysis suggests that the model term originally proposed for the nonlinear energy transfer in the α equation should be modified, so that it vanishes in the 2D limit. A unique set of model coefficients could be determined, which makes the model consistent with theory and experiments for interaction numbers Nranging from zero to infinity. The model coincides with the standard K- ε model when there is no magnetic field. In the linear regime of large N, it produces the $K \sim t^{-1/2}$ energy decay and length scale evolution predicted earlier by Moffatt, and Sommeria and Moreau. For intermediate interaction numbers (typically $N \sim 1$) where nonlinear effects are important, $K \sim t^{-1.7}$ and $L_{\parallel} \sim t^{0.65}$, in agreement with the classical experiments by Alemany et al.

1. Introduction

Electrostatic magnetic fields have found widespread use in many industrial materials processing applications. In continuous casting of steel, for example, a static magnetic field is often applied to brake and control the mean flow of liquid metal in the mould. Numerical simulations of this and other turbulent MHD flows generally suffer from the inability of conventional turbulence models (like the $K-\varepsilon$ model, or a full Reynolds stress closure) to deal with the large anisotropies of length scales encountered in MHD turbulence. To improve the situation, it has been suggested to include information about length-scale anisotropy in an extended Reynolds stress model for MHD applications (Widlund et al. [12]).

The so-called dimensionality tensor, Y_{ij} , was first introduced by Reynolds [6] to help describe the effect of rapid rotation on turbulence. While the Reynolds stress tensor R_{ij} accounts for the kinetic energy of fluctuations in different directions, the dimensionality tensor carries information about the length scales in different directions. The latter information seems vital for a correct description of Joule dissipation. The scalar Joule dissipation rate can, for example, be exactly expressed in terms of the component of the dimensionality tensor which is

parallel with the magnetic field,

$$\mu = \frac{1}{2}\mu_{nn} = \frac{\sigma B^2}{\rho} n_i n_j Y_{ji},\tag{1}$$

where n_i is a unit direction vector of the magnetic field.

A conventional Reynolds stress transport (RST) model includes transport equations for the six independent Reynolds stresses and the scalar viscous dissipation rate. Inspired by (1), Widlund *et al.* [12] extended a RST model with a model transport equation for a dimensionality anisotropy variable α , defined as

$$\alpha \equiv \frac{n_i n_j Y_{ji}}{2K}.\tag{2}$$

The anisotropic Joule dissipation tensor is then modeled with an invariant tensor function in R_{ij} and α . An exact transport equation for α can be derived from the Navier–Stokes equations, including magnetic and inertial effects, as well as effects of mean shear and strain [13]. All terms in the equation require modeling, however.

The strength of magnetic damping of turbulence, relative to nonlinear inertial mechanisms, is measured by the interaction number, or Stuart number, defined as

$$N \equiv \frac{\sigma B^2}{\rho} \frac{l}{u},\tag{3}$$

where u and l are characteristic velocity and length scales of the turbulence, B is the magnetic flux density, ρ density, and σ electric conductivity.

A recent paper by Widlund et al. [13] showed that, in the linear regime of large interaction numbers (where Joule dissipation dominates), the proposed model equations have analytic solutions. By choosing one model constant appropriately, these are made consistent with the energy decay $K \sim t^{-1/2}$ predicted earlier by Moffatt [5], and the parallel length scale growth $l_{\parallel} \sim t^{1/2}$ proposed by Sommeria and Moreau [10].

For moderate values of N, the model has been shown to compare well with results from the few available direct numerical simulations of decaying homogeneous turbulence [12]. Experimental data is scarse; the experiment by Alemany et al. [1] is unique among MHD turbulence experiments, as their setup is the only one in which wall effects and other inhomogeneities have negligible impact on results (see also Caperan and Alemany [2]). It is thus the only experiment useful for validating models of homogeneous MHD turbulence.

In the present paper we study the dynamical properties of the model equations, especially for intermediate interaction numbers, $N \sim 1$; in this case we have to deal with the combination of nonlinear energy transfer, viscous and magnetic effects. Section 2 presents governing equations, and model equations for the homogeneous case. The dynamical properties of the model equations are examined in Sec. 3. Some numerical results are presented in Sec. 4, including

(in Sec. 4.2) a comparison with the classical experimental results by Alemany *et al.* [1]. Results and future work are discussed briefly in Sec. 5.

2. Theory

2.1. Governing equations. With spatial coordinates \mathbf{x} and time t, the Navier–Stokes equations for the instantaneous velocity field $u_i(\mathbf{x}, t)$ of an incompressible fluid are

$$\frac{\partial u_i}{\partial t} + u_j \frac{\partial u_i}{\partial x_j} = -\frac{1}{\rho} \frac{\partial p}{\partial x_i} + \nu \frac{\partial^2 u_i}{\partial x_i \partial x_j} + f_i, \tag{4}$$

$$\frac{\partial u_i}{\partial x_i} = 0, (5)$$

where $p(\mathbf{x}, t)$ is the pressure field, ρ the fluid density, ν the kinematic viscosity, and f_i is the Lorentz force (per unit mass).

The Lorentz force f_i in (4) is governed by the non-relativistic Maxwell equations. The magnetic Reynolds number is defined as $\text{Rm}_L \equiv \mu \sigma u l$ (μ is here magnetic permeability). If the magnetic Reynolds number is small ($\text{Rm}_L \ll 1$), convective disturbances to the magnetic field will be small compared to the external field \mathbf{B} , and we can use the so-called quasistatic approximation (see [13] for details). Using lower-case letters to denote instantaneous values, we have

$$f_i \approx \frac{1}{\rho} \epsilon_{ikn} j_k B_n,$$
 (6)

where the instantaneous electric current density j_i is given by Ohm's law,

$$j_i \approx \sigma(e_i + \epsilon_{ikn} u_k B_n). \tag{7}$$

and e_i is the electric field. The scalar electrostatic potential ϕ is defined by

$$e_i = -\frac{\partial \phi}{\partial x_i}. (8)$$

The current field is divergence free, so it follows from (7) that

$$\frac{\partial^2 \phi}{\partial x_i \partial x_i} \approx \epsilon_{ijk} \frac{\partial}{\partial x_i} (u_j B_k). \tag{9}$$

If we consider the case of homogeneous shear-free turbulence, the governing equations can be Fourier transformed. In the spectral domain we can eliminate pressure from the equations, and find an explicit expression for the Lorentz force (see [13], and Schumann [9]). The Fourier coefficients of velocity are then given by

$$\frac{d\hat{u}_i}{dt} = -ik_j(\widehat{u_i u_j}) + i\frac{k_i k_m k_j}{k^2}(\widehat{u_m u_j}) - \nu k^2 \hat{u}_i - \frac{\sigma}{\rho} \frac{(\mathbf{B} \cdot \mathbf{k})^2}{k^2} \hat{u}_i.$$
 (10)

The spectral energy tensor is defined as the ensemble averaged second moments of $\hat{\mathbf{u}}$,

$$\hat{\Phi}_{ij}(\mathbf{k},t) = \langle \hat{u}_i(-\mathbf{k},t)\hat{u}_j(\mathbf{k},t)\rangle = \langle \hat{u}_i^*\hat{u}_j\rangle, \tag{11}$$

which correspond to the two-point velocity correlations in physical space. Here \hat{u}_i^* is the complex conjugate of \hat{u}_i .

An evolution equation for $\hat{\Phi}_{ij}$ can be derived from (10) (see [13]), and from this we can in turn formulate equations for several one-point turbulence quantities [13]. The turbulent kinetic energy, for example, is

$$K = \frac{1}{2} \int \hat{\Phi}_{nn} d^3 \mathbf{k},\tag{12}$$

given by

$$\frac{dK}{dt} = -\varepsilon - \mu,\tag{13}$$

where

$$\varepsilon = \nu \int k^2 \hat{\Phi}_{nn} d^3 \mathbf{k} \tag{14}$$

$$\mu = \frac{\sigma}{\rho} \int \frac{(\mathbf{B} \cdot \mathbf{k})^2}{k^2} \hat{\Phi}_{nn} d^3 \mathbf{k}. \tag{15}$$

The Reynolds stress tensor can be defined in the same way, as

$$R_{ij} = \int \hat{\Phi}_{ij} d^3 \mathbf{k}. \tag{16}$$

In the shear-free case it is given by

$$\frac{dR_{ij}(t)}{dt} = \Pi_{ij}^{(s)} - \varepsilon_{ij} - \mu_{ij}, \tag{17}$$

with

$$\Pi_{ij}^{(s)} = \int ik_m \left\{ \Delta_{in} \int \hat{T}_{mnj}^*(\mathbf{k}, \mathbf{k}') d^3 \mathbf{k}' \right\}$$
(18)

$$-\Delta_{jn} \int \hat{T}_{mni}(\mathbf{k}, \mathbf{k}') d^3 \mathbf{k}' \left\} d^3 \mathbf{k}, \tag{19}$$

$$\varepsilon_{ij} = 2\nu \int k^2 \hat{\Phi}_{ij} d^3 \mathbf{k}, \qquad (20)$$

$$\mu_{ij} = 2\frac{\sigma}{\rho} \int \frac{(\mathbf{B} \cdot \mathbf{k})^2}{k^2} \hat{\Phi}_{ij} d^3 \mathbf{k}, \qquad (21)$$

where ε_{ij} is the dissipation rate tensor, μ_{ij} is the Joule dissipation tensor, and $\Pi_{ij}^{(s)}$ represents nonlinear intercomponent energy transfer.

The Joule dissipation of turbulent kinetic energy in (15) can be written as

$$\mu = \frac{\sigma B^2}{\rho} n_i n_j Y_{ji},\tag{22}$$

where \mathbf{n} is a unit vector parallel with the magnetic field, and \mathbf{Y} is the so-called dimensionality tensor introduced by Reynolds and co-workers [6, 7],

$$Y_{ij} = \int \frac{k_i k_j}{k^2} \hat{\Phi}_{ij}(\mathbf{k}, t) d^3 \mathbf{k}.$$
 (23)

Reynolds showed that Y contains information related to turbulent length scales in different directions.

2.2. Model equations. Based on (22), Widlund et al. [12] proposed a Reynolds stress transport (RST) model for MHD turbulence, which included an extra transport equation for a dimensionality anisotropy variable, α , defined as

$$\alpha \equiv \frac{n_i n_j Y_{ji}}{2K}.\tag{24}$$

If we introduce a magnetic time scale as $\tau = \rho/(2\sigma B^2)$, we have

$$\mu = \frac{\alpha K}{\tau}.\tag{25}$$

This expression for Joule dissipation is exact for homogeneous turbulence.

A transport equation for α can be derived from the Navier–Stokes equations, but all terms require modeling [13].

Assume cartesian coordinates oriented so that the magnetic field vector is in the x_3 -direction, i.e. $\mathbf{B} = B\mathbf{e}_3$. For the case of homoegenous shear-free MHD turbulence, axisymmetric about the magnetic field vector, there is only two independent Reynolds stress components, R_{11} and R_{33} , so that the turbulent kinetic energy is $K = 2R_{11} + R_{33}$. For this case, the Reynolds stress closure proposed by Widlund et al. [12, 13] reduces to

$$\frac{dK}{dt} = -\varepsilon - \frac{\alpha K}{\tau}, \qquad (26)$$

$$\frac{d\varepsilon}{dt} = -\varepsilon_{\varepsilon} - \mu_{\varepsilon}, \qquad (27)$$

$$\frac{d\alpha}{dt} = \pi_{\alpha} - \mu_{\alpha}, \qquad (28)$$

$$\frac{d\varepsilon}{dt} = -\varepsilon_{\varepsilon} - \mu_{\varepsilon}, \tag{27}$$

$$\frac{d\alpha}{dt} = \pi_{\alpha} - \mu_{\alpha}, \tag{28}$$

$$\frac{dR_{33}}{dt} = \pi_{33} - \frac{2}{3}\varepsilon - \frac{G+H}{\tau}R_{33}.$$
 (29)

An equation for the R_{11} component is redundant, as it can be computed from Kand R_{33} . The K equation is exact, as the Joule dissipation term follow from the definition of α . The viscous destruction term in the ε equation is modeled in the usual way, and Widlund et al. used an analogous model for the Joule destruction term—in principal a rescaling of the corresponding terms in the K equation. We have

$$\varepsilon_{\varepsilon} = C_{\varepsilon 2} \frac{\varepsilon^2}{K}, \tag{30}$$

$$\mu_{\varepsilon} = C_{\varepsilon \alpha} \frac{\alpha \varepsilon}{\tau}. \tag{31}$$

The terms in the α equation represent nonlinear energy transfer, and Joule destruction, respectively. In analogy with (30) and (31), the simplest dimensionally correct model of the Joule destruction is

$$\mu_{\alpha} = C_{\alpha 1} \frac{\alpha^2}{\tau}.\tag{32}$$

The model originally proposed by Widlund et al. for the nonlinear term is a simple linear "return-to-isotropy" expression of Rotta type,

$$\pi_{\alpha} = C_{\alpha 2} \frac{\varepsilon}{K} \left(\frac{1}{3} - \alpha \right), \tag{33}$$

assuming the energy transfer rate is governed by the turbulent time scale K/ε .

In (29), π_{33} is a component of a return-to-isotropy model for modeling of slow pressure-strain. Here we use the model of Sarkar & Speziale [8], but the choice is not critical for the results presented here. The anisotropy of the Joule dissipation is governed by the model functions G and H, here given by

$$G(\alpha, R_{33}/K) = \alpha + \frac{9}{10} \frac{R_{33}}{K} \alpha^2,$$
 (34)

$$H(\alpha) = -\frac{9}{5}\alpha^2. \tag{35}$$

3. Dynamical properties of the model

The dynamical properties of the turbulence model are determined by the three equations for K, ε and α (since they are independent of the stress anisotropy).

Let us define the magnetic interaction number using variables of the closure,

$$N \equiv \frac{2\sigma B^2 K}{\rho \varepsilon} = \frac{K}{2\tau \varepsilon}.$$
 (36)

In the absence of a magnetic field (N=0), the model reduces to the common $K-\varepsilon$ model, with analytic power-law solutions. For large times, turbulent kinetic energy decays as $K \sim t^{-n}$, where $n = 1/(C_{\varepsilon^2} - 1)$. The standard value of C_{ε^2} used in most turbulence closures is 1.92, which gives $n \approx 1.09$ (see, e.g., Launder & Spalding [4]). For large times, an integral length scale estimated as $L \sim K^{1.5}/\varepsilon$ would then grow slowly as $L \sim t^{0.46}$. These results are well documented in the literature, and in good agreement with experiments on grid generated turbulence.

Below we look at the model properties in the presence of a magnetic field.

3.1. Decay in a strong magnetic field. For large interaction numbers, $N \gg$ 1, Joule dissipation dominates, at least for a time of order $N_0\tau$; Moffatt studied this case using the linearized inviscid Fourier transformed equations [5]. For this regime of linear decay, the energy was found to decay as $K \sim t^{-1/2}$.

When Joule dissipation dominates, the model equations (26), (27) and (28) are approximated by

$$\frac{dK}{dt} = -\frac{1}{\tau}K\alpha, \qquad (37)$$

$$\frac{d\varepsilon}{dt} = -\frac{C_{\varepsilon\alpha}}{\tau}\varepsilon\alpha, \qquad (38)$$

$$\frac{d\varepsilon}{dt} = -\frac{C_{\varepsilon\alpha}}{\tau}\varepsilon\alpha,\tag{38}$$

$$\frac{dt}{d\alpha} = -\frac{C_{\alpha 1}}{\tau} \alpha^2. \tag{39}$$

Note that the equation for ε is retained here, although ε is assumed small enough to be neglected in the right-hand sides of the equations. This enables us to study how the magnetic destruction terms affect the turbulent time and length scales we can construct from K an ε ,

$$\tau_{tr} \sim \frac{K}{\varepsilon},$$
(40)

$$L \sim \frac{K^{3/2}}{\varepsilon}.$$
 (41)

Equations (37) through (39) have analytic solutions,

$$K(t) = K_0 (\beta t + 1)^{-1/C_{\alpha 1}}, (42)$$

$$\varepsilon(t) = \varepsilon_0 \left(\beta t + 1\right)^{-\frac{C_{\varepsilon\alpha}}{C_{\alpha 1}}} \tag{43}$$

$$\alpha(t) = \alpha_0 (\beta t + 1)^{-1}, \qquad (44)$$

where $\beta = C_{\alpha 1}\alpha_0/\tau$, and variables with a zero subscript represent initial conditions.

The decay rate of turbulent kinetic energy is governed by the model coefficient $C_{\alpha 1}$ in the magnetic destruction term in the α equation. By choosing $C_{\alpha 1} = 2$, we obtain the asymptotic decay rate $K \sim t^{-1/2}$ predicted by Moffatt [5].

The significance of $C_{\alpha 1}$ can be understood from an examination of the exact destruction term. Widlund et al. [13] used the linearized equations and the concept of rapid distortion theory (RDT) to compare the exact Joule destruction terms in the Reynolds stress and α equations, with the proposed model terms. Figure 1 compares the ratio $\mu_{\alpha}\tau/\alpha$, as predicted by RDT and the simple model (32). A coefficient $C_{\alpha 1}=0.8$ was found to give the correct value for isotropic turbulence (for which $\alpha=1/3$), while $C_{\alpha 1}=2$ gives a good description near the 2D limit ($\alpha=0$). With the information in Fig. 1 it would be fairly straightforward to devise a more accurate higher-order model term for μ_{α} , although this is beyond the scope of the present paper. Figure 2, showing decay of turbulent kinetic energy, compares model predictions with a numerical integration of the exact RDT equations; See [13] for details. In the following we will use $C_{\alpha 1}=2$, which gives the desired asymptotic behavior for small α .

Equation 43 shows that the decay rate of ε is determined by the ratio $C_{\varepsilon\alpha}/C_{\alpha 1}$, and the value of $C_{\varepsilon\alpha}$ thus affects the development of turbulent time and length scales (40) and (41). Combining solutions (42) and (43), we get

$$\tau_{tr}(t) = \frac{K_0}{\varepsilon_0} \left(\beta t + 1\right)^{\frac{C_{\varepsilon\alpha} - 1}{C_{\alpha 1}}}, \tag{45}$$

$$L(t) = \frac{K_0^{3/2}}{\varepsilon_0} \left(\beta t + 1\right)^{\frac{C_{\varepsilon\alpha} - 3/2}{C_{\alpha 1}}}.$$
 (46)

Assuming $C_{\alpha 1}=2$, we can identify two values of $C_{\varepsilon\alpha}$ with special meaning. $C_{\varepsilon\alpha}=1$ leaves the turbulent time scale unaffected by the magnetic field, with a slow decline of the integral length scale, $L \sim t^{-1/4}$. If instead $C_{\varepsilon\alpha}=3/2$, the integral length scale L is unaffected, but there is slow growth of the time scale, $\tau_{tr}\sim t^{1/4}$. It is generally held that the length scale estimated by (41) is not

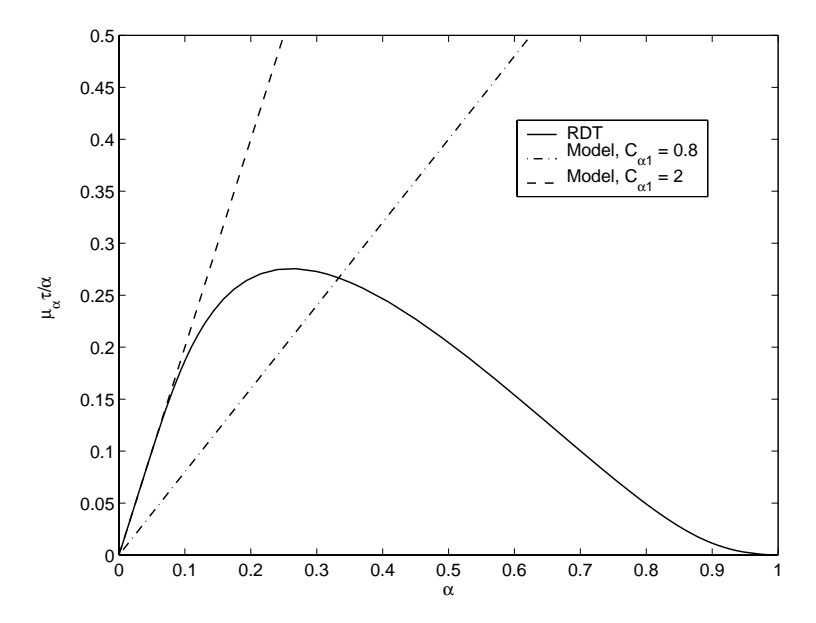


FIGURE 1. With the model term (32), the non-dimensional ratio $\mu_{\alpha}\tau/\alpha$ is given by the linear expression $C_{\alpha 1}\alpha$. Here this model is compared with the exact term in the linearized equations, as a function of α (see Widlund *et al.* [13] for details).

affected by the magnetic field (see, e.g., Davidson [3] and Moffatt [5]). In the following we will therefor expect $C_{\varepsilon\alpha}$ to take a value close to 3/2.

The model variable α represents an anisotropy of length scales, relative to the direction of the magnetic field. The definition of α , and comparison with scale estimates in earlier work (e.g. Davidson [3]), suggests the scale relation

$$\alpha \sim \left(\frac{L}{L_{\parallel}}\right)^2,$$
 (47)

where L_{\parallel} is a characteristic length scale in the direction of the magnetic field. Provided the change in L is small, Eq. (44) then yields the length-scale growth $L_{\parallel} \sim t^{1/2}$ for large times. This is consistent with the results of Sommeria and Moreau [10], and Davidson [3].

3.2. Moderate interaction numbers. When the interaction number is of order one, the situation is more complicated. The equations for K, ε , and α , are nonlinear and strongly coupled. No analytic solutions can be found for this case. The most important change is perhaps that the α equation is now strongly coupled to the other two, through the nonlinear return-to-isotropy term, π_{α} . We will see that the behavior of this term is very important for the dynamical properties of the whole system.

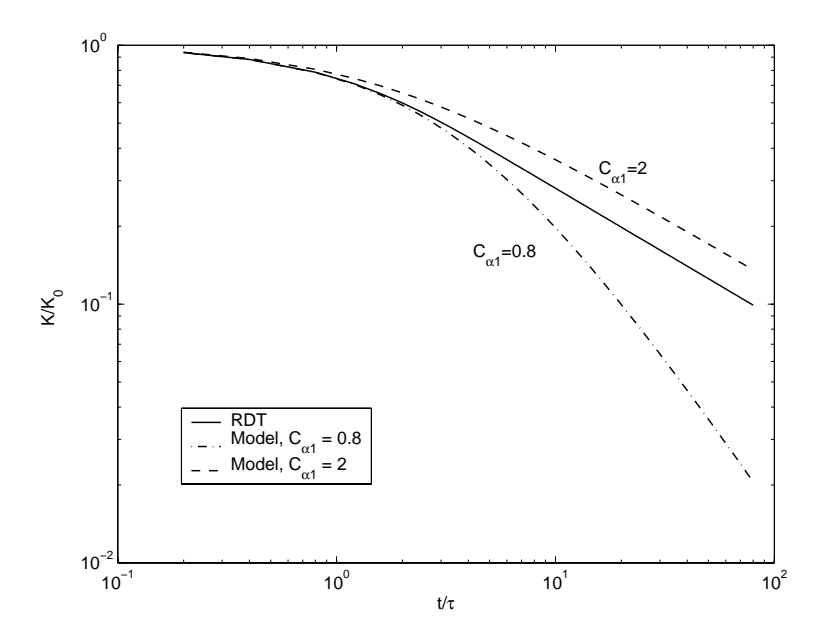


Figure 2. Decaying turbulence in the limit of large N, where Joule dissipation dominates. The graphs show time development $[\tau = \rho/(2\sigma B^2)]$ of turbulent kinetic energy. Solid line represents the RDT solution, and dashed lines the analytic solution of the model equations (37) and (39), for two values of $C_{\alpha 1}$. (Initially isotropic turbulence, $\alpha_0 = 1/3$.)

We assume the model variables have power-law behavior for sufficiently large times. We could introduce the variable transformation s = 1/t, so that solutions for large times correspond to solutions for small s. For small s, a Frobenius series expansion of a variable φ has the form

$$\varphi(s) = s^m (a_0 + a_1 s + a_2 s^2 + \cdots),$$
 (48)

where the exponent m may be any real number. We retain only the first term, and look for solutions of the form

$$K(s) = a_0 s^x, (49)$$

$$K(s) = a_0 s^x, (49)$$

$$\varepsilon(s) = b_0 s^y, (50)$$

$$\alpha(s) = c_0 s^z. (51)$$

For large times, $\alpha \to 0$, so that the return-to-isotropy model (33) is approximately

$$\pi_{\alpha} \approx \frac{C_{\alpha 2} \varepsilon}{3K}.\tag{52}$$

For small values of s, the transformed equations (26), (27), and (28) then read as

$$0 = s^2 \frac{dK}{ds} - \varepsilon - \frac{1}{\tau} K\alpha, \tag{53}$$

$$0 = s^2 \frac{d\varepsilon}{ds} - C_{\varepsilon 2} \frac{\varepsilon^2}{K} - \frac{C_{\varepsilon \alpha}}{\tau} \varepsilon \alpha, \tag{54}$$

$$0 = s^2 \frac{d\alpha}{ds} + \frac{C_{\alpha 2}\varepsilon}{3K} - \frac{C_{\alpha 1}}{\tau} \alpha^2.$$
 (55)

Inserting our ansatz (49), (50), and (51) yields (after simplification)

$$0 = x - \frac{b_0}{a_0} s^{(-x+y-1)} - \frac{c_0}{\tau} s^{(z-1)}, \tag{56}$$

$$0 = y - \frac{C_{\varepsilon 2}b_0}{a_0}s^{(-x+y-1)} - \frac{C_{\varepsilon \alpha}c_0}{\tau}s^{(z-1)}, \tag{57}$$

$$0 = z + \frac{C_{\alpha 2}b_0}{3a_0c_0}s^{(-x+y-z-1)} - \frac{C_{\alpha 1}c_0}{\tau}s^{(z-1)}.$$
 (58)

The first constant term of each equation above must be balanced by at least one other term of zeroth order. Presumably the magnetic terms (last) are active also at large times, so that z=1. Since z=1, the second terms in (56) and (57) are a factor s larger than the second term in (58). For this case to be different from the linear problem of Sec. 3.1, we conclude that also the second term in (58) is constant, so that y=x+2; the second terms in (56) and (57) are then 1st order in s, and vanish for small s (large times). Equations (56) and (57) now reduce to

$$0 = x - \frac{c_0}{\tau}, \tag{59}$$

$$0 = y - \frac{C_{\varepsilon\alpha}c_0}{\tau}, \tag{60}$$

which we can solve for x and y. We find

$$x = \frac{2}{C_{\varepsilon\alpha} - 1},\tag{61}$$

$$y = \frac{2C_{\varepsilon\alpha}}{C_{\varepsilon\alpha} - 1},\tag{62}$$

$$z = 1. (63)$$

With the ansatz (49), (50), and (51), we have for large times $K \sim t^{-x}$, $\varepsilon \sim t^{-y}$, and $\alpha \sim t^{-z}$, while the length scales evolve as $L \sim t^{(-3x/2+y)}$, and $L_{\parallel} \sim t^{(-3x/2+y+1/2)}$. The coefficient value $C_{\varepsilon\alpha} = 3/2$ proposed in Sec. 3.1 gives an energy decay $K \sim t^{-4}$, while the length scales develop as in the linear case. The experiment by Alemany et al. indicated that $K \sim t^{-1.7}$. To obtain this decay, we would have to choose $C_{\varepsilon\alpha} = 2.2$, but then the length scales would evolve as $L \sim t^{1.2}$ and $L_{\parallel} \sim t^{1.7}$. This is not consistent with neither theory, nor experiments.

The unwanted properties of the model is caused by the unphysical behavior of the return-to-isotropy term π_{α} when we approach $\alpha=0$. As explained in spectral terms by Alemany et~al., we will eventually reach a balance between Joule dissipation and nonlinear angular energy transfer. The angular energy transfer is represented by the return term π_{α} , which counteracts the magentic destruction term μ_{α} in the α equation. One can argue that the spectral triad interactions responsible for the angular energy transfer should vanish in the limit of 2D turbulence, where all the energy is concentrated in the wave number plane $k_{\parallel}=0$. This means that π_{α} should be zero for $\alpha=0$. In contrast, the linear model term (33) has its maximum value for $\alpha=0$. Since $\mu_{\alpha}=0$ in the 2D limit, $\alpha=0$ is not a fixed point of the system, and the 2D limit is approached only slowly, as the growth of the turbulent time scale K/ε gradually shifts the balance of the two terms towards lower α .

The shortcomings of the original model are addressed in the following section.

3.3. Modified nonlinear term. We repeat the analysis in the previous section with a modified version of the return-to-isotropy term π_{α} . For a physically correct description near the 2D limit, π_{α} should be zero not only for isotropic turbulence ($\alpha = 1/3$), but also in the 2D limit, where $\alpha = 0$. Any such model can be written as a series expansion

$$\pi_{\alpha} = C'_{\alpha 2} \frac{\varepsilon}{K} \alpha (1 + d_1 \alpha + d_2 \alpha^2 + \cdots). \tag{64}$$

For our analysis we assume small values of α , and retain only the leading-order term,

$$\pi_{\alpha} \approx C'_{\alpha 2} \frac{\varepsilon}{K} \alpha.$$
 (65)

The primed coefficient $C'_{\alpha 2}$ can here be interpreted as the slope of $\pi_{\alpha}K/\varepsilon$, as a function of α , near the 2D limit.

With the new expression (65), the transformed equation (55) for α is altered, so that

$$0 = s^2 \frac{d\alpha}{ds} + \frac{C'_{\alpha 2} \varepsilon \alpha}{K} - \frac{C_{\alpha 1}}{\tau} \alpha^2.$$
 (66)

We insert the ansatz (49), (50), and (51) to obtain

$$0 = z + \frac{C'_{\alpha 2}b_0}{a_0}s^{(-x+y-1)} - \frac{C_{\alpha 1}c_0}{\tau}s^{(z-1)}.$$
 (67)

The exponent of the second term in (67) has changed, compared with the original (58), and the exponent is now the same as the second terms in (56) and (57). For this case to be different from the linear problem, we then conclude that all terms in (56), (57), and (67) must be of equal order, so that z = 1, and y = x + 1.

Eqs. (56), (57), and (67) then reduce to

$$0 = x - \frac{b_0}{a_0} - \frac{c_0}{\tau}, \tag{68}$$

$$0 = y - \frac{C_{\varepsilon 2}b_0}{a_0} - \frac{C_{\varepsilon \alpha}c_0}{\tau}, \tag{69}$$

$$0 = z + \frac{C'_{\alpha 2}b_0}{a_0} - \frac{C_{\alpha 1}c_0}{\tau}. \tag{70}$$

The non-trivial solution to this system of equations yields

$$x = \frac{C_{\varepsilon 2} + C_{\alpha 1} - C_{\varepsilon \alpha} + C'_{\alpha 2}}{C_{\alpha 1}(C_{\varepsilon 2} - 1) + C'_{\alpha 2}(C_{\varepsilon \alpha} - 1)},$$
(71)

$$y = \frac{C_{\varepsilon 2} + C_{\varepsilon 2}C_{\alpha 1} - C_{\varepsilon \alpha} + C_{\varepsilon \alpha}C'_{\alpha 2}}{C_{\alpha 1}(C_{\varepsilon 2} - 1) + C'_{\alpha 2}(C_{\varepsilon \alpha} - 1)},$$
(72)

$$z = 1. (73)$$

The result y = x + 1 relates the power-law decay of energy to the evolution of the time and length scales. We saw earlier that $L \sim t^q$, where q = -3x/2 + y. If y = x + 1, then q = 1 - x/2. The same relationship between energy decay and length scale growth is obtained for the standard $K - \varepsilon$ model, and with $C_{\varepsilon\alpha} = 3/2$ this holds also for the linear case in Sec. 3.1. In contrast, the original model in Sec. 3.2 makes y = x + 2. This gives q = 2 - x/2, and explains the inconsistency between predicted energy decay and length scale growth for the original model.

Inertial effects are governed by the turbulent time scale K/ε , while the Joule energy dissipation is governed by an effective magnetic time scale τ/α , rather than τ . The analysis shows that, for large times, both these time scales grow as $K/\varepsilon \sim \tau/\alpha \sim t$. This corresponds to an equilibrium between nonlinear energy transfer, and Joule dissipation. As pointed out by Sreenivasan and Alboussière [11], these time scales define a "true" interaction number, N^* . We here define it in terms of the variables of the closure,

$$N^* \equiv \frac{\alpha K}{\tau \varepsilon} = \frac{\mu}{\varepsilon} = \frac{2\sigma B^2 \alpha K}{\rho \varepsilon}.$$
 (74)

In the "nonlinear" phase of decay occurring for large times, Sreenivasan *et al.* proposed that N^* is constant and of order unity. This is consistent with our analysis: the ansatz (49), (50) and (51), and the solution to the system (68) through (70), gives

$$N^* = \frac{C_{\varepsilon 2} + C'_{\alpha 2} - 1}{C_{\alpha 1} - C_{\varepsilon \alpha} + 1} = \text{const.}$$
 (75)

The power-law exponent (71) for energy decay at large times depend on all model coefficients $C_{\varepsilon 2}$, $C_{\alpha 1}$, $C_{\varepsilon \alpha}$, and $C'_{\alpha 2}$. By choosing $C_{\varepsilon 2}=1.92$ and $C_{\alpha 1}=2$, the model predicts the correct energy decay both for high N, and for N=0 (no magnetic field). The asymptotic energy decay for finite N is then determined by our choice of $C'_{\alpha 2}$ and $C_{\varepsilon \alpha}$, although we prefer a value of $C_{\varepsilon \alpha}$ close to 3/2, to get the expected length scale evolution in the linear regime. Figure 3 shows

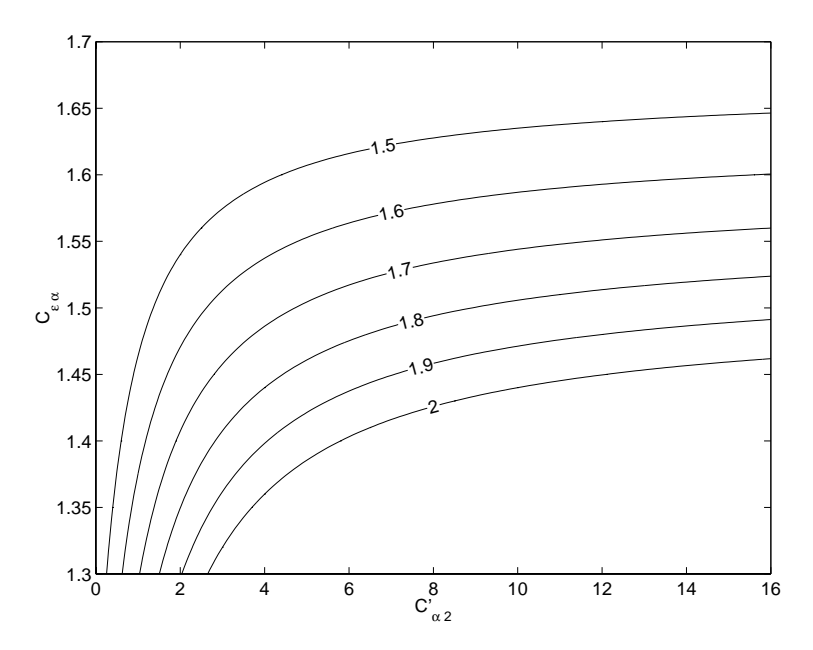


FIGURE 3. Contours of the power-law exponent x in the asymptotic decay $K \sim t^{-x}$, as a function of the coefficients $C_{\varepsilon\alpha}$ and $C'_{\alpha 2}$ (assuming $C_{\varepsilon 2} = 1.92$ and $C_{\alpha 1} = 2$).

how the power-law exponent x in $K \sim t^{-x}$ depend on the model coefficients $C'_{\alpha 2}$ and $C_{\varepsilon \alpha}$ (assuming $C_{\varepsilon 2}=1.92$ and $C_{\alpha 1}=2$). If $C_{\varepsilon \alpha}=3/2$, the value $C'_{\alpha 2}=4.72$ reproduces the energy decay $K \sim t^{-1.7}$ found by Alemany et~al.. The length scales then develop as $L \sim t^{0.15}$ and $L_{\parallel} \sim t^{0.65}$ for large times. The true interaction parameter tends to a constant value $N^* \approx 3.76$, given by (75).

4. Numerical simulations

The model equations can be solved numerically with a standard ODE solver, and approriate initial conditions. For this purpose, we need to define a return-to-isotropy model term π_{α} which presumably behaves roughly as the original model (33) away from the 2D limit, but with the asymptotically correct behavior (65) when we approach $\alpha = 0$.

A simple combination of Eqs. (33) and (65) yields

$$\pi_{\alpha} = \frac{\varepsilon}{K} \min \left[C'_{\alpha 2} \alpha; \ C_{\alpha 2} \left(\frac{1}{3} - \alpha \right) \right]. \tag{76}$$

For a given value of $C'_{\alpha 2}$, the value of $C_{\alpha 2}$ decides how fast π_{α} grows as we move away from the isotropic state, and also fixes the distinct value of α where the model term abrubtly changes behavior and falls off towards zero. Equation (76) is a gross simplification of the true mechanism, but we can use it here to demonstrate some properties of the model.

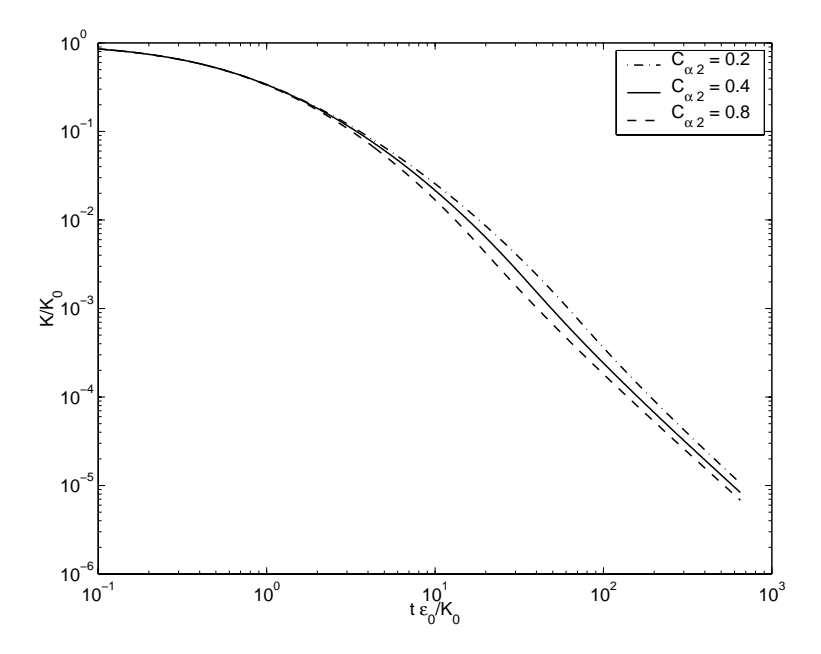


FIGURE 4. Predicted energy decay for three values of the coefficient $C_{\alpha 2}$, and initial interaction number $N_0 = 1$.

4.1. Variation of $C_{\alpha 2}$ and N. Initial values for K and ε can be chosen arbitrarily as $K_0 = 1$, and ε_0 . We presume initially isotropic turbulence, $\alpha_0 = 1/3$, and $R_{33} = 2K/3$. The initial magnetic interaction parameter is $N_0 = K_0/(2\tau\varepsilon_0)$.

The analysis above shows that the following set of model coefficients gives an asymptotic energy decay in agreement with theory and experiments, for all values of N:

$$\{C_{\varepsilon 2}, C_{\alpha 1}, C_{\varepsilon \alpha}, C'_{\alpha 2}\} = \{1.92, 2, 1.5, 4.72\}.$$
 (77)

Figure 4 shows predicted energy decay for $N_0 = 1$ and three different values of the undetermined coefficient $C_{\alpha 2}$, which governs the magnitude of the return term (76). Figure 5 shows the evolution of the true interaction parameter, $N^* = \alpha K/(\tau \varepsilon)$. Both figures show that $C_{\alpha 2}$ affects how fast we reach the final "nonlinear" phase of decay; the stronger the return term, the faster we reach the point where π_{α} starts to decrease with decreasing α .

Figure 6 shows the evolution of the true interaction parameter for three intial interaction parameters $N_0 = \{0.1, 1, 10\}$, and $C_{\alpha 2} = 0.4$. We asymptotically reach a constant value $N^* \approx 3.8$, given by (75).

4.2. Comparison with experiments. The experiments by Alemany *et al.* [1] measured the r.m.s. velocity parallel with the magnetic field, u_{\parallel} , and the parallel integral scale, l_{\parallel} (from the one-dimensional spectrum in this direction). The MHD turbulence model we want to compare with, on the other hand, features the

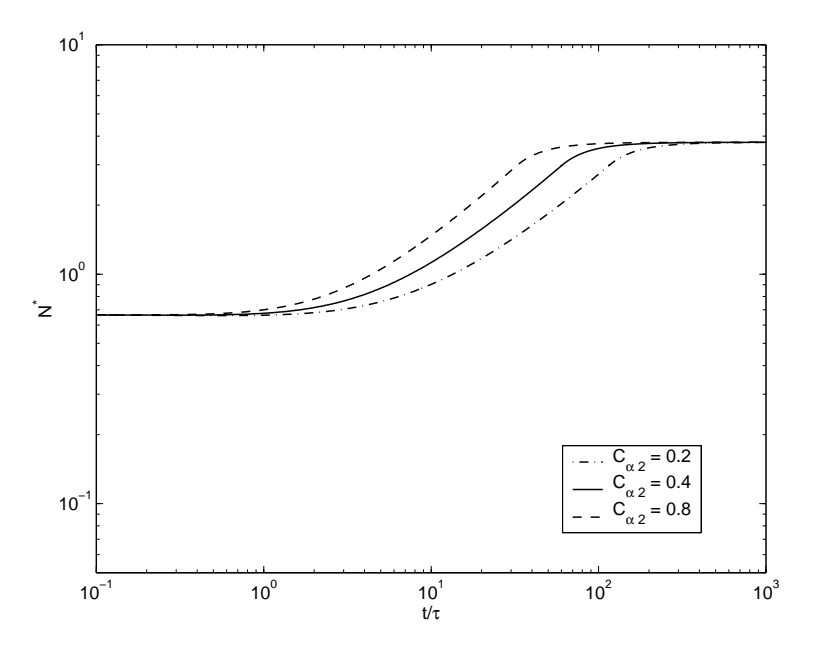


Figure 5. Predicted evolution of the true interaction number N^* , for three values of the coefficient $C_{\alpha 2}$ ($N_0=1$).

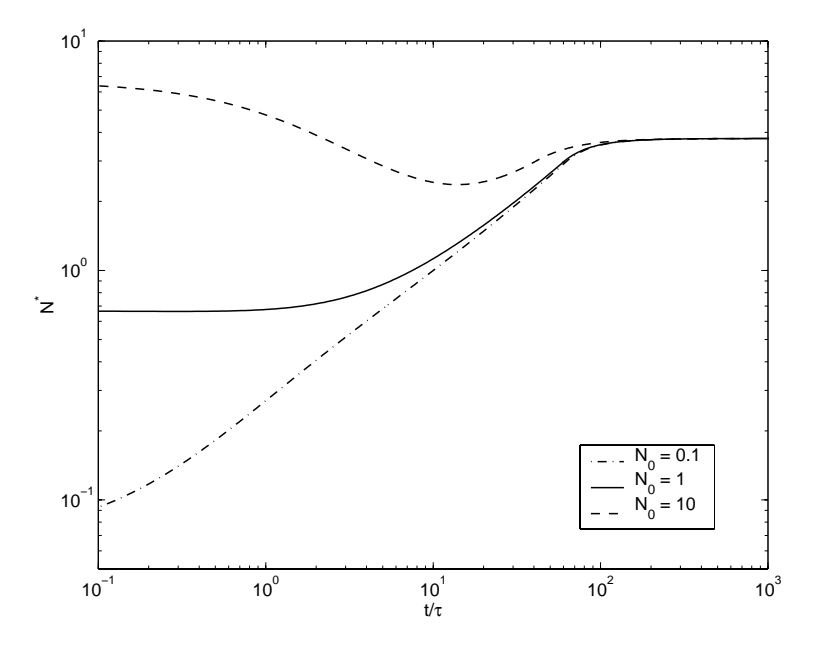


FIGURE 6. Predicted evolution of the true interaction number N^* for three values of initial interaction number, $N_0 = \{0.1, 1, 10\}$, and with $C_{\alpha 2} = 0.4$.

independent variables K, ε , α , and R_{33} ; only R_{33} can be compared directly with the measured $\overline{u_{\parallel}^2}$. Based on previously introduced scale estimates, we therefor assume that a turbulent length scale L and a parallel length scale L_{\parallel} can be related to the closure variables through

$$L = A \frac{K^{3/2}}{\varepsilon},\tag{78}$$

$$\left(\frac{L}{L_{\parallel}}\right)^2 = \frac{\alpha}{\alpha_{\rm iso}},\tag{79}$$

where A is a constant of order one, and $\alpha_{iso} = 1/3$ is the isotropic value of α .

Like Alemany et al., we will present results with the non-dimensional time scale $Z - Z_0 = tU/M$, where M = 2 cm is the mesh size, $Z_0 = 4$ is the location of the effective origin, and t is real time in the simulation. Initial conditions are computed from measured data in $Z - Z_0 = 2$, corresponding to a time t_1 in the simulations. An ODE solver can then be run forwards and backwards in time, so we can check the model behavior near the effective origin.

4.2.1. Viscous decay (B=0). Alemany et al. performed experiments with and without magnetic field, and for three different mean velocities, U=[5,10,20] cm/s. Without magnetic field, we should find good agreement between the standard K- ε model and experiments if the Reynolds number is high enough. Experimental data at $Z-Z_0=2$ gives approximately $\overline{u_{\parallel}^2}/U^2=18\cdot 10^{-3}$, and $l_{\parallel}=0.27$ cm. We assume U=20 cm/s, and specify initial conditions at $t=t_1$ as $R_{33,1}=\overline{u_{\parallel}^2}$, and due to isotropic conditions, $K_1=3R_{33,1}/2$ and $L_1=l_{\parallel}$. The initial ε_1 is then computed from (78), where A=0.31 is chosen to match the measured energy decay.

Results are shown in Figs. 7 and 8. The predicted evolution of the length scale agree well with measurements only for the highest mean velocity, U = 20 cm/s. For the lower mean velocities, the measured length scale evolution is inconsistent with the observed energy decay. This is probably an effect of the low Reynolds numbers realized in the experiments; based on u_{\parallel} and l_{\parallel} measured at $Z - Z_0 = 2$, the turbulent Reynolds number was Re = {157, 315, 629}, for mean velocities $U = \{5, 10, 20\}$ cm/s, respectively. In the following we consider only results obtained with U = 20 cm/s.

4.2.2. With magnetic field. To get the desired asymptotic evolution of energy and length scales, we use the model coefficients defined in (77), together with $C_{\alpha 2} = 0.4$.

For magnetic field B=0.25 T and mean velocity U=20 cm/s, the first measurement in $Z-Z_0=2$ gives $\overline{u_{\parallel}^2}/U^2=17\cdot 10^{-3}$, and $l_{\parallel}=0.36$ cm. For the time $t=t_1$, the experimental data thus provide the initial conditions $R_{33,1}=\overline{u_{\parallel}^2}$, and $L_{\parallel,1}=l_{\parallel}$. Assuming we can *estimate* L and R_{11} at time $t=t_1$, we can compute the remaining initial conditions as follows: (i) $K_1=(2R_{11,1}+R_{33,1})$,

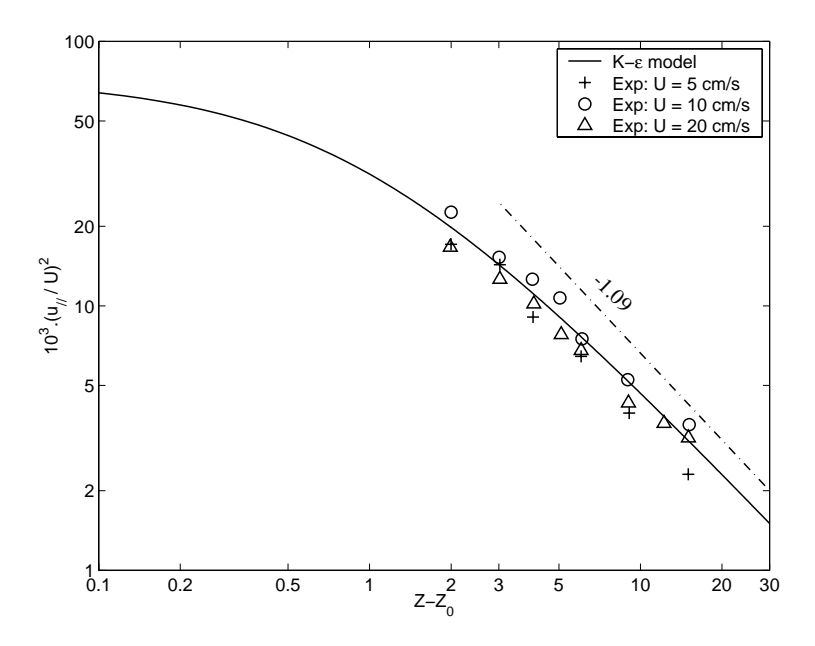


FIGURE 7. Viscous decay of turbulent kinetic energy. Comparsion between Alemany's experimental data (for B=0), and predictions with the standard $K-\varepsilon$ model.

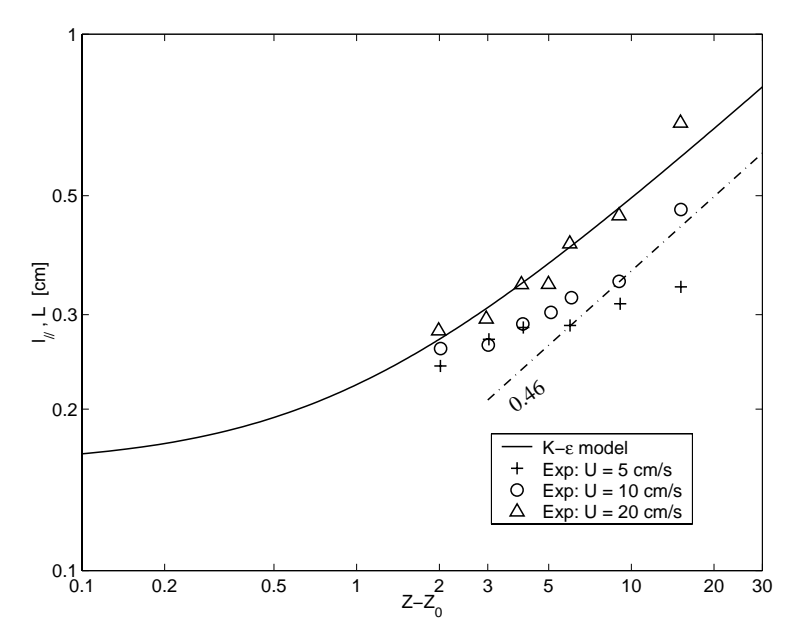


FIGURE 8. Growth of integral length scale, as measured by Alemany et al., and predicted by the standard $K-\varepsilon$ model. Predicted length scale is computed from Eq. (78), with A=0.31.

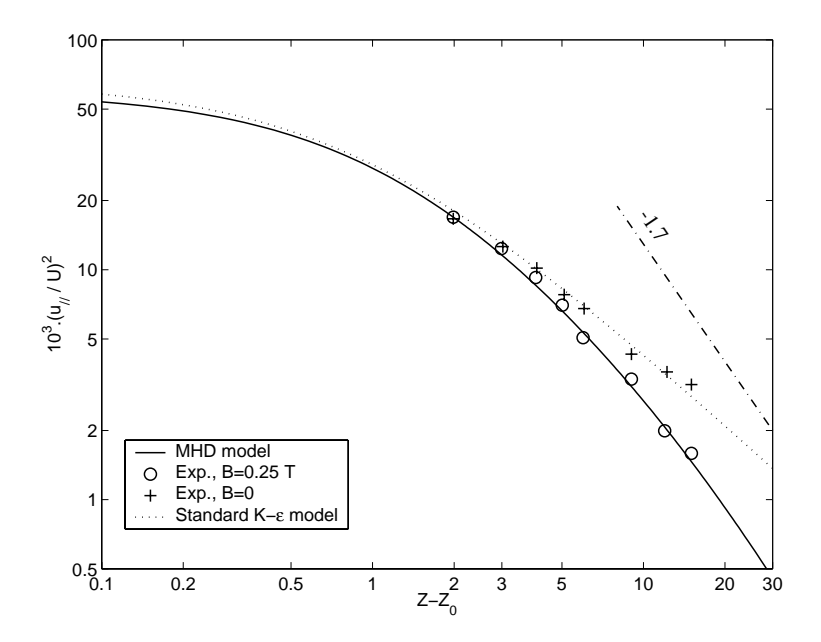


FIGURE 9. Decay of field-parallel Reynolds stress. Comparison between model predictions and Alemany's experimental data ($B=0.25~\mathrm{T},\,U=20~\mathrm{cm/s}$). Predictions with the standard $K-\varepsilon$ model and experimental data for B=0 are shown for comparison. The dashed line represents the asymptotic power-law behavior of the model.

(ii) α_1 is computed from Eq. (79), and (iii) ε_1 is computed using Eq. (78). We have chosen $L_1 = 0.251$ cm and $R_{11,1} = 0.85R_{33,1}$; with these values, backward integration to the virtual origin (t = 0, $Z - Z_0 = 0$) gives $R_{11,0} \approx R_{33,0}$, and $L_0 \approx L_{\parallel,0}$ (isotropic turbulence). As in the viscous case, we adjust A in (78) to match the measured energy decay; here A = 0.22.

Figure 9 shows measured and predicted decay of the field-parallel Reynolds stress. Results with B=0 are included for comparison. The Reynolds stress anisotropies are relatively small, so there is little difference between the evolution of K, and the individual stress components (not shown here).

Equations (78) and (79) can be used to compute L and L_{\parallel} from predicted values of K, ε , and α . Computed length scales are compared with the measured parallel scale l_{\parallel} in Fig. 10. Non-magnetic results are shown for comparison. Compared to the non-magnetic case, the integral scale L evolves slower in the presence of a magnetic field, while the parallel scale L_{\parallel} grows faster.

5. Discussion and summary

In earlier papers, Widlund et al. proposed to model MHD turbulence by including an extra transported scalar α in standard eddy-viscosity and Reynolds stress

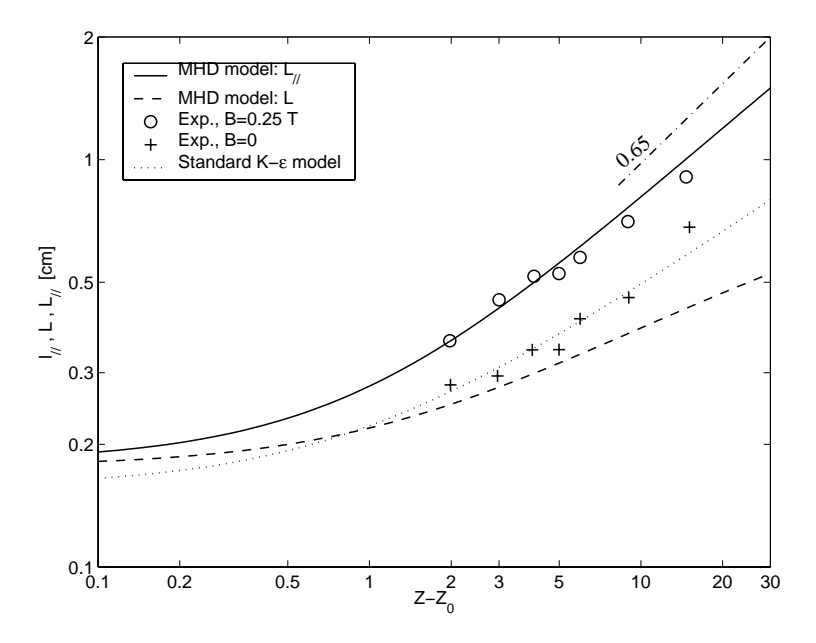


FIGURE 10. Development of computed length scales (see text), compared with the parallel length scale measured in Alemany's experiment. Predictions with the standard $K-\varepsilon$ model and experimental data for B=0 are shown for comparison. The dashed line represents the asymptotic power-law behavior of L_{\parallel} , according to the model.

closures [12, 13]. The new scalar measures anisotropy of length scales, with respect to the direction of the magnetic field.

In this paper we have studied the dynamical properties of of proposed model equations, for the case of homogeneous decaying turbulence. On physical grounds, we proposed a modification of the nonlinear return-to-isotropy term π_{α} in the α equation, so that π_{α} falls off linearly towards zero when we approach the 2D limit $(\alpha=0)$. We could then determine a consistent set of model coefficients, that makes the asymptotic behavior of the model for large times consistent with theory and experiments, for interaction parameters N ranging from zero to infinity. When N=0, the model coincides with a standard K- ε model. For the linear regime of large N, the model predicts energy decay $K \sim t^{-1/2}$ and $L_{\parallel} \sim t^{1/2}$, in agreement with earlier theoretical results (Moffatt [5] and Davidson [3]). For intermediate values of N, finally, the model reproduces the energy decay $K \sim t^{-1.7}$ and the length scale evolution measured in the classical experiment by Alemany $et\ al.\ [1]$.

Davidson [3] obtained his results for large N from scale estimates, assuming conservation of angular momentum about an axis parallel with the magnetic field. For intermediate interaction numbers, typically $N \sim 1$, Sreenivasan and Alboussière [11] analysed the dynamics of a single vortex in the late nonlinear

phase of decay, where there is an equilibrium between Joule dissipation and nonlinear energy transfer. They assumed conservation of angular momentum, and further that a true interaction parameter $N_t = N(L/L_{\parallel})^2$ tends to a constant value of order one. From a modeling perspective, these assumptions are not necessary. The properties themselves are confirmed, however, provided that the proposed model equations capture the essential properties of the underlying physical mechanisms. The most important aspects we have seen here are, (i) an exact expression of the Joule dissipation in terms of the closure variables $(\mu \equiv \alpha K/\tau)$, (ii) a dimensionally correct linear model of Joule destruction in the ε equation (31), (iii) a magnetic destruction of α matching the asymptotic behavior of the exact term in the linearized equations (Fig. 1), and finally, (iv) a return-to-isotropy term in the α equation, which approaches zero in the 2D limit.

The nonlinear energy transfer mechanisms are still not well understood. We have, for example, not considered the effect of the magnetic field on the nonlinear energy transfer rate. The magnetic field may effect the rate of nonlinear angular energy transfer (the return term in the α equation), and intercomponent transfer, but also the energy cascade leading to viscous dissipation of energy in the small scales. The study of nonlinear effects will be one of the priorities for future work.

References

- A. Alemany, R. Moreau, P. L. Sulem, and U. Frisch. Influence of an external magnetic field on homogeneous mhd turbulence. *Journal de Mécanique*, 28:277–313, 1979.
- [2] Ph. Caperan and A. Alemany. Turbulence homogène m.h.d. a faible nombre de reynolds magnétique. Étude de la transition vers la phase quasi bidimensionnelle et charactérisation de son anisotropie. *Journal de Mécanique théoretique et appliquée*, 4(2):175–200, 1985.
- [3] P. A. Davidson. The role of angular momentum in the magnetic damping of turbulence. *Journal of Fluid Mechanics*, 336:123–150, 1997.
- [4] B. E. Launder and D. B. Spalding. The numerical computation of turbulent flows. Computer Methods in Appl. Mech. and Eng., 3:269–289, 1974.
- [5] H. K. Moffatt. On the suppression of turbulence by a uniform magnetic field. *Journal of Fluid Mechanics*, 28:571–592, 1967.
- [6] William C. Reynolds. Effects of rotation on homogeneous turbulence. In Proc. 10th Australasian Fluid Mechanics Conference, Melbourne, Australia, 1989. University of Melbourne.
- [7] William C. Reynolds and S. C. Kassinos. One-point modelling of rapidly deformed homogeneous turbulence. *Proceedings of the Royal Society of Lon*don, Series A, 451(1941):87–104, Oct 1995.
- [8] S. Sarkar and C. G. Speziale. A simple nonlinear model for the return to isotropy in turbulence. *Physics of Fluids A*, 2(1):84–93, 1990.

- [9] U. Schumann. Numerical simulation of transition from three- to twodimensional turbulence under a uniform magnetic field. *Journal of Fluid Mechanics*, 74:31–58, 1976.
- [10] J. Sommeria and R. Moreau. Why, how, and when, MHD turbulence becomes two-dimensional. *Journal of Fluid Mechanics*, 118:507–518, 1982.
- [11] B. Sreenivasan and T. Alboussière. Evolution of a vortex in magnetic field. Eur. J. Mech. B - Fluids, 19:403–421, 2000.
- [12] O. Widlund, S. Zahrai, and F. H. Bark. Development of a Reynolds stress closure for modeling of homogeneous MHD turbulence. *Physics of Fluids*, 10(8):1987–1996, 1998.
- [13] O. Widlund, S. Zahrai, and F. H. Bark. Structure information in rapid distortion analysis and one-point modeling of axisymmetric magnetohydrodynamic turbulence. *Physics of Fluids*, 12(10):2609–2620, 2000.